CAPITAL UNIVERSITY OF SCIENCE AND TECHNOLOGY, ISLAMABAD

Scattering of Non-Axisymmetric Shell Radiation with Membrane Disc

by

Nabeela Waheed

A thesis submitted in partial fulfillment for the degree of Master of Philosophy

in the

Faculty of Computing
Department of Mathematics

2025

First and foremost, I am profoundly grateful to ***Allah Almighty*** *for His countless blessings, guidance, and mercy that made this achievement possible. This thesis is dedicated to my beloved parents,* ***Tazeem Akhtar*** *and* ***Abdul Waheed****, whose unwavering support and sacrifices have been my greatest strength. To my brothers,* ***Faisal Junaid*** *and* ***Umar Waheed****, whose unwavering support and encouragement have been my strength throughout this journey. And to my dearest nephew,* ***Muhammad Azlan Umar****, whose laughter and playful mischief have filled my journey with endless smiles and warmth.*

CERTIFICATE OF APPROVAL

Scattering of Non-Axisymmetric Shell Radiation with Membrane Disc

by

Nabeela Waheed

(Registration No: MMT231016)

THESIS EXAMINING COMMITTEE

S. No.	Examiner	Name	Organization
(a)	External Examiner	Dr. Muhammad Ayub	QAU, Islamabad
(b)	Internal Examiner	Dr. Abdul Rehman Kashif	CUST, Islamabad
(c)	Supervisor	Dr. Muhammad Afzal	CUST, Islamabad

Dr. Muhammad Afzal
Thesis Supervisor
March 2025

Dr. Muhammad Sagheer
Head
Dept. of Mathematics
March 2025

Dr. M. Abdul Qadir
Dean
Faculty of Computing
March 2025

Author's Declaration

I, **Nabeela Waheed**, certify that my MPhil thesis titled "**Scattering of Non-axisymmetric Shell Radiation with Membrane Disc**" is entirely my own work and has not been submitted previously at Capital University of Science and Technology, Islamabad, or any other institution, either nationally or internationally, for the award of any degree.

If, at any stage, this declaration is found to be untrue, the University holds the authority to annul my MPhil degree.

(Nabeela Waheed)

Registration No: MMT231016

Plagiarism Undertaking

I hereby solemnly declare that the research presented in this thesis titled "**Scattering of Non-Axisymmetric Shell Radiation with Membrane Disc**", is entirely my own work, with no substantial contribution from any other individual. Any minor assistance or input received has been appropriately acknowledged, and the entire thesis has been written by me.

I am fully aware of the zero-tolerance policy regarding plagiarism upheld by both the HEC and Capital University of Science and Technology. As the author of this thesis, I affirm that no part of my work has been plagiarized, and all referenced material has been properly cited.

I understand that if any instance of formal plagiarism is detected in my thesis, even after the award of my MPhil degree, the University has the right to revoke my degree. Additionally, both the HEC and the University may publish my name on their websites, listing students whose work has been found to contain plagiarism.

(Nabeela Waheed)

Registration No: MMT231016

Acknowledgement

I am deeply grateful to **Almighty Allah**, the most merciful and benevolent, whose blessings are countless and ever-present. I also extend my sincere gratitude to **Prophet Muhammad (PBUH)**, the final messenger of **Almighty Allah**, the ultimate reformer of the world and a source of knowledge for humanity.

I wish to express my heartfelt thanks to everyone who supported and encouraged me throughout this journey. My deepest appreciation goes to my thesis supervisor, **Dr. Muhammad Afzal**, for his invaluable guidance and encouragement in completing this thesis. This work would not have been possible without his unwavering support.

I am sincerely grateful to all my **teachers** who have imparted knowledge and wisdom throughout my academic journey. Their dedication, support, and encouragement have been instrumental in shaping my academic and professional growth.

I am profoundly thankful to my **parents** for their constant prayers, moral support, and encouragement, which have been a constant source of strength for me.

Lastly, I would like to express my sincere gratitude to my **friends** who have helped and supported me throughout my MPhil journey.

(Nabeela Waheed)

Registration No: MMT231016

Abstract

This thesis investigates acoustic scattering in flexible cylindrical membrane shells, with a particular focus on non-axisymmetric transverse motion. The system consists of two flexible cylindrical shells, with one shell connected to a membrane disc, and both shells are placed in a surrounding fluid. The aim of this study is to explore the dynamic interaction between the flexible shells, membrane disc, and the surrounding fluid, specifically under non-axisymmetric excitation in transverse modes. The governing equations are developed based on the wave equation, Donnell-Mushtari theory for cylindrical shells, and the membrane equation, considering both dimensional and non-dimensional formulations. The membrane is modeled with a spring-like edge condition, representing a restoring force at its boundary, which plays a key role in the system's behavior. The research employs a mode-matching (MM) technique to analyze non-axisymmetric modes in transverse motion, focusing on both symmetric and anti-symmetric modes. This method is used to derive solutions for the displacement fields in the flexible shell and membrane system, accounting for the interaction with the surrounding fluid, represented by three velocity potential fluids. The edge conditions and boundary conditions are also considered in this framework. The findings provide important insights into the acoustic scattering phenomena within flexible shell systems, highlighting the role of non-axisymmetric transverse modes in wave propagation and fluid-structure interaction. The results are particularly valuable for understanding the dynamic behavior of flexible membranes and shells in applications related to acoustic scattering, vibration analysis, and fluid-structure interaction in various engineering domains.

Contents

List of Figures

Abbreviations

DM	Donnell-Mushtari
HVAC	Heating, Ventilation and Air Conditioning
MM	Mode-matching

Symbols

r_a	Non-dimensional radius of shell I
r_b	Non-dimensional radius of shell II
$\bar{r_a}$	Dimensional radius of shell I
$\bar{r_b}$	Dimensional radius of shell II
φ	Longitudinal displacement
ϑ	Circumferential displacement
Ω	Angular displacement
ϖ	Poisson's ratio for shell
k	Fluid wave number
γ	Scaling factor
ϱ_m	Membrane mass density
ϱ	Density of fluid
$\bar{\omega}$	Dimensional angular frequency
T	Membrane tension
P	Membrane pressure
c	Speed of sound
ϱ_s	Density of shell
$\bar{\chi_1}$	Fluid velocity potential of shell I
$\bar{\chi_2}$	Fluid velocity potential of shell 1I
ℓ	Indicator for incident forcing mode
h	Shell thickness
κ	Sound speed of the shell

Chapter 1

Introduction

In modern engineering, minimizing noise pollution is a critical objective due to its harmful effects on both humans and animals. Noise pollution is particularly significant in systems such as vehicle exhausts and HVAC (heating, ventilation, and air conditioning) systems, where unwanted sound and vibrations can cause discomfort and reduce efficiency.Vehicle exhaust systems are a major source of outdoor noise, driving research into innovative designs that reduce sound transmission and vibration. One common approach involves the use of silencers, which contain small perforations that redirect exhaust gases into a chamber. This design dissipates energy, reduces vibrations, and blocks noise before it exits the system, significantly lowering the environmental impact of vehicle noise.

Similarly, HVAC systems, which are essential for maintaining indoor air quality and comfort, also face noise-related challenges. These systems rely on ducts or waveguides to transport air for heating, cooling, and ventilation. However, noise generated by fans or external sources can propagate through the ducts, disrupting the indoor environment. While HVAC ducts are often rectangular, circular or cylindrical ducts are also widely used in specialized applications. The geometry of these ducts plays a crucial role in sound and vibration propagation. Changes in the size, shape, or material of these ducts can alter sound transmission characteristics, for instance [1–9]. By focusing on cylindrical structures, this research aims to provide deeper insights into how sound waves interact with such geometries, aiding

in the development of effective noise control measures for practical engineering applications.

Circular ducts, a fundamental form of waveguide, can be either rigid or flexible. A rigid circular duct does not absorb sound, and its walls remain fixed under acoustic excitation. In contrast, a flexible circular duct, often modeled as a flexible shell, deforms under pressure, leading to more complex acoustic interactions. Flexible shells are often combined with membrane discs at junctions of ducts or waveguides, where the flexible, vibrating membrane significantly influences sound propagation and energy dissipation [10–14].

A flexible shell, typically a thin, curved structure, is widely used in acoustic applications due to its ability to resonate and interact with sound waves. The displacement of the shell under acoustic loading plays a crucial role in fluid-structure interactions, affecting the system's acoustic behavior. Similarly, the membrane disc is a thin, circular structure that deforms in response to pressure or vibrations. When coupled with a flexible shell, it alters the flow of acoustic energy by affecting how sound waves are reflected, transmitted, or dissipated at junctions between different duct or waveguide sections. The interaction between the flexible shell and membrane disc is therefore a key factor in controlling acoustic scattering and wave behavior in cylindrical systems.

1.1 Literature Review

This thesis focuses on the interaction between a flexible shell and a membrane disc at the junction of cylindrical ducts. This system is analyzed using the Mode-Matching (MM) method, which facilitates the study of acoustic scattering and wave propagation. The MM method ensures the consistency of normal velocity and pressure at the junction of the flexible shell and membrane disc, allowing for accurate predictions of radiated energy. By understanding the acoustic behavior of such configurations, this research contributes to the broader goal of noise reduction in engineering systems, including vehicle exhausts and HVAC ducts. Cylindrical ducts, with their distinct wave propagation characteristics, provide an ideal model

for studying how structural flexibility and membrane interactions influence sound transmission. The study of sound propagation in cylindrical ducts has been an area of interest for many researchers. One of the earliest contributions was made by Miles [15], who investigated acoustic scattering in an infinite, rigid, cylindrical duct. His research focused on the propagation of plane waves and examined the effects of evanescent modes generated by an abrupt change in radius. By solving the boundary value problem for an analogous electrical system, Miles derived fundamental governing equations for acoustic propagation near a discontinuity and developed a systematic method to determine the reflected and transmitted coefficients. Shenderov [16] advanced the study of wave propagation by solving the Helmholtz equation for waveguides with impedance walls. His research explored the impact of eigenfunctions and characteristic roots on wave behavior, offering deeper insights into sound transmission in ducts with complex boundary conditions.

Further developments were made by Cummings [17], who examined sound propagation in cylindrical ducts with sudden expansions. His research analyzed different velocity profiles to predict sound reflection and provided insights into wave interactions at expansion junctions. Similarly, Homentcovschi and Miles [18] studied wave scattering at points where rigid cylindrical ducts changed size, focusing on the impact of expansion chambers on sound transmission and reflection.

Lawrie and Abrahams [19] studied the effects of size variations and gaps on sound propagation in cylindrical ducts. Lawrie [20] further examined the influence of flexible shells bonded to cylindrical structures on their acoustic and structural response. They applied MM technique with generalized orthogonality relations to solve their problem. Their adopted technique has been followed to many authors to solve structural discontinuitiesinvolving problems [21–30] bifurcated problems and trifuracted waveguide problems [31–33]. Leissa [34] compared various theoretical approaches for modeling vibrations in cylindrical shells and analyzed their effects on sound propagation. Munjal and Prasad [35] conducted a transfer matrix analysis to study sound propagation in rigid cylindrical ducts with hot mean flow,

modeling the effects of temperature variations and flow velocity on wave transmission and reflection. Their findings improved the understanding of acoustic behavior in high-temperature environments like exhaust systems and aeroengine ducts.

Munjal [36] analyzed acoustic wave behavior in ducts and cylindrical shells, offering critical insights into wave propagation and noise reduction in silencers. His work, which involves flexible cylindrical shells, is relevant for understanding how membrane discs and flexible shells influence sound attenuation. This research builds upon Munjal's foundational contributions to modeling sound transmission and scattering in flexible waveguides.

Peat [37–39] refined theoretical models for higher-order modes, enhancing the understanding of acoustic wave behavior in cylindrical ducts and silencers.

In the early 21st century, research increasingly focused on fluid-structure interactions. Pullen [40] advanced modal analysis in cylindrical shells, providing key insights into acoustic scattering and laying the foundation for the fluid-structure interaction modeling in this thesis. Shafique et al. [3] conducted a mode-matching analysis of fluid-structure coupled wave scattering between two flexible waveguides. Their study provided valuable insights into wave transmission and reflection in elastic waveguides, contributing to the understanding of acoustic interactions in flexible structures. Recent studies have continued to refine the understanding of wave propagation, scattering, and fluid-structure interactions in cylindrical shells and waveguide structures. Several important contributions in this field provide insights directly relevant to [41–50] the focus of this thesis, which investigates the interaction between flexible shells, membrane discs, and surrounding fluids. Nazarov and Kamenetsky [51] explored acoustic wave scattering by a circular membrane within a cylindrical shell. Their study provides valuable insights into wave interactions with thin membranes, which is critical for understanding the role of membrane discs in this research. By analyzing wave behavior at junctions between cylindrical shells and waveguides, their work lays a foundation for the acoustic modeling developed in this thesis.

Lee [52] developed a comprehensive theory on elastic wave propagation in cylindrical shells, focusing on their interaction with surrounding fluids. His study is essential for understanding fluid-structure interactions in this thesis, particularly regarding the acoustic behavior of flexible cylindrical shells. The theoretical models he proposed enhance the accuracy of wave propagation predictions in flexible shell systems. Raju [53] conducted a detailed analysis of wave scattering in cylindrical shells using the MM method, with a focus on wave interactions with thin membranes. His work is directly applicable to this research, as the MM method is a key technique for analyzing wave scattering in cylindrical waveguides. By refining the MM method with more complex boundary conditions, Raju provides a more precise framework for modeling the interaction between flexible shells and membrane discs.

Mitchell et al. [54] investigated the acoustic behavior of flexible shells and membranes, developing a theoretical framework to describe their interaction with acoustic waves. Their findings provide crucial insights into wave propagation in flexible structures, which directly relate to the study of flexible shells and membrane discs in this thesis. The models they introduced contribute to a deeper understanding of acoustic wave behavior in cylindrical systems. Lawrie and Abrahams [55] established an orthogonality relation for problems involving high-order boundary conditions, which has significant applications in sound-structure interactions. Their work provides a mathematical foundation for analyzing wave behavior in coupled systems, particularly in cylindrical geometries with complex boundary conditions. This orthogonality relation is relevant to the mode-matching approach used in this thesis to study wave scattering in flexible shells. Afzal et al. [56] analyzed the impact of flexible shells and sound-absorbent linings on acoustic wave behavior in ducts. Their study provides valuable insights into how flexible structures influence sound propagation and attenuation in waveguides.

Yaseen and Nawaz [57] investigated acoustic radiation through a flexible shell in a bifurcated circular waveguide, contributing to the understanding of wave interactions in complex duct systems. Their findings are relevant to the study of wave scattering in cylindrical waveguides with membrane interfaces.

1.2 Thesis Contribution

This thesis contributes to the field of acoustic scattering and wave propagation in flexible membrane discs and cylindrical shells through several key advancements. First, a novel MM method is introduced to analyze wave propagation at the interface between flexible cylindrical shells and membrane discs. This method, grounded in generalized orthogonality relation, simplifies the governing equations and reduces computational complexity, offering an efficient approach to study wave interaction with flexible structures. Furthermore, this research presents a new approach to understanding the interaction of waves or pistons at the interface between flexible membrane discs and cylindrical shells. The study provides valuable insights into the dynamics of this interface and the wave propagation between the flexible shell and the membrane disc.

The governing equations for both the fluid and the shell-membrane system are derived, leading to the establishment of a dispersion relation that defines the velocity potential and wavenumbers for each section of the waveguide. This formulation contributes to a better understanding of wave behavior and dynamics within the system. Finally, the MM method is applied at the junction between the shell and membrane to ensure continuity of normal velocity and pressure. This allows for an accurate analysis of how waves reflect and transmit, further enhancing the understanding of their interactions in the coupled fluid-structure system.

1.3 Objectives

This thesis aims to investigate the energy emitted by a wave or piston at the interface of membrane discs and flexible circular cylindrical shells. The interaction between the flexible shell and the membrane disc results in energy radiation and wave propagation, where the membrane disc plays a crucial role in understanding the system's vibrations and acoustics. Specifically, this study analyzes the energy release at the interface between the membrane disc and the shell. To achieve this, a MM method based on generalized orthogonality relations is developed and

implemented to simplify the governing equations. Furthermore, the fundamental equations governing fluid motion and waveguide dynamics are derived to establish the dispersion relation. The MM method is also applied to ensure the continuity of normal velocity and pressure at the junction. Finally, the radiated energy is computed using the derived energy expressions under harmonic time dependence.

1.4 Thesis Layout

This thesis is further composed of the following chapter:

•**Chapter 2** introduces essential definitions and key concepts that form the basis for the entire thesis. It also discusses the boundary conditions that govern the system's behavior, particularly in relation to the flexible cylindrical shells and membrane discs. This chapter ensures that the reader has a solid understanding of the foundational terms and conditions that will be used in the mathematical formulations in later chapters.

Chapter 3 develops the mathematical framework for analyzing flexible shell–membrane disc interactions. It derives the orthogonality relation, applies the MM method to enforce velocity and pressure continuity, and uses the Galerkin approach for non-axisymmetric transverse motion. The theoretical models introduced here form the foundation for subsequent chapters.

•**Chapter 4** presents the results of the analysis and the corresponding discussions. It focuses on the calculation of reflected and transmitted amplitudes using the MM method. The chapter also explores the symmetric and anti-symmetric modes and their impact on wave transmission in flexible cylindrical shells and membrane discs. The results are analyzed, with a detailed discussion on their implications for noise reduction and wave behavior.

•**Chapter 5** summarizes the key findings, highlighting the contribution to understanding wave propagation and fluid-structure interactions in cylindrical systems. The study emphasizes the role of flexible shells and membrane discs in controlling acoustic behavior and their impact on wave scattering and radiation. The use

of MM techniques and the analysis of non-axisymmetric modes provide valuable insights into the dynamic behavior of these systems.

The references cited in this chapter are compiled and listed in the bibliography section.

Chapter 2

Preliminaries

This chapter introduces the fundamental concepts and governing equations necessary for the understanding of the thesis. It provides an overview of acoustics, the wave equation, boundary conditions, the Galerkin method, orthogonality relations, and other essential concepts relevant to the study of acoustic scattering in cylindrical membrane shells.

2.1 Acoustic Fundamentals

Acoustics, derived from the Greek word *akouein* meaning "to hear," is the scientific study of sound. Initially, acoustics was concerned with audible pressure waves, but it has since enlarge to include both subsonic (infrasound) and ultrasonic waves. Acoustics is now a branch of physics that explores mechanical vibrations over a broad range of frequencies, including those outside the hearing range of humans.

In this thesis, the focus is primarily on structural acoustics, particularly the way flexible structures such as cylindrical shells and membrane discs interact with sound waves. The behavior of these structures under acoustic excitation is of primary interest, as they exhibit unique responses due to their flexible nature. Specifically, this study delves into the phenomenon of acoustic scattering caused by membrane discs placed within cylindrical shells. Here, the complex interaction between acoustic waves and the structure is examined, particularly with regard to

how these membranes deform under acoustic pressures, affecting the transmission and reflection of sound.

The primary objective is to understand the nature of acoustic wave interaction with flexible membrane discs and cylindrical shells, exploring both the wave propagation and the resulting structural deformations. This interaction is crucial for applications in areas such as noise control, vibration analysis, and the design of acoustic chambers or devices where sound-wave interactions with materials play a pivotal role.

2.2 Acoustic Wave Equation

The propagation of acoustic waves is governed by a differential equation derived from basic conservation laws, including the conservation of mass, momentum, and energy. Though the resulting equations are inherently nonlinear, linear approximations are often employed for simplicity. This section derives the linear acoustic wave equation.

2.2.1 Conservation of Mass

The conservation of mass for a fluid is expressed as:

$$\frac{\partial \varrho}{\partial t} + \nabla \cdot (\varrho \mathbf{v}) = 0, \tag{2.1}$$

where ϱ is the fluid density, $\mathbf{v}$ is the velocity vector.

For small perturbations induced by acoustic waves, the physical quantities are approximated as:

$$\varrho = \varrho_0 + \varrho', \quad \mathbf{v} = \mathbf{v}', \quad \varrho' \ll \varrho_0,$$

where ϱ_0 is the equilibrium (mean) density, ϱ' is the small perturbation in density, $\mathbf{v}'$ is the perturbation in velocity. Substituting these into the continuity equation

and neglecting higher-order terms yields:

$$\frac{\partial \varrho'}{\partial t} + \varrho_0 \nabla \cdot \mathbf{v}' = 0. \tag{2.2}$$

2.2.2 Conservation of Momentum

The conservation of momentum for an inviscid fluid is given by Euler's equation:

$$\varrho \frac{\partial \mathbf{v}}{\partial t} + \varrho(\mathbf{v} \cdot \nabla)\mathbf{v} = -\nabla p, \tag{2.3}$$

where p is the pressure. For small perturbations, we have:

$$\varrho = \varrho_0 + \varrho', \quad \mathbf{v} = \mathbf{v}', \quad p = p_0 + p', \quad p' \ll p_0,$$

where p_0 is the equilibrium pressure, p' is the small perturbation in pressure. Substituting these into Euler's equation and neglecting higher-order terms gives:

$$\varrho_0 \frac{\partial \mathbf{v}'}{\partial t} = -\nabla p'. \tag{2.4}$$

2.2.3 Equation of State

For a compressible fluid, the relationship between pressure p and density ϱ is defined by the equation of state. Under adiabatic conditions and for small perturbations:

$$p' = c^2 \varrho', \tag{2.5}$$

where c is the speed of sound in the medium.

2.2.4 Combining the Equations

From the continuity equation (2.2):

$$\frac{\partial \varrho'}{\partial t} = -\varrho_0 \nabla \cdot \mathbf{v}'. \tag{2.6}$$

Substituting $\varrho' = \frac{p'}{c^2}$ (from the equation of state):

$$\frac{\partial}{\partial t}\left(\frac{p'}{c^2}\right) = -\varrho_0 \nabla \cdot \mathbf{v}'. \tag{2.7}$$

Simplifying, we get:

$$\frac{\partial p'}{\partial t} = -\varrho_0 c^2 \nabla \cdot \mathbf{v}'. \tag{2.8}$$

From the momentum equation (2.4):

$$\frac{\partial \mathbf{v}'}{\partial t} = -\frac{1}{\varrho_0}\nabla p'. \tag{2.9}$$

Taking the divergence of both sides:

$$\nabla \cdot \frac{\partial \mathbf{v}'}{\partial t} = -\frac{1}{\varrho_0}\nabla^2 p'. \tag{2.10}$$

Using $\frac{\partial}{\partial t}(\nabla \cdot \mathbf{v}')$ from equation (2.8):

$$\nabla^2 p' = \frac{\varrho_0}{c^2}\frac{\partial^2 p'}{\partial t^2}. \tag{2.11}$$

2.2.5 Wave Equation

Rearranging the equation gives the wave equation for the pressure perturbation p':

$$\nabla^2 p' - \frac{1}{c^2}\frac{\partial^2 p'}{\partial t^2} = 0. \tag{2.12}$$

2.3 Boundary Conditions

The following boundary conditions are used to model the boundary value problem (BVP):

1. Soft boundary conditions,

2. Rigid boundary conditions,

3. Impedance boundary conditions,

4. Clamped edge conditions.

2.3.1 Soft Conditions

Soft boundary conditions are Dirichlet-type, where the pressure or displacement is assumed to be zero:

$$\psi(x, y) = 0. \tag{2.13}$$

2.3.2 Rigid Conditions

Rigid boundary conditions are Neumann-type, where the normal velocity is assumed to be zero:

$$\frac{\partial \psi}{\partial x} = 0. \tag{2.14}$$

2.3.3 Impedance Conditions

Impedance boundary conditions are Robin-type, combining both Dirichlet and Neumann conditions. These are expressed as:

$$\beta_1 \psi(x, y) + \beta_2 \frac{\partial \psi(x, y)}{\partial x} = 0, \tag{2.15}$$

where β_1 and β_2 are constants.

2.3.4 Clamped Edge Conditions

For a cylindrical shell with displacements φ (axial), ϑ (circumferential), and w (radial), the clamped edge conditions at $z = 0$ and $z = z_0$ are:

1. No displacement (fixed edges):

$$\varphi = 0, \quad \vartheta = 0, \quad \Omega = 0.$$

2. No slope (no rotation):

$$\frac{\partial \varphi}{\partial z} = 0, \quad \frac{\partial \vartheta}{\partial z} = 0, \quad \frac{\partial \Omega}{\partial z} = 0.$$

These conditions ensure that the edges of the shell are fully constrained with no motion or rotation.

2.4 Types of Motion

2.4.1 Transverse Motion

Transverse motion refers to the displacement of a structure perpendicular to its surface, such as the radial displacement of a membrane or shell under acoustic pressure. This motion plays a crucial role in the scattering of sound waves, as it directly influences how the structure deforms in response to acoustic pressure. In cylindrical shells, transverse motion can be axisymmetric or non-axisymmetric, depending on whether the deformation is uniform along the circumference or varies with angular position.

2.4.2 Longitudinal Motion

Longitudinal motion involves displacements along the axis of the structure, such as the axial displacement of a cylindrical shell. While it does not contribute directly to the acoustic scattering in this study, it is important for the overall structural dynamics of the system. Longitudinal motion interacts with transverse motion, particularly in coupled systems where the displacements are interdependent.

2.4.3 Axisymmetric Motion

Axisymmetric motion refers to the type of motion in which the displacement or deformation of a structure is independent of the angular coordinate around the

axis of symmetry. In the context of cylindrical shells or membranes, axisymmetric motion occurs when the physical properties and displacements of the system are invariant in the angular direction, meaning that they only depend on the radial distance and axial position. This type of motion is typically observed in systems where the excitation or disturbance is uniformly distributed around the circumference, leading to a symmetric response across all angles.

2.4.4 Non-Axisymmetric Motion

Non-axisymmetric motion refers to deformations that vary with both radial and angular positions along the circumference of the structure. In the case of a cylindrical shell or membrane disc, this type of motion introduces additional complexity, as it involves modes that are not symmetric about the axis of rotation. Non-axisymmetric modes are crucial for understanding the scattering behavior of the structure under non-uniform acoustic excitations and are often more complex to model compared to axisymmetric modes.

2.5 Galerkin Approach

The Galerkin method is a powerful tool for solving differential equations, particularly in the context of boundary value problems. In this method, the solution is approximated by a weighted sum of basis functions that satisfy the boundary conditions. The key idea is to multiply the governing equation by a test function (often the same as the trial function) and integrate over the domain, leading to a system of algebraic equations that approximate the solution. For acoustic scattering in cylindrical membrane shells, the Galerkin method is used to approximate the displacement of the membrane and the shell. The displacement functions are chosen to satisfy the boundary conditions and to capture the essential behavior of the system.The resulting system of equations can then be resolved using the Galerkin method to provide a way to calculate the amplitudes of transmitted and reflected waves.

2.6 Basic Definitions

2.6.1 Waveguides

Waveguides are structures that direct waves, such as sound or electromagnetic waves, and are characterized by their geometry and material properties. In this thesis, waveguides refer to the cylindrical shells and membrane discs, which serve as the primary medium for acoustic wave propagation.

2.6.2 Amplitude

The amplitude of a vibrating body is the maximum displacement from its equilibrium position.

2.6.3 Time Period

The time period of a vibrating body is the time taken to complete one full cycle of motion. It is denoted by T and is given by:

$$T = \frac{2\pi}{\omega}, \tag{2.16}$$

where ω is the angular frequency of vibration.

2.7 Mode-Matching Scheme

The Mode-Matching (MM) technique is a widely used analytical approach for studying wave behavior in waveguides, particularly in systems with structural discontinuities and varying impedance distributions. This method is highly effective in handling complex boundary conditions by dividing the structure into segments and expressing the field potentials within each segment in terms of unknown amplitudes. These amplitudes are then determined by enforcing the continuity of

pressure and velocity at the interfaces, converting the governing differential equations into a solvable algebraic system. Due to its accuracy and adaptability, the MM technique is extensively applied in various engineering fields, including acoustics, structural mechanics, and fluid dynamics. In industries such as automotive engineering and HVAC systems, where controlling vibrational energy and minimizing noise is crucial, MM provides an efficient tool for analyzing and optimizing wave propagation. The technique allows for a systematic study of wave interactions in duct-like structures, enabling better design strategies for noise reduction. This thesis employs the MM method to investigate wave propagation through cylindrical shells with membrane disc interfaces. The method's ability to handle discontinuities makes it particularly suitable for analyzing the scattering, transmission, and reflection of waves in the given system. The practical implementation and effectiveness of this approach are further explored in Chapters 3 and 4.

Chapter 3

Non-Axisymmetric Radiation in Infinite Waveguide with Bridging membrane Disc

This chapter examines the propagation of waves in thin, circular, cylindrical, flexible shells undergoing non-axisymmetric motion. By incorporating the DM equations for the flexible shell with the wave equation, the dispersion relation is derived. Using this dispersion relation, a generalized orthogonality condition is formulated for the eigenfunctions associated with the non-axisymmetric motion of the flexible shell. The wave mode amplitudes for selected prototype problems are obtained by applying this orthogonality relation through the MM technique. The chapter introduces a novel generalized orthoganality relation for flexible shells, derived from the DM equations of motion. The methods and formulations presented here contribute to a deeper understanding of wave propagation in flexible cylindrical shells subjected to non-axisymmetric disturbances. This chapter formulates the problem by presenting the governing equations in both dimensional and nondimensional forms. It details the mode-matching solution, including eigenfunction expansion, the Galerkin approach for membrane responses, and matching conditions. Numerical results analyze eigenfunctions, mode amplitudes, and their interpretations for specific cases.

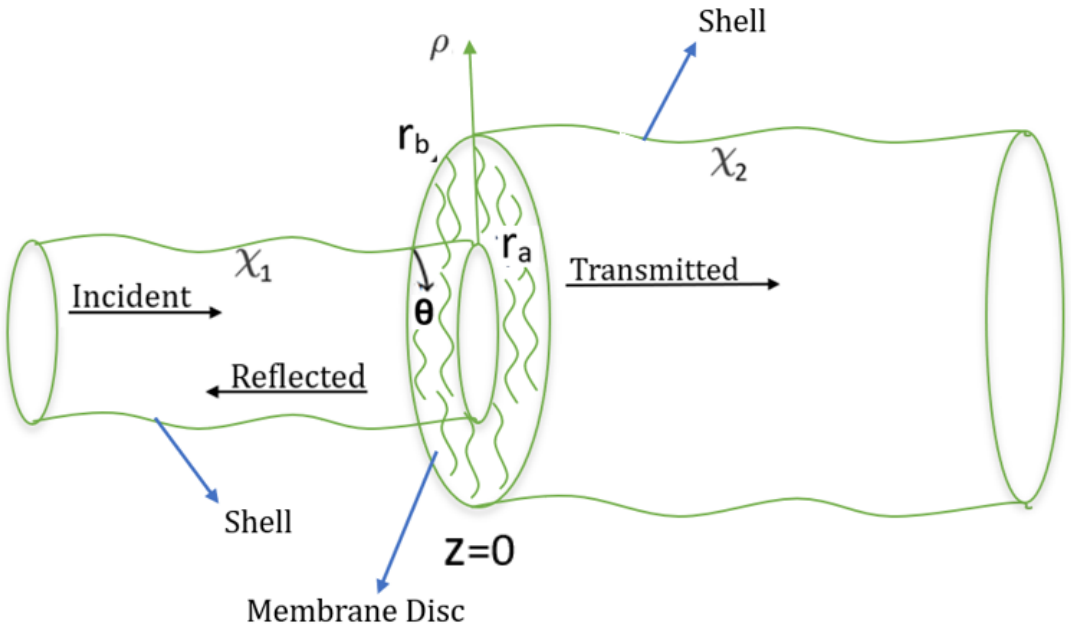

FIGURE 3.1: Configuration of the flexible shells and the membrane disc

3.1 Problem Formulation

In this section, we explore a thin, flexible cylindrical shell connected to a membrane disc. The system consists of two extended cylindrical shells. The left shell lies within the region $0 \leq \bar{\rho} \leq \bar{r_a}, \quad \bar{z} \leq 0$, where it interacts with a fluid having the velocity potential $\bar{\chi}_1$. Likewise, the right shell extends over the section $0 \leq \bar{\rho} \leq \bar{r_b}, \quad \bar{z} > 0$, where the fluid is associated with the velocity potential $\bar{\chi}_2$. These fluid velocity potentials, $\bar{\chi}_1$ and $\bar{\chi}_2$, are defined as a piecewise function, as shown in Figure 3.1.

$$\bar{\chi}(\bar{\rho}, \bar{z}) = \begin{cases} \bar{\chi}_1(\bar{\rho}, \bar{z}), & \text{for } \bar{z} \leq 0, \\ \bar{\chi}_2(\bar{\rho}, \bar{z}), & \text{for } \bar{z} > 0. \end{cases}$$

At $\bar{z} = 0$, a membrane disc spans the radial range $\bar{r_a} < \bar{\rho} < \bar{r_b}$, influencing the interaction between the shells and the surrounding fluid. A wave traveling in the positive $\bar{z}$-direction generates the forcing at the shell boundary. This section derives the dimensional and non-dimensional forms of key equations, including the wave equation, Donnell-Mushtari equations, membrane equation, and edge conditions. The membrane equation characterizes the disc's radial displacement and its interaction with the fluid and shells. The flexible shell's motion is described by

three displacement parameters: longitudinal ($\bar{\varphi}$), circumferential ($\bar{\vartheta}$), and angular ($\bar{\Omega}$), representing shell deformation under external forces and fluid effects. This chapter establishes the foundation for understanding shell-membrane interactions and analyzing different motion modes. The wave equation describes acoustic wave propagation in the cylindrical shell and is given by:

$$\left\{ \frac{\partial^2}{\partial \bar{\rho}^2} + \frac{1}{\bar{\rho}} \frac{\partial}{\partial \bar{\rho}} + \frac{1}{\bar{\rho}^2} \frac{\partial^2}{\partial \bar{\theta}^2} + \frac{\partial^2}{\partial \bar{z}^2} + k^2 \right\} \bar{\chi}(\bar{\rho}, \bar{\theta}, \bar{z}) = 0, \tag{3.1}$$

where $\bar{\rho}, \bar{\theta}, \bar{z}$ denote the radial, angular, and axial coordinates, respectively, and $\bar{\chi}$ represents the fluid velocity potential.

The behavior of a thin cylindrical shell, which supports energy propagation, is governed by the Donnell-Mushtari (DM) equations, assuming small displacements and a thin structure. For a shell of radius $\bar{r_a}$, thickness h, and density ϱ_s, the governing equations at $\bar{\rho} = \bar{r_a}$ are:

$$\frac{\partial^2 \bar{\varphi}}{\partial \bar{z}^2} + \frac{1-\varpi}{2\bar{r_a}^2} \frac{\partial^2 \bar{\varphi}}{\partial \bar{\theta}^2} + \frac{1+\varpi}{2\bar{r_a}} \frac{\partial^2 \bar{\vartheta}}{\partial \bar{z} \partial \bar{\theta}} + \frac{i\varpi}{\bar{r_a}} \frac{\partial^2 \bar{\chi}}{\partial \bar{\rho} \partial \bar{z}} + \beta^2 \bar{\varphi} = 0, \tag{3.2}$$

$$\frac{1+\varpi}{2\bar{r_a}} \frac{\partial^2 \bar{\varphi}}{\partial \bar{z} \partial \bar{\theta}} + \frac{1-\varpi}{2} \frac{\partial^2 \bar{\vartheta}}{\partial \bar{z}^2} + \frac{1}{\bar{r_a}^2} \frac{\partial^2 \bar{\vartheta}}{\partial \bar{\theta}^2} + \frac{i}{\bar{r_a}^2} \frac{\partial^2 \bar{\chi}}{\partial \bar{\rho} \partial \bar{z}} + \beta^2 \bar{\vartheta} = 0, \tag{3.3}$$

$$\begin{aligned} -i\varpi \bar{r_a} \frac{\partial \bar{\varphi}}{\partial \bar{z}} - i \frac{\partial \bar{\vartheta}}{\partial \bar{\theta}} + \frac{\partial \bar{\chi}}{\partial \bar{\rho}} + \frac{1}{\tau_1} \frac{\partial^5 \bar{\chi}}{\partial \bar{\rho} \partial \bar{z}^4} + \frac{2}{\tau_1 \bar{r_a}^2} \frac{\partial^5 \bar{\chi}}{\partial \bar{\rho} \partial \bar{z}^2 \partial \bar{\theta}^2} + \frac{1}{\tau_1 \bar{r_a}^4} \frac{\partial^5 \bar{\chi}}{\partial \bar{\rho} \partial \bar{\theta}^4} \\ -\bar{r_a}^2 \beta^2 \frac{\partial \bar{\chi}}{\partial \bar{\rho}} - \frac{\bar{r_a}^2 \beta^2 \varrho}{\varrho_s h k} \bar{\chi} = 0, \end{aligned} \tag{3.4}$$

where $\beta = \dfrac{\bar{\omega}}{c_s k}$ and $\tau_1 = \dfrac{12}{k^2 h^2 \bar{r_a}^2}$.

To ensure the physical consistency of the system, the following boundary conditions are applied at the edges, which will be incorporated into the DM equation:

$$\bar{\varphi}_1 = \bar{\vartheta}_1 = \frac{\partial \bar{\chi}_1}{\partial \bar{\rho}} = \frac{\partial^2 \bar{\chi}_1}{\partial \bar{\rho} \partial \bar{z}} = 0, \quad 0 < \bar{\rho} < \bar{r_a}, \quad \bar{z} < 0. \tag{3.5}$$

$$\bar{\varphi}_2 = \bar{\vartheta}_2 = \frac{\partial \bar{\chi}_2}{\partial \bar{\rho}} = \frac{\partial^2 \bar{\chi}_2}{\partial \bar{\rho} \partial \bar{z}} = 0, \quad 0 < \bar{\rho} < \bar{r_b}, \quad \bar{z} \geq 0. \tag{3.6}$$

Further at $\bar{z} = 0$, there is a membrane disc that extends over the radial region $\bar{r_a} < \bar{\rho} < \bar{r_b}$. This membrane plays a key role in the interaction between the

flexible cylindrical shells and the surrounding fluid. The membrane's displacement is described by the membrane equation, which accounts for the deformation of the disc due to external forces such as pressure and tension. The membrane equation is given by:

$$T\left(\frac{\partial^2}{\partial\bar{\rho}^2}+\frac{1}{\bar{\rho}}\frac{\partial}{\partial\bar{\rho}}+\frac{1}{\bar{\rho}^2}\frac{\partial^2}{\partial\bar{\theta}^2}\right)\bar{U}(\bar{\rho},\bar{\theta})-\varrho_m\omega^2\bar{U}=\bar{P}_2-\bar{P}_1. \tag{3.7}$$

In this equation, $\bar{U}(\bar{\rho},\bar{\theta})$ represents the displacement of the membrane in the z-direction, which depends on the radial coordinate $\bar{\rho}$ and the angular coordinate $\bar{\theta}$. $\bar{P}(\bar{\rho},\bar{\theta})$ is the pressure applied to the membrane, with $\bar{P}_1$ and $\bar{P}_2$ being the pressures acting on the membrane. T is the tension in the membrane, and ϱ_m represents the mass density of the membrane. $\bar{\omega}$ is the dimensional angular frequency. The first two terms on the left-hand side describe the changes in displacement due to the radial and angular directions, while the last term represents the effect of the inertial forces (due to membrane mass) and the pressure difference acting on the membrane. In this study, the membrane equation will be used to model the behavior of the disc at $\bar{z}=0$, considering the interaction between the fluid and the flexible shells. This equation is important for understanding how the system behaves under different forces and fluid conditions. The boundary conditions at $\bar{\rho}=\bar{r_a}$ describe the behavior of the membrane at its edge. These conditions are crucial for solving the membrane equation and modeling the system's response under different edge constraints.

Boundary Conditions

1. Fixed Edge Condition (Clamped Edge): At a fixed edge, both the displacement and the slope (derivative) of the membrane are constrained to zero. This implies that the membrane cannot move or rotate at the edge.

$$\bar{U}(\bar{r_a},\bar{\theta})=0,\quad \frac{\partial\bar{U}}{\partial\bar{\rho}}(\bar{r_a},\bar{\theta})=0.$$

2. Free Edge Condition: A free edge means that the membrane is unconstrained, and no force acts on the edge. The displacement at the edge is free

to vary, but the radial derivative (slope) is related to the tension in the membrane. This condition follows from the membrane theory, which assumes that in the absence of external forces or constraints, the membrane's natural response is governed by equilibrium equations in the absence of bending rigidity.

$$\frac{\partial^2 \bar{U}}{\partial \bar{\rho}^2}(\bar{r_a}, \bar{\theta}) + \frac{1}{\bar{r_a}} \frac{\partial \bar{U}}{\partial \bar{\rho}}(\bar{r_a}, \bar{\theta}) = 0, \quad \frac{\partial^2 \bar{U}}{\partial \bar{\theta}^2}(\bar{r_a}, \bar{\theta}) = 0.$$

3. Spring-Like Edge Condition: A spring-like edge models a scenario where the displacement at the boundary is proportional to the restoring force, similar to a spring. This condition is used when the membrane is connected to a spring or elastic material that applies a restoring force at the edge.

$$T \frac{\partial \bar{U}}{\partial \bar{\rho}}(\bar{r_a}, \bar{\theta}) = k \bar{U}(\bar{r_a}, \bar{\theta}).$$

These boundary conditions describe different physical constraints on the membrane at $\bar{\rho} = \bar{r_a}$ and will be used to solve the governing equations for the system, helping to determine the behavior of the membrane under various conditions. As previously defined, the same edge conditions will also apply to region II, where $0 < \bar{\rho} < \bar{r_b}$ and $\bar{z} > 0$. The wave equation in non-dimensional form is expressed as:

$$\left\{ \frac{\partial^2}{\partial \rho^2} + \frac{1}{\rho} \frac{\partial}{\partial \rho} + \frac{1}{\rho^2} \frac{\partial^2}{\partial \theta^2} + \frac{\partial^2}{\partial z^2} + k^2 \right\} \chi(\rho, \theta, z) = 0. \tag{3.8}$$

This section presents the DM equations in non-dimensional form, as described by Junger and Feit [58]. These equations describe a flexible shell, assuming negligible displacements relative to its thickness. Furthermore, the shell's thickness is assumed to be much smaller than its radius. The DM equations for a cylindrical shell are:

$$\frac{\partial^2 \varphi}{\partial z^2} + \frac{1 - \varpi}{2 r_a^2} \frac{\partial^2 \varphi}{\partial \theta^2} + \frac{1 + \varpi}{2 r_a} \frac{\partial^2 \vartheta}{\partial z \partial \theta} + \frac{i \varpi}{r_a} \frac{\partial^2 \chi}{\partial \rho \partial z} + \beta^2 \varphi = 0, \tag{3.9}$$

$$\frac{1 + \varpi}{2 r_a} \frac{\partial^2 \varphi}{\partial z \partial \theta} + \frac{1 - \varpi}{2} \frac{\partial^2 \vartheta}{\partial z^2} + \frac{1}{r_a^2} \frac{\partial^2 \vartheta}{\partial \theta^2} + \frac{i}{r_a^2} \frac{\partial^2 \chi}{\partial \rho \partial z} + \beta^2 \vartheta = 0, \tag{3.10}$$

$$-i\varpi r_a\frac{\partial\varphi}{\partial z}-i\frac{\partial\vartheta}{\partial\theta}+\frac{\partial\chi}{\partial\rho}+\frac{1}{\tau_1}\frac{\partial^5\chi}{\partial\rho\partial z^4}+\frac{2}{\tau_1 r_a^2}\frac{\partial^5\chi}{\partial\rho\partial z^2\partial\theta^2}+\frac{1}{\tau_1 r_a^4}\frac{\partial^5\chi}{\partial\rho\partial\theta^4} \\ -r_a^2\beta^2\frac{\partial\chi}{\partial\rho}\ -\frac{r_a^2\beta^2\varrho}{\varrho_s hk}\chi=0. \tag{3.11}$$

At the edges, the boundary conditions are as follows:

$$\varphi_1=\vartheta_1=\frac{\partial\chi_1}{\partial\rho}=\frac{\partial^2\chi_1}{\partial\rho\partial z}=0,\quad 0\le\rho\le r_a,\quad z<0. \tag{3.12}$$

$$\varphi_2=\vartheta_2=\frac{\partial\chi_2}{\partial\rho}=\frac{\partial^2\chi_2}{\partial\rho\partial z}=0,\quad 0\le\rho\le r_b,\quad z>0. \tag{3.13}$$

In the non-dimensional form, the membrane disc located at $z=0$ spans the radial region $r_a<\rho<r_b$. This membrane facilitates the interaction between the flexible cylindrical shells and the surrounding fluid. The displacement of the membrane is governed by the non-dimensional membrane equation, which incorporates the effects of external forces such as pressure and tension on the deformation of the disc. The non-dimensional membrane equation is expressed as:

$$\left(\frac{\partial^2}{\partial\rho^2}+\frac{1}{\rho}\frac{\partial}{\partial\rho}+\frac{1}{\rho^2}\frac{\partial^2}{\partial\theta^2}+\mu^2\right)U(\rho,\theta)=\gamma\chi_2, \tag{3.14}$$

where$\mu^2=\dfrac{\varrho\omega^2}{K^2T}$, $\gamma=\dfrac{i\omega\varrho_m}{TK}$. This non-dimensional form of the equation will be employed to analyze the dynamic behavior of the disc at $z=0$ in relation to the interaction between the fluid and the flexible shells.

The edge conditions for the membrane disc are as follows: At a clamped edge, both the displacement and the slope are zero:

$$U(r_a,\theta)=0,\quad \frac{\partial U}{\partial\rho}(r_a,\theta)=0.$$

At a free edge, the net force and moment must vanish, leading to the following conditions:

$$\frac{\partial^2U}{\partial\rho^2}(r_a,\theta)+\frac{1}{r_a}\frac{\partial U}{\partial\rho}(r_a,\theta)=0,\quad \frac{\partial^2U}{\partial\theta^2}(r_a,\theta)=0.$$

A spring-like edge means the boundary displacement is proportional to the restoring force, like a spring. This happens when the membrane is connected to a spring

or elastic material at the edge.

$$T\frac{\partial U}{\partial \rho}(r_a, \theta) = kU(r_a, \theta).$$

The same edge conditions will also apply to region $0 < \rho < r_b$ and $z > 0$.

3.2 Mode Matching Solutions

A thin and flexible cylindrical shell is studied using cylindrical polar coordinates (ρ, θ, z). Inside the shell, there is a compressible fluid with density ϱ and a speed of sound c, while the outside is assumed to be a vacuum. To simplify the analysis, a time-dependent factor of $e^{-i\omega t}$ is used, where t denotes time and $\omega = ck$, with k representing the wave number. The non-dimensional Helmholtz equation governs the motion of the internal fluid:

$$\left\{\frac{\partial^2}{\partial \rho^2} + \frac{1}{\rho}\frac{\partial}{\partial \rho} + \frac{1}{\rho^2}\frac{\partial^2}{\partial \theta^2} + \frac{\partial^2}{\partial z^2} + 1\right\}\chi = 0, \tag{3.15}$$

where χ represents the velocity potential of the fluid. We use the separation of variables method to solve this. The expression for $\chi(\rho, \theta, z)$ is represented as:

$$\chi(\rho, \theta, z) = R(\rho)\Theta(\theta)Z(z). \tag{3.16}$$

By substituting this form into equation (3.15) and multiplying through by $\frac{\rho^2}{R\Theta Z}$, the equation separates into:

$$\frac{\rho^2 R''(\rho)}{R(\rho)} + \frac{\rho R'(\rho)}{R(\rho)} + \frac{\Theta''(\theta)}{\Theta(\theta)} + \frac{\rho^2 Z''(z)}{Z(z)} + \rho^2 = 0. \tag{3.17}$$

To ensure periodicity in θ, the terms involving Θ require a negative separation constant, resulting in the equation:

$$\frac{\Theta''(\theta)}{\Theta(\theta)} = -p^2, \tag{3.18}$$

where p represents the separation constant. The solution to this equation is:

$$\Theta(\theta) = c_1 \cos(p\theta) + c_2 \sin(p\theta), \tag{3.19}$$

with c_1 and c_2 being constants. In a simpler case, the solution simplifies to:

$$\Theta(\theta) = \cos(p\theta). \tag{3.20}$$

Next, by dividing the differential equation (3.17) by ρ^2 and introducing a constant for separation, we arrive at:

$$\frac{R''(\rho)}{R(\rho)} + \frac{1}{\rho}\frac{R'(\rho)}{R(\rho)} - \frac{p^2}{\rho^2} + 1 = -\frac{Z''(z)}{Z(z)} = s^2. \tag{3.21}$$

For $Z(z)$, we get

$$Z''(z) + s^2 Z(z) = 0. \tag{3.22}$$

The solution is

$$Z(z) = c_3 e^{isz} + c_4 e^{-isz}, \tag{3.23}$$

where c_3 and c_4 are arbitrary constants. Multiplying equation (3.21) by $R(\rho)$, we obtain:

$$R''(\rho) + \frac{R'(\rho)}{\rho} + \left(\tau^2 - \frac{p^2}{\rho^2}\right) R(\rho) = 0, \tag{3.24}$$

or equivalently,

$$R''(\rho) + \frac{R'(\rho)}{\rho} + \frac{1}{\rho^2}\left(\tau^2\rho^2 - p^2\right) R(\rho) = 0, \tag{3.25}$$

where $\tau^2 = 1 - s^2$.

This equation is identified as Bessel's differential equation of order p, with a solution of the form:

$$R_p(\rho) = c_5 J_p(\tau\rho) + c_6 N_p(\tau\rho), \tag{3.26}$$

The Bessel functions of the first and second kinds of order p are represented by J_p and N_p, respectively. As $r \to 0$, $N_p(\tau\rho)$ becomes singular, thus the solution is:

$$R_p(\rho) = J_p(\tau\rho). \tag{3.27}$$

Since we are considering only non-axisymmetric motion, we have $p \geq 1$. Consequently, the velocity potential's single mode can be expressed as follows:

$$\chi_{pn}(\rho, \theta, z) = A_{pn} J_p(\tau_n \rho) \cos(p\theta) e^{is_{pn}z}, \tag{3.28}$$

where A_{pn} is the amplitude and $(\tau_n)^2 = 1 - s_n^2$. This chapter examines the eigensystem of flexible shells in non-axisymmetric motion for $p \geq 1$. Using the dimensionless motion equations (3.9) and (3.10), the longitudinal and circumferential displacements in a shell of structural depth h, radial measure $\bar{a}$, and material density ϱ_s are:

$$\varphi(\rho, \theta, z) = W_m \cos(p\theta) e^{is_{pm}z}, \tag{3.29}$$

$$\vartheta(\rho, \theta, z) = X_m \sin(p\theta) e^{is_{pm}z}, \tag{3.30}$$

where W_m and X_m are displacement amplitudes of Bessel order p. Substituting these into equation (3.9) along with (3.28) yields the coupled equation.

$$W_m \left[\beta^2 - s_m^2 - \frac{p^2(1-\varpi)}{2r_a^2}\right] + \frac{imp(1+\varpi)}{2r_a} X_m = \frac{\varpi s_m R'_{pm}(r_a)}{r_a}, \tag{3.31}$$

A second equation is derived by replacing the displacement forms (3.29)-(3.30) and the velocity potential form (3.28) in equation (3.10):

$$W_m \frac{-(1+\varpi)}{2r_a} ips_m + X_m \left[\beta^2 - \frac{s_m^2(1-\varpi)}{2} - \frac{p^2}{r_a^2}\right] = \frac{ipR'_{pm}(r_a)}{r_a^2}. \tag{3.32}$$

To obtain the displacement amplitudes, these simultaneous equations need to be solved. Their matrix representation is given as:

$$\begin{bmatrix} \frac{p^2(1-\varpi)}{2} - r_a^2\beta^2 + r_a^2 s_m^2 & \frac{-ipr_a s_m(1+\varpi)}{2} \\ -ipr_a(1+\varpi)s_m & 2r_a^2\beta^2 - r_a^2 s_m^2(1-\varpi) - 2p^2 \end{bmatrix} \begin{bmatrix} W_m \\ X_m \end{bmatrix}$$

$$= R'_{pm}(r_a) \begin{bmatrix} -r_a s_m \varpi \\ 2ip \end{bmatrix}.$$

It follows that:

$$\begin{bmatrix} W_m \\ X_m \end{bmatrix} = \frac{1}{\eta_p(s_m)} \begin{bmatrix} 2r_a^2\beta^2 - r_a^2 s_m^2(1-\varpi) - 2p^2 & \dfrac{ipr_a s_m(1+\varpi)}{2} \\ ipr_a(1+\varpi)s_m & \dfrac{p^2(1-\varpi)}{2} - r_a^2\beta^2 + r_a^2 s_m^2 \end{bmatrix} \times \begin{bmatrix} -r_a s_m \varpi \\ 2ip \end{bmatrix} R'_{pm}(r_a).$$

where $\eta_p(s_m)$ represents the determinant, expressed as:

$$\eta_p(s_m) = \left(\frac{p^2(1-\varpi)}{2} - r_a^2\beta^2 + r_a^2 s_m^2\right) \times \left(2r_a^2\beta^2 - r_a^2 s_m^2(1-\varpi) - 2p^2\right) + \frac{p^2 r_a^2 s_m^2(1+\varpi)^2}{2}. \tag{3.33}$$

The longitudinal displacement is therefore given by:

$$\varphi_m = \left[\frac{-2r_a^3\beta^2\varpi s_m + r_a^3 s_m^3(\varpi - \varpi^2) + 2r_a p^2 \varpi s_m - p^2 r_a(1+\varpi)s_m}{\eta_p(s_m)}\right] \times R'_{pm}(r_a)\cos(p\theta)e^{is_{mp}z}. \tag{3.34}$$

In a similar manner, the expression for the circumferential displacement is:

$$\vartheta_m = \left[\frac{-ir_a^2 p(\varpi + \varpi^2)s_m^2 + ip^3(1-\varpi) - 2ipr_a^2\beta^2 + 2ipr_a^2 s_m^2}{\eta_p(s_m)}\right] \times R'_{pm}(r_a)\sin(p\theta)e^{is_{mp}z}. \tag{3.35}$$

The displacement expressions in (3.34) and (3.35) are inserted into the third governing equation (3.11) to obtain the fundamental equation:

$$Q_p(s_m) = \tau_1\left[\varpi r_a s_m W_m - ipX_m\right] + R'_{pm}(r_a)\left[s_m^4 + \frac{2p^2 s_m^2}{r_a^2} - \mu_p^4\right] - \alpha R_{pm}(r_a) = 0. \tag{3.36}$$

where $\tau_1 = \dfrac{12}{r_a^2 k^2 h^2}$, $\mu^4 = (\alpha^2\beta^2 - 1)\tau_1 - \dfrac{p^4}{r_a^4}$, and $\alpha = \dfrac{12\beta^2\varrho}{h^3 k^3 \varrho_s}$.The wavenumbers of the waves moving inside the shell are defined by the roots s_{pn} of the characteristic equation. The largest real root is at the top of the list, followed by roots with progressively more imaginary components.

3.2.1 Eigen Value Problem and Properties of Eigen System

The characteristic function (3.36) can be written as:

$$Q_p(s_m) = G_p(s_m)R'_{pm}(r_a) - \alpha\eta_p(s_m)R_{pm}(r_a). \tag{3.37}$$

The expressions $G_p(s_m)$ and $\eta_p(s_m)$ are characteristic polynomials.The polynomial $G_p(s_m)$ is given by:

$$G_p(s_m) = G_8^a s_m^8 + G_6^a s_m^6 + G_4^a s_m^4 + G_2^a s_m^2 + G_0^a. \tag{3.38}$$

The coefficients in the above expression are given by:

$$G_8^a = r_a^4(\varpi - 1), \tag{3.39}$$

$$G_6^a = r_a^2\left\{r_a^2\beta^2(3-\varpi) + 4p^2(\varpi-1)\right\}, \tag{3.40}$$

$$G_4^a = 5p^4(\varpi-1) + 3r_a^2\beta^2p^2(3-\varpi) + r_a^4\left\{(1-\varpi)\mu^4 - \tau(\varpi^3-\varpi^2) - 2\beta^4\right\}, \tag{3.41}$$

$$G_2^a = r_a^4\beta^2\tau\left\{r_a^2\beta^2(\varpi-3) - 2\varpi^2 - \varpi + 3\right\} - 2r_a^2p^2\beta^2\left\{2\beta^2 + r_a^2\tau(\varpi-1)\right\} - 3p^4\beta^2(\varpi-3) + \frac{4p^6(\varpi-1)}{r_a^2}. \tag{3.42}$$

These coefficients define the eigensystem behavior in non-axisymmetric motion.

$$G_0^a = \left(2r_a^2\beta^2 + p^2(\varpi-1)\right)\left(p^2\left(-\mu^4 - \tau_1\right) + r_a^2\beta^2\mu^4\right). \tag{3.43}$$

and

$$\eta_p(s_m) = \eta_4^a s_m^4 + \eta_2^a s_m^2 + \eta_0^a, \tag{3.44}$$

with

$$\eta_4^a = r_a^4(\varpi - 1), \tag{3.45}$$

$$\eta_2^a = r_a^2\left\{r_a^2\beta^2(3-\varpi) + 2p^2(\varpi-1)\right\}, \tag{3.46}$$

$$\eta_0^a = \left(p^2 - r_a^2\beta^2\right)\left\{2r_a^2\beta^2 + p^2(\varpi - 1)\right\}. \tag{3.47}$$

For each integer p, the equation $Q_p(s_m) = 0$ has infinitely many roots, as in (3.28). For simplicity, s_n replaces s_{np} in this section.

Let s_m and s_n $(m, n = 0, 1, 2, \ldots)$ be the roots of the characteristic function, satisfying the relation:

$$Q_p(s_m)\eta_p(s_n)R'_{pn}(r_a) - Q_p(s_n)\eta_p(s_m)R'_{pm}(r_a) = 0, \tag{3.48}$$

where $G_p(s_m)$ and $\eta_p(s_m)$ are given in (3.38) and (3.44), respectively. Substituting the characteristic function $Q_p(s_m)$ from (3.37) into (3.48) gives:

$$\begin{aligned}\Big[G_p(s_m)\eta_p(s_n) - G_p(s_n)\eta_p(s_m)\Big]R'_{pn}(r_a)R'_{pm}(r_a)\\ +\frac{\alpha}{r_a}\eta_p(s_m)\eta_p(s_n)\left[\rho\Big(R_{pn}(\rho)R'_{pm}(\rho) - R_{pm}(\rho)R'_{pn}(\rho)\Big)\right]_{\rho=0}^{r_a} = 0.\end{aligned} \tag{3.49}$$

The square bracket terms are first differentiated and then rewritten as an integral. Then, similar terms are grouped together:

$$\begin{aligned}\frac{\alpha}{r_a}\eta_p(s_m)\eta_p(s_n)\int_0^{r_a}\left[R_{pn}(\rho)\{\rho R''_{pm}(\rho) + R'_{pm}(\rho)\} - R_{pm}(\rho)\{R'_{pn}(\rho) + \rho R''_{pn}(\rho)\}\right]d\rho\\ = -\{G_p(s_m)\eta_p(s_n) - G_p(s_n)\eta_p(s_m)\}R'_{pn}(r_a)R'_{pm}(r_a).\end{aligned} \tag{3.50}$$

Bessel's equation shows that

$$\begin{aligned}(s_m^2 - s_n^2)\frac{\alpha}{r_a}\eta_p(s_m)\eta_p(s_n)\int_0^{r_a}\rho R_{pn}(\rho)R_{pm}(\rho)d\rho\\ = -\{G_p(s_m)\eta_p(s_n) - G_p(s_n)\eta_p(s_m)\}R'_{pn}(r_a)R'_{pm}(r_a).\end{aligned} \tag{3.51}$$

Hence

$$\begin{aligned}\frac{\alpha}{r_a}\int_0^{r_a}\rho R_{pn}(\rho)R_{pm}(\rho)d\rho + \frac{Q_p(s_n)\eta_p(s_m)R'_{pm}(r_a)}{(s_m^2 - s_n^2)\eta_p(s_m)\eta_p(s_n)} - \frac{Q_p(s_m)\eta_p(s_n)R'_{pn}(r_a)}{(s_m^2 - s_n^2)\eta_p(s_m)\eta_p(s_n)}\\ = -\frac{\{G_p(s_m)\eta_p(s_n) - G_p(s_n)\eta_p(s_m)\}R'_{pn}(r_a)R'_{pm}(r_a)}{(s_m^2 - s_n^2)\eta_p(s_m)\eta_p(s_n)}.\end{aligned}$$

The constant A_{pn}, which is non-zero, is expressed as:

$$A_{pn} = \frac{R'_{pn}(r_a)}{\eta_p(s_n)} \lim_{s_m \to s_n} \frac{Q_p(s_n) - Q_p(s_m)}{s_m^2 - s_n^2}. \tag{3.52}$$

The form of the equation above enables the use of l'Hôpital's rule:

$$A_{pn} = \frac{Q'_p(s_{1n}) R'_{1pn}(r_a)}{2 s_{1n} \eta_p(s_{1n})}. \tag{3.53}$$

The generalized orthogonality relation is thus

$$\frac{\alpha}{r_a} \int_0^{r_a} \rho R_{1pm}(\rho) R_{1pn}(\rho) d\rho = \delta_{mn} A_{pn} - \frac{H_p(s_{1m}, s_{1n}) R'_{1pn}(r_a) R'_{1pm}(r_a)}{\eta_p(s_{1n}) \eta_p(s_{1m})}. \tag{3.54}$$

where δ_{mn} is the Kronecker delta and

$$H_p(s_{1m}, s_{1n}) = \frac{G_p(s_{1m}) \eta_p(s_{1n}) - G_p(s_{1n}) \eta_p(s_{1m})}{s_{1m}^2 - s_{1n}^2}. \tag{3.55}$$

That can also be written as

$$H_p(s_{1m}, s_{1n}) = H_p^6 s_{1n}^6 + H_p^4 s_{1n}^4 + H_p^2 s_{1n}^2 + H_p^0, \tag{3.56}$$

where

$$H_p^6 = G_8^a \eta_p(s_{1m}), \tag{3.57}$$

$$H_p^4 = G_8^a \eta_p(s_{1m}) + G_6^a \eta_p(s_{1m}), \tag{3.58}$$

$$H_p^2 = G_8^a \eta_2^a s_{1m}^6 + (G_8^a \eta_0^a + G_6^a \eta_2^a) s_{1m}^2 + (G_6^a \eta_0^a + G_4^a \eta_2^a - G_2^a \eta_4^a) s_{1m}^2 + G_4^a \eta_0^a - G_0^a \eta_4^a, \tag{3.59}$$

$$H_p^0 = G_8^a \eta_0^a s_{1m}^6 + G_6^a \eta_0^a s_{1m}^4 + (G_4^a \eta_0^a - G_0^a \eta_4^a) s_{1m}^2 + G_2^a \eta_0^a - G_0^a \eta_2^a. \tag{3.60}$$

In a similar manner, for a shell with radius r_b, the corresponding generalized orthogonality relation is:

$$\frac{\alpha}{r_a} \int_0^{r_a} \rho R_{2pn}(\rho) R_{2pm}(\rho) d\rho = \delta_{mn} B_{pn} - \frac{H_p(s_{2m}, s_{2n}) R'_{2pn}(r_a) R'_{2pm}(r_a)}{\eta_p(s_{2m}) \eta_p(s_{2n})}. \tag{3.61}$$

where G_m^a and η_m^a are replaced by G_m^b and η_m^b, $\tau_2 = \frac{12}{k^2 h^2 r_b^2}$, s_{2n} are the equivalent wavenumbers, $\tau_{2n} = \sqrt{(1 - s_{2n}^2)}$, and

$$B_{pn} = \frac{Q'_p(s_{2n})R'_{2pn}(r_b)}{2s_{2n}\eta_p(s_{2n})}. \tag{3.62}$$

3.2.2 Eigenfunction Expansion

This section explores the determination of transmitted and reflected energy when an incident wave encounters a sudden expansion in radius. Two semi-unbounded shells comprise the system: the shell on the left spans $0 \leq \rho \leq r_a$, $z \leq 0$, and the right shell spans $0 \leq \rho \leq r_b$, $z \geq 0$, where $r_a \leq r_b$. A membrane disc, positioned at $r_a \leq \rho \leq r_b$, $z = 0$, closes the waveguide. The force is provided by a wave travelling in the positive z-direction, approaching the sudden expansion in radius. The flow potential χ_1 represents both the incident and reflected waves at the junction within the region defined by $z \leq 0$ and $0 \leq \rho \leq r_a$, as expressed by:

$$\chi_1(\rho,\theta,z) = F_{1\ell}R_{1p\ell}(\rho)\cos(p\theta)e^{is_{1p\ell}z} + \sum_{p=1}^{\infty}\sum_{n=0}^{\infty} C_{pn}R_{1pn}(\rho)\cos(p\theta)e^{-is_{1pn}z}. \tag{3.63}$$

In this case, ℓ represents the mode chosen for the applied forcing, with the amplitude of the incident wave given by $F_{1\ell}$. For the fundamental propagating mode ($\ell = 0$) or the first propagating mode in the left-side shell ($\ell = 1$), it is expressed as

$$F_{1\ell} = \left(\frac{1}{s_{1\ell}A_{1\ell}}\right)^{1/2}.$$

Here, C_{pn} denotes the nth reflected mode amplitude, and s_{1n} and $\tau_{1n} = \sqrt{1-(s_{1n})^2}$ are the wave numbers.

Using $\Omega = i\chi_r$, the velocity potential (3.63) is incorporated into equations (3.34) and (3.35) to determine the eigenfunction-based longitudinal, circumferential, and radial displacements for the left-side shell.

$$\varphi_1(\theta,z) = W_{1p\ell}F_{1\ell}R_{1p\ell}(r_a)\cos(p\theta)e^{is_{1p\ell}z} - \sum_{p=1}^{\infty}\sum_{n=0}^{\infty} W_{1pn}C_{pn}R_{1pn}(r_a)\cos(p\theta)e^{-is_{1pn}z},$$

$$\vartheta_1(\theta,z) = X_{1p\ell}F_{1\ell}R_{1p\ell}(r_a)\sin(p\theta)e^{is_{1p\ell}z} + \sum_{p=1}^{\infty}\sum_{n=0}^{\infty} X_{1pn}C_{pn}R_{1pn}(r_a)\sin(p\theta)e^{-is_{1pn}z},$$

$$\Omega_1(\theta,z) = -F_{1\ell}R_{1p\ell}(r_a)\cos(p\theta)e^{is_{1p\ell}z} - \sum_{p=1}^{\infty}\sum_{n=0}^{\infty} C_{pn}R_{1pn}(r_a)\cos(p\theta)e^{-is_{1pn}z}. \quad (3.64)$$

In the region $z \geq 0$, $0 \leq \rho \leq r_b$, the velocity potential consists of the transmitted waves that propagate through the junction:

$$\chi_2(\rho,\theta,z) = \sum_{p=1}^{\infty}\sum_{n=0}^{\infty} D_{pn}R_{2pn}(\rho)\cos(p\theta)e^{is_{2pn}z}. \quad (3.65)$$

The amplitude of the nth mode of transmission is denoted by D_{pn}, the roots of the dispersion function in the right-hand shell are denoted by s_{2pn}, and $\tau_{2n} = \sqrt{1-s_{2n}^2}$. The expressions for the eigenfunctions corresponding to the longitudinal, circumferential, and radial displacements in the right-hand shell are given by:

$$\varphi_2(\theta,z) = \sum_{p=1}^{\infty}\sum_{n=0}^{\infty} W_{2pn}D_{pn}R_{2pn}(r_b)\cos(p\theta)e^{is_{2pn}z},$$

$$\vartheta_2(\theta,z) = \sum_{p=1}^{\infty}\sum_{n=0}^{\infty} X_{2pn}D_{pn}R_{2pn}(r_b)\sin(p\theta)e^{is_{2pn}z},$$

$$\Omega_2(\theta,z) = \sum_{p=1}^{\infty}\sum_{n=0}^{\infty} D_{pn}R_{2pn}(r_b)\cos(p\theta)e^{is_{2pn}z}.$$

In the region $z = 0$, $0 \leq \rho \leq r_a$, the pressure is continuous, which leads to the expression:

$$\chi_1(\rho,\theta,z) = \chi_2(\rho,\theta,z). \quad (3.66)$$

By inserting the velocity potentials (3.63) and (3.65) into this equation, we get:

$$F_{1\ell}R_{1p\ell}\cos(p\theta) + \sum_{p=1}^{\infty}\sum_{n=0}^{\infty} C_{pn}R_{1pn}(\rho)\cos(p\theta) = \sum_{p=1}^{\infty}\sum_{n=0}^{\infty} D_{pn}R_{2pn}(\rho)\cos(p\theta). \quad (3.67)$$

Multiplying the above equation with $\cos(q\theta)$ and integrating over $0 \leq \theta \leq 2\pi$, we get:

$$F_{1\ell}R_{1p\ell}\delta_{pq} + \sum_{n=0}^{\infty} C_{qn}R_{1qn}(\rho) = \sum_{n=0}^{\infty} D_{qn}R_{2qn}(\rho), \quad (3.68)$$

The equation (3.68)is multiplied through by $\frac{\alpha}{r_a}\rho R_{1qm}(\rho)$ and integrated with respect to ρ over $0 \leq \rho \leq r_a$, we obtain:

$$F_{1\ell}\delta_{pq}\int_0^{r_a}\frac{\alpha}{r_a}\rho R_{1qm}(\rho)R_{1p\ell}(\rho)\,d\rho+\sum_{n=0}^{\infty}C_{qn}\int_0^{r_a}\frac{\alpha}{r_a}\rho R_{1qm}(\rho)R_{1qn}(\rho)\,d\rho=\sum_{n=0}^{\infty}D_{qn}\int_0^{r_a}\frac{\alpha}{r_a}\rho R_{1qm}(\rho)R_{2qn}(\rho)\,d\rho, \tag{3.69}$$

where:

$$P_{mn}=\int_0^{r_a}\rho R_{2qn}(\rho)R_{1qm}(\rho)\,d\rho.$$

By applying the generalized orthogonality relation (3.54), After rearranging the integrals on the left-hand side, the first coupled equation is produced:

$$C_{qm}=-\frac{F_{1\ell}\delta_{pq}\delta_{m\ell}A_{q\ell}}{A_{qm}}+\frac{\alpha}{r_aA_{qm}}\sum_{n=0}^{\infty}D_{qn}P_{mn}+\frac{R'_{1qm}(r_a)}{\eta_q(s_{1m})A_{qm}}\left[E_1H_q^6(s_{1m})+E_2H_q^4(s_{1m})+E_3H_q^2(s_{1m})+E_4H_q^0(s_{1m})\right]. \tag{3.70}$$

The constants E_1, E_2, E_3, and E_4 are defined as:

$$E_1=\frac{F_{1\ell}s_{1p\ell}^6R'_{1p\ell}(r_a)\delta_{pq}}{\eta_q(s_{1\ell})}+\sum_{n=0}^{\infty}\frac{C_{qn}s_{1qn}^6R'_{1qn}(r_a)}{\eta_q(s_{1qn})},$$

$$E_2=\frac{F_{1\ell}s_{1p\ell}^4R'_{1p\ell}(r_a)\delta_{pq}}{\eta_q(s_{1\ell})}+\sum_{n=0}^{\infty}\frac{C_{qn}s_{1qn}^4R'_{1qn}(r_a)}{\eta_q(s_{1qn})},$$

$$E_3=\frac{F_{1\ell}s_{1p\ell}^2R'_{1p\ell}(r_a)\delta_{pq}}{\eta_q(s_{1\ell})}+\sum_{n=0}^{\infty}\frac{C_{qn}s_{1qn}^2R'_{1qn}(r_a)}{\eta_q(s_{1qn})},$$

$$E_4=\frac{F_{1\ell}R'_{1p\ell}(r_a)\delta_{pq}}{\eta_q(s_{1\ell})}+\sum_{n=0}^{\infty}\frac{C_{qn}R'_{1qn}(r_a)}{\eta_q(s_{1qn})}.$$

The constants E_1 to E_4 are determined by enforcing the edge conditions at the left-hand shell-membrane disc connection. Applying the boundary condition on Region I, the system is expressed in matrix form as:

$$\begin{bmatrix}S_{11}&S_{12}&S_{13}&S_{14}\\S_{21}&S_{22}&S_{23}&S_{24}\\S_{31}&S_{32}&S_{33}&S_{34}\\S_{41}&S_{42}&S_{43}&S_{44}\end{bmatrix}\begin{bmatrix}E_1\\E_2\\E_3\\E_4\end{bmatrix}=\begin{bmatrix}I_{11}\\I_{21}\\I_{31}\\I_{41}\end{bmatrix}, \tag{3.71}$$

where

$$I_{11} = F_{1\ell}\delta_{pq}\left[W_{1p\ell}R_{1p\ell}(r_a) + W_{1q\ell}R_{1q\ell}(r_a)\right] - \frac{\alpha}{r_a}\sum_{n=0}^{\infty}\sum_{m=0}^{\infty}\frac{D_{qn}W_{1qm}R_{1qm}(r_a)P_{mn}}{A_{qm}},$$

$$I_{21} = F_{1\ell}\delta_{pq}\left[X_{1q\ell}R_{1q\ell}(r_a) - X_{1p\ell}R_{1p\ell}(r_a)\right] - \frac{\alpha}{r_a}\sum_{n=0}^{\infty}\sum_{m=0}^{\infty}\frac{D_{qn}X_{1qm}R_{1qm}(r_a)P_{mn}}{A_{qm}},$$

$$I_{31} = F_{1\ell}\delta_{pq}\left[R'_{1q\ell}(r_a) - R'_{1p\ell}(r_a)\right] - \frac{\alpha}{r_a}\sum_{n=0}^{\infty}\sum_{m=0}^{\infty}\frac{D_{qn}R'_{1qm}(r_a)P_{mn}}{A_{qm}},$$

$$I_{41} = F_{1\ell}\delta_{pq}\left[s_{1p\ell}R'_{1p\ell}(r_a) + s_{1q\ell}R'_{1q\ell}(r_a)\right] - \frac{\alpha}{r_a}\sum_{n=0}^{\infty}\sum_{m=0}^{\infty}\frac{D_{qn}s_{1qm}R'_{1qm}(r_a)P_{mn}}{A_{qm}},$$

$$S_{11} = \sum_{m=0}^{\infty}\frac{W_{1qm}R_{1qm}(r_a)R'_{1qm}(r_a)H_q^6(s_{1m})}{\eta_q(s_{1m})A_{qm}},$$

$$S_{12} = \sum_{m=0}^{\infty}\frac{W_{1qm}R_{1qm}(r_a)R'_{1qm}(r_a)H_q^4(s_{1m})}{\eta_q(s_{1m})A_{qm}},$$

$$S_{12} = \sum_{m=0}^{\infty}\frac{W_{1qm}R_{1qm}(r_a)R'_{1qm}(r_a)H_q^4(s_{1m})}{\eta_q(s_{1m})A_{qm}},$$

$$S_{13} = \sum_{m=0}^{\infty}\frac{W_{1qm}R_{1qm}(r_a)R'_{1qm}(r_a)H_q^2(s_{1m})}{\eta_q(s_{1m})A_{qm}},$$

$$S_{14} = \sum_{m=0}^{\infty}\frac{W_{1qm}R_{1qm}(r_a)R'_{1qm}(r_a)H_q^0(s_{1m})}{\eta_q(s_{1m})A_{qm}},$$

$$S_{21} = \sum_{m=0}^{\infty}\frac{X_{1qm}R_{1qm}(r_a)R'_{1qm}(r_a)H_q^6(s_{1m})}{\eta_q(s_{1m})A_{qm}},$$

$$S_{22} = \sum_{m=0}^{\infty}\frac{X_{1qm}R_{1qm}(r_a)R'_{1qm}(r_a)H_q^4(s_{1m})}{\eta_q(s_{1m})A_{qm}}$$

$$S_{23} = \sum_{m=0}^{\infty}\frac{X_{1qm}R_{1qm}(r_a)R'_{1qm}(r_a)H_q^2(s_{1m})}{\eta_q(s_{1m})A_{qm}},$$

$$S_{24} = \sum_{m=0}^{\infty}\frac{X_{1qm}R_{1qm}(r_a)R'_{1qm}(r_a)H_q^0(s_{1m})}{\eta_q(s_{1m})A_{qm}},$$

$$S_{31} = \sum_{m=0}^{\infty} \frac{R'_{1qm}(r_a)R'_{1qm}(r_a)H_q^6(s_{1m})}{\eta_q(s_{1m})A_{qm}},$$

$$S_{32} = \sum_{m=0}^{\infty} \frac{R'_{1qm}(r_a)R'_{1qm}(r_a)H_q^4(s_{1m})}{\eta_q(s_{1m})A_{qm}},$$

$$S_{33} = \sum_{m=0}^{\infty} \frac{R'_{1qm}(r_a)R'_{1qm}(r_a)H_q^2(s_{1m})}{\eta_q(s_{1m})A_{qm}},$$

$$S_{34} = \sum_{m=0}^{\infty} \frac{R'_{1qm}(r_a)R'_{1qm}(r_a)H_q^0(s_{1m})}{\eta_q(s_{1m})A_{qm}},$$

$$S_{41} = \sum_{m=0}^{\infty} \frac{R'_{1qm}(r_a)R'_{1qm}(r_a)H_q^6(s_{1m})s_{1qm}}{\eta_q(s_{1m})A_{qm}},$$

$$S_{42} = \sum_{m=0}^{\infty} \frac{R'_{1qm}(r_a)R'_{1qm}(r_a)H_q^4(s_{1m})s_{1qm}}{\eta_q(s_{1m})A_{qm}},$$

$$S_{43} = \sum_{m=0}^{\infty} \frac{R'_{1qm}(r_a)R'_{1qm}(r_a)H_q^2(s_{1m})s_{1qm}}{\eta_q(s_{1m})A_{qm}},$$

$$S_{44} = \sum_{m=0}^{\infty} \frac{R'_{1qm}(r_a)R'_{1qm}(r_a)H_q^0(s_{1m})s_{1qm}}{\eta_q(s_{1m})A_{qm}}.$$

At the interface, continuity of the normal velocity component is maintained within the fluid region, while also satisfying the vertical membrane condition.

The membrane's boundary condition is given by:

$$U(\rho,\theta) = 0 \quad \text{at} \quad \rho = r_a \text{ and } \rho = r_b,$$

where $U(\rho,\theta)$ represents the displacement function. The governing differential equation for the non-axisymmetric disc modes is:

$$\left(\frac{\partial^2}{\partial\rho^2} + \frac{1}{\rho}\frac{\partial}{\partial\rho} + \frac{1}{\rho^2}\frac{\partial^2}{\partial\theta^2} + \mu^2\right) U(\rho,\theta) = \gamma\chi_2, \tag{3.72}$$

where χ_2 is the source function, μ^2 is a membrane wavenumber, and γ is a fluid loading parameter. The displacement function $U(\rho,\theta)$ is then expressed as a sum of modes:

$$U(\rho,\theta) = \sum_{n=0}^{\infty}\sum_{m=0}^{\infty} g_{mn}\chi_{mn}(\rho,\theta), \tag{3.73}$$

where g_{mn} are the coefficients to be determined, and $\chi_{mn}(\rho, \theta)$ are the eigenfunctions associated with the radial and angular components.

The eigenvalue problem for non-axisymmetric modes is given by:

$$\left(\frac{\partial^2}{\partial\rho^2} + \frac{1}{\rho}\frac{\partial}{\partial\rho} + \frac{1}{\rho^2}\frac{\partial^2}{\partial\theta^2} + \lambda_{mn}^2\right)\chi_{mn}(\rho, \theta) = 0. \tag{3.74}$$

To solve this equation, we assume a solution in the form of a product of radial and angular functions:

$$\chi_{mn}(\rho, \theta) = R_{mn}(\rho)\Theta_{mn}(\theta). \tag{3.75}$$

Substituting this expression into equation (3.74) leads to:

$$R''_{mn}(\rho)\Theta_{mn}(\theta) + \frac{1}{\rho}R'_{mn}(\rho)\Theta_{mn}(\theta) + \frac{1}{\rho^2}R_{mn}(\rho)\Theta''_{mn}(\theta) + \lambda_{mn}^2 R_{mn}(\rho)\Theta_{mn}(\theta) = 0. \tag{3.76}$$

Dividing (3.76) through by $R_{mn}(\rho)\Theta_{mn}(\theta)$ and multiplying the resulting equation by ρ^2, we obtain:

$$\rho^2\frac{R''_{mn}(\rho)}{R_{mn}(\rho)} + \rho\frac{R'_{mn}(\rho)}{R_{mn}(\rho)} + \rho^2\lambda_{mn}^2 = -\frac{\Theta''_{mn}(\theta)}{\Theta_{mn}(\theta)} = m^2, \tag{3.77}$$

where m^2 is a constant.

The angular function $\Theta_{mn}(\theta)$ satisfies a simple harmonic equation, and its solution is:

$$\Theta_{mn}(\theta) = c_7\cos(m\theta) + c_8\sin(m\theta), \tag{3.78}$$

where c_7 and c_8 represent constants that can take any value. The radial equation becomes:

$$\rho^2 R''_{mn}(\rho) + \rho R'_{mn}(\rho) + (\rho^2\lambda_{mn}^2 - m^2)R_{mn}(\rho) = 0. \tag{3.79}$$

This represents a standard Bessel equation of order m, with the general solution given as:

$$R_{mn}(\rho) = b_1 J_m(\lambda_{mn}\rho) + b_2 Y_m(\lambda_{mn}\rho), \tag{3.80}$$

where J_m and Y_m are the Bessel functions of the first and second kinds, respectively, and b_1 and b_2 are constants to be determined. Using the boundary condition

$R_{mn}(r_a) = 0$, we derive a relationship between the constants:

$$b_1 = -\frac{b_2 Y_m(\lambda_{mn} r_a)}{J_m(\lambda_{mn} r_a)}.$$

Thus, the radial displacement function is:

$$R_{mn}(\rho) = -b_2 \left[\frac{J_m(\lambda_{mn}\rho) Y_m(\lambda_{mn} r_a)}{J_m(\lambda_{mn} r_a)} - Y_m(\lambda_{mn}\rho) \right]. \tag{3.81}$$

Applying the second boundary condition $R_{mn}(r_b) = 0$, we obtain the dispersion relation:

$$\frac{J_m(\lambda_{mn} r_a)}{Y_m(\lambda_{mn} r_a)} = \frac{J_m(\lambda_{mn} r_b)}{Y_m(\lambda_{mn} r_b)}.$$

The eigenfunction is:

$$\chi_{mn}(\rho) = \left[\frac{J_m(\lambda_{mn}\rho) Y_m(\lambda_{mn} r_a)}{J_m(\lambda_{mn} r_a)} - Y_m(\lambda_{mn}\rho) \right] \cos(m\theta). \tag{3.82}$$

Here λ_{mn} are the roots of dispersion relation. Substituting this into the series solution for $U(r)$, we get:

$$\sum_{n=0}^{\infty} g_{mn} \{\mu^2 - \lambda_{mn}^2\} \chi_{mn}(\rho) = \gamma \chi_2(\rho, \theta). \tag{3.83}$$

Further simplifying:

$$\sum_{n=0}^{\infty} g_{mn} \chi_{mn}(\rho) \Delta_{mn} = \gamma \sum_{p=1}^{\infty} \sum_{n=0}^{\infty} D_{pn} R_{2pn}(\rho) \cos(p\theta). \tag{3.84}$$

where $\Delta_{mn} = \mu^2 - \lambda_{mn}^2$.

Next, we apply the Galerkin method to obtain the coefficients g_{mn}. By multiplying the governing equation by $r\chi_{m'n'}(r, \theta)$ and integrating over the domain, we obtain:

$$\sum_{m=0}^{\infty} \sum_{n=0}^{\infty} g_{mn} \Delta_{mn} \delta_{mm'} \delta_{nn'} N_{mn} = \gamma \sum_{p=1}^{\infty} \sum_{n=0}^{\infty} D_{pn} I_{m'n'} \delta_{m'p}, \tag{3.85}$$

where

$$I_{m'nn'} = \int_{r_a}^{r_b} \rho R_{2pn}(\rho) R_{m'n'}(\rho)\, d\rho,$$

$$\int_0^{2\pi} \cos(p\theta)\cos(m'\theta)\, d\theta = \pi\delta_{pm'},$$

$$\int_0^{2\pi}\int_{r_a}^{r_b} \rho R_{m'n'}^2 \cos^2(m'\theta)\, d\rho\, d\theta = \pi N_{m'n'}\delta_{mm'}\delta_{nn'},$$

By solving the above equation for g_{mn}, we obtain:

$$g_{m'n'} = \frac{\gamma}{\Delta_{m'n'}N_{m'n'}} \sum_{n=0}^{\infty} D_{m'n} I_{m'nn'}. \tag{3.86}$$

This expression provides the relationship between the unknown coefficients $g_{m'n'}$ and the system's parameters. The normal velocity condition is formulated as:

$$\frac{\partial \chi_2}{\partial z}(\rho,\theta,0) = \begin{cases} \dfrac{\partial \chi_1}{\partial z}(\rho,\theta,0) & \text{if } 0 \le \rho \le r_a, \\ U(\rho,\theta) & \text{if } r_a \le \rho \le r_b. \end{cases} \tag{3.87}$$

After substituting velocity potentials (3.63) and (3.65) and membrane displacement (3.73) into (3.87), multiplying by $\dfrac{\alpha}{r_b}\rho R_{2qm}(\rho)$, and integrated over $0 \le \rho \le r_b$ the result is

$$\sum_{n=0}^{\infty} s_{2qn} D_{qn} \frac{\alpha}{r_b} \int_0^{r_b} \rho R_{2qn}(\rho) R_{2qm}(\rho)\, d\rho =$$
$$\frac{\alpha}{r_b} s_{1p\ell} F_{1\ell} \delta_{pq} P_{\ell m} - \frac{\alpha}{r_b} \sum_{n=0}^{\infty} C_{qn} s_{1qn} P_{nm} - i\frac{\alpha}{r_b} \sum_{n=0}^{\infty} g_{qn} h_{qmn}, \tag{3.88}$$

where

$$\int_0^{r_a} \rho R_{1qn}(\rho) R_{2qm}(\rho) d\rho = P_{nm}, \quad \int_0^{r_a} \rho R_{1q\ell}(\rho) R_{2qm}(\rho) d\rho = P_{\ell m},$$

$$\int_{r_a}^{r_b} \rho R_{qn}(r) R_{2qm}(\rho) d\rho = h_{qmn}.$$

By applying the generalized orthogonality relation (3.61), the left-hand integral in (3.88) is simplified. After some rearrangement, we get:

$$D_{qm} = \frac{\alpha s_{1p\ell} F_{1\ell} P_{\ell m} \delta_{pq}}{r_b s_{2qm} B_{qm}} - \frac{\alpha}{r_b} \sum_{n=0}^{\infty} \frac{C_{qn} s_{1qn} P_{nm}}{s_{2qm} B_{qm}} - i \frac{\alpha}{r_b} \sum_{n=0}^{\infty} \frac{g_{qn} h_{qmn}}{B_{qm} s_{2qm}} + \frac{R'_{2qm}(r_b)}{s_{2qm} B_{qm} \eta_q(s_{2m})} \left[H_q^6(s_{2m}) E_5 + H_q^4(s_{2m}) E_6 + H_q^2(s_{2m}) E_7 + H_q^0(s_{2m}) E_8 \right], \tag{3.89}$$

where the terms E_5, E_6, E_7, and E_8 are explicitly defined in the following expressions, representing the coefficients that arise from the imposed boundary and continuity conditions.

$$E_5 = \frac{\sum_{n=0}^{\infty} D_{qn} s_{2qn} s_{2qn}^6 R'_{2qn}(r_b)}{\eta_q(s_{2n})}, E_6 = \frac{\sum_{n=0}^{\infty} D_{qn} s_{2qn} s_{2qn}^4 R'_{2qn}(r_b)}{\eta_q(s_{2n})},$$

$$E_7 = \frac{\sum_{n=0}^{\infty} D_{qn} s_{2qn} s_{2qn}^2 R'_{2qn}(r_b)}{\eta_q(s_{2n})}, E_8 = \frac{\sum_{n=0}^{\infty} D_{qn} s_{2qn} R'_{2qn}(r_b)}{\eta_q(s_{2n})}.$$

The values of E_5, E_6, E_7, and E_8 are obtained from the edge conditions governing the shell-membrane interaction. Applying the boundary conditions, the system is written in matrix form:

$$\begin{bmatrix} \Psi_{11} & \Psi_{12} & \Psi_{13} & \Psi_{14} \\ \Psi_{21} & \Psi_{22} & \Psi_{23} & \Psi_{24} \\ \Psi_{31} & \Psi_{32} & \Psi_{33} & \Psi_{34} \\ \Psi_{41} & \Psi_{42} & \Psi_{43} & \Psi_{44} \end{bmatrix} \begin{bmatrix} E_5 \\ E_6 \\ E_7 \\ E_8 \end{bmatrix} = \begin{bmatrix} \zeta_{11} \\ \zeta_{21} \\ \zeta_{31} \\ \zeta_{41} \end{bmatrix}, \tag{3.90}$$

where

$$\Psi_{11} = \sum_{m=0}^{\infty} \frac{W_{2qm} R_{2qm}(r_b) H_q^6(s_{2m}) R'_{2qm}(r_b)}{\eta_q(s_{2m}) B_{qm} s_{2qm}}, \Psi_{12} = \sum_{m=0}^{\infty} \frac{W_{2qm} R_{2qm}(r_b) H_q^4(s_{2m}) R'_{2qm}(r_b)}{\eta_q(s_{2m}) B_{qm} s_{2qm}},$$

$$\Psi_{13} = \sum_{m=0}^{\infty} \frac{W_{2qm} R_{2qm}(r_b) H_q^2(s_{2m}) R'_{2qm}(r_b)}{\eta_q(s_{2m}) B_{qm} s_{2qm}}, \Psi_{14} = \sum_{m=0}^{\infty} \frac{W_{2qm} R_{2qm}(r_b) H_q^0(s_{2m}) R'_{2qm}(r_b)}{\eta_q(s_{2m}) B_{qm} s_{2qm}},$$

$$\Psi_{21}=\sum_{m=0}^{\infty}\frac{X_{2qm}R_{2qm}(r_b)H_q^6(s_{2m})R'_{2qm}(r_b)}{\eta_q(s_{2m})B_{qm}s_{2qm}},\Psi_{22}=\sum_{m=0}^{\infty}\frac{X_{2qm}R_{2qm}(r_b)H_q^4(s_{2m})R'_{2qm}(r_b)}{\eta_q(s_{2m})B_{qm}s_{2qm}},$$

$$\Psi_{23}=\sum_{m=0}^{\infty}\frac{X_{2qm}R_{2qm}(r_b)H_q^2(s_{2m})R'_{2qm}(r_b)}{\eta_q(s_{2m})B_{qm}s_{2qm}},\Psi_{24}=\sum_{m=0}^{\infty}\frac{X_{2qm}R_{2qm}(r_b)H_q^0(s_{2m})R'_{2qm}(r_b)}{\eta_q(s_{2m})B_{qm}s_{2qm}},$$

$$\Psi_{31}=\sum_{m=0}^{\infty}\frac{R'_{2qm}(r_b)H_q^6(s_{2m})R'_{2qm}(r_b)}{\eta_q(s_{2m})B_{qm}s_{2qm}},\Psi_{32}=\sum_{m=0}^{\infty}\frac{R'_{2qm}(r_b)H_q^4(s_{2m})R'_{2qm}(r_b)}{\eta_q(s_{2m})B_{qm}s_{2qm}},$$

$$\Psi_{33}=\sum_{m=0}^{\infty}\frac{R'_{2qm}(r_b)H_q^2(s_{2m})R'_{2qm}(r_b)}{\eta_q(s_{2m})B_{qm}s_{2qm}},\Psi_{34}=\sum_{m=0}^{\infty}\frac{R'_{2qm}(r_b)H_q^0(s_{2m})R'_{2qm}(r_b)}{\eta_q(s_{2m})B_{qm}s_{2qm}},$$

$$\Psi_{41}=\sum_{m=0}^{\infty}\frac{R'_{2qm}(r_b)H_q^6(s_{2m})R'_{2qm}(r_b)}{\eta_q(s_{2m})B_{qm}},\quad\Psi_{42}=\sum_{m=0}^{\infty}\frac{R'_{2qm}(r_b)H_q^4(s_{2m})R'_{2qm}(r_b)}{\eta_q(s_{2m})B_{qm}},$$

$$\Psi_{43}=\sum_{m=0}^{\infty}\frac{R'_{2qm}(r_b)H_q^2(s_{2m})R'_{2qm}(r_b)}{\eta_q(s_{2m})B_{qm}},\quad\Psi_{44}=\sum_{m=0}^{\infty}\frac{R'_{2qm}(r_b)H_q^0(s_{2m})R'_{2qm}(r_b)}{\eta_q(s_{2m})B_{qm}},$$

$$\zeta_{11}=-\frac{\alpha}{r_b}F_{1\ell}s_{1p\ell}\sum_{m=0}^{\infty}\frac{W_{2qm}R_{2qm}(r_b)P_{\ell m}\delta_{pq}}{B_{qm}s_{2qm}}+\frac{\alpha}{r_b}\sum_{n=0}^{\infty}\sum_{m=0}^{\infty}\frac{C_{qn}W_{2qm}R_{2qm}(r_b)s_{1qn}P_{nm}}{B_{qm}s_{2qm}}$$
$$+i\frac{\alpha}{r_b}\sum_{m=0}^{\infty}\sum_{n=0}^{\infty}\frac{W_{2qm}R_{2qm}(r_b)g_{qn}h_{qmn}}{B_{qm}s_{2qm}},$$

$$\zeta_{21}=-\frac{\alpha}{r_b}F_{1\ell}s_{1p\ell}\sum_{m=0}^{\infty}\frac{X_{2qm}R_{2qm}(r_b)P_{\ell m}\delta_{pq}}{B_{qm}s_{2qm}}+\frac{\alpha}{r_b}\sum_{n=0}^{\infty}\sum_{m=0}^{\infty}\frac{C_{qn}X_{2qm}R_{2qm}(r_b)s_{1qn}P_{nm}}{B_{qm}s_{2qm}}$$
$$+i\frac{\alpha}{r_b}\sum_{m=0}^{\infty}\sum_{n=0}^{\infty}\frac{X_{2qm}R_{2qm}(r_b)g_{qn}h_{qmn}}{B_{qm}s_{2qm}},$$

$$\zeta_{31}=-\frac{\alpha}{r_b}F_{1\ell}s_{1p\ell}\sum_{m=0}^{\infty}\frac{R'_{2qm}(r_b)P_{\ell m}\delta_{pq}}{B_{qm}s_{2qm}}+\frac{\alpha}{r_b}\sum_{n=0}^{\infty}\sum_{m=0}^{\infty}\frac{C_{qn}R'_{2qm}(r_b)s_{1qn}P_{nm}}{B_{qm}s_{2qm}}$$
$$+i\frac{\alpha}{r_b}\sum_{m=0}^{\infty}\sum_{n=0}^{\infty}\frac{R'_{2qm}(r_b)g_{qn}h_{qmn}}{B_{qm}s_{2qm}},$$

$$\zeta_{41}=-\frac{\alpha}{r_b}F_{1\ell}s_{1p\ell}\sum_{m=0}^{\infty}\frac{R'_{2qm}(r_b)P_{\ell m}\delta_{pq}}{B_{qm}}+\frac{\alpha}{r_b}\sum_{n=0}^{\infty}\sum_{m=0}^{\infty}\frac{C_{qn}R'_{2qm}(r_b)s_{1qn}P_{nm}}{B_{qm}}$$
$$+i\frac{\alpha}{r_b}\sum_{m=0}^{\infty}\sum_{n=0}^{\infty}\frac{R'_{2qm}(r_b)g_{qn}h_{qmn}}{B_{qm}}.$$

By truncating and solving equations (3.70) and (3.89), the transmitted and reflected amplitudes are determined.

3.3 Numerical Solution

To ensure accurate results and proper amplitude formation, it is essential to verify the matching conditions. This verification is performed for the case where the non-dimensional shell radii are $\bar{a} = 0.2$ m and $\bar{b} = 0.28$ m, considering first-mode forcing and clamped edge conditions.

The pressure matching condition, given by equation (3.66), is evaluated for $p = 1$ against the non-dimensional radius of the shell using 15 modes at a frequency of 1000 Hz. The results are presented in Figure (3.2,3.3). It is observed that while the real part of the pressure exhibits a good match on both sides of the shell, a discrepancy appears at the shell's edge. However, the imaginary part does not match accurately, indicating that using only 15 modes is insufficient for correctly determining the amplitudes. This suggests that a greater number of modes are required for an accurate solution. To improve accuracy, the pressure matching condition is re-evaluated using 30 modes at 1000 Hz, as depicted in Figure (3.4,3.5). With this increased number of modes, both the real and imaginary components align well, confirming that a higher mode count provides better accuracy in determining the amplitudes.

Similarly, the normal velocity matching condition is examined under the same conditions. Initially, the condition is tested using 15 modes at 1000 Hz, with the results for the real and imaginary parts illustrated in Figure (3.6,3.7). These results indicate a poor match, reinforcing that 15 modes are insufficient for capturing the correct behavior of normal velocity. To enhance the accuracy, the analysis is repeated using 30 modes at 1000 Hz, as shown in Figure (3.8,3.9). While the results exhibit an improved match, a discrepancy remains, particularly due to the presence of a singularity. This mismatch arises because the normal velocity is continuous within the fluid but becomes zero at the rigid annular disc. The abrupt transition leads to an inconsistency in the matching condition at the interface.

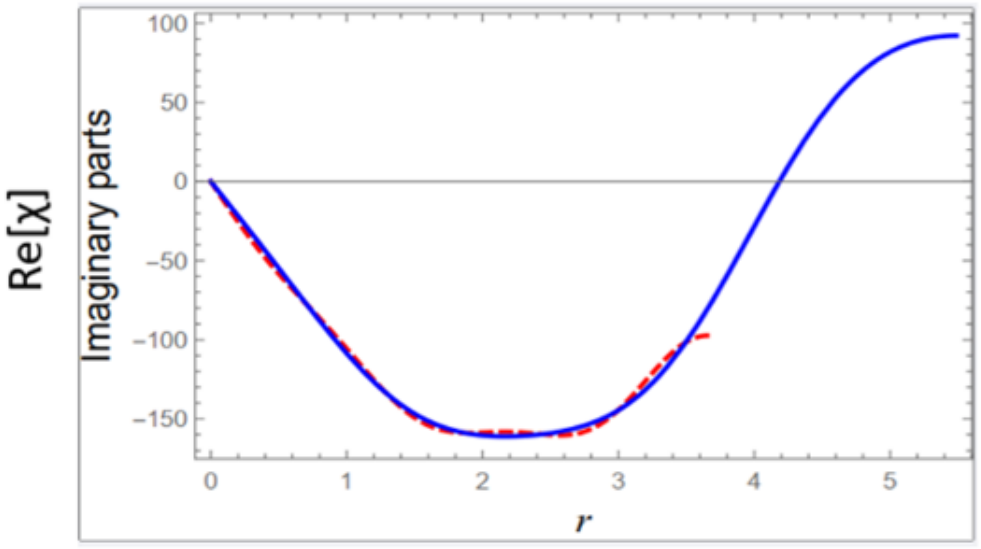

FIGURE 3.2: Real part of the pressure matching condition with 15 terms (χ_1: left shell, dotted line; χ_2: right shell, blue line).

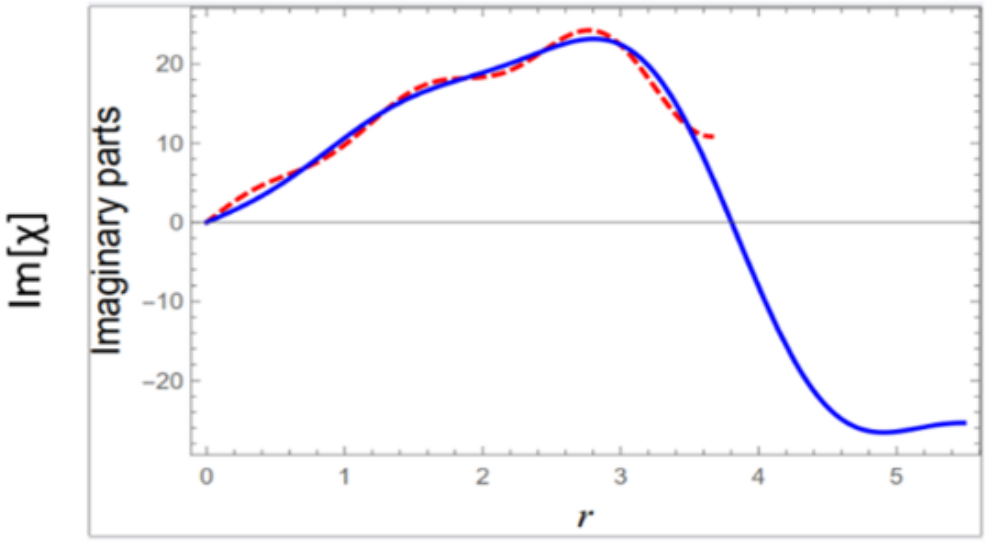

FIGURE 3.3: Imaginary part of the pressure matching condition with 15 terms (χ_1: left shell, dotted line; χ_2: right shell, blue line).

Note: In the graphs, the variable ρ represents the radial coordinate r.

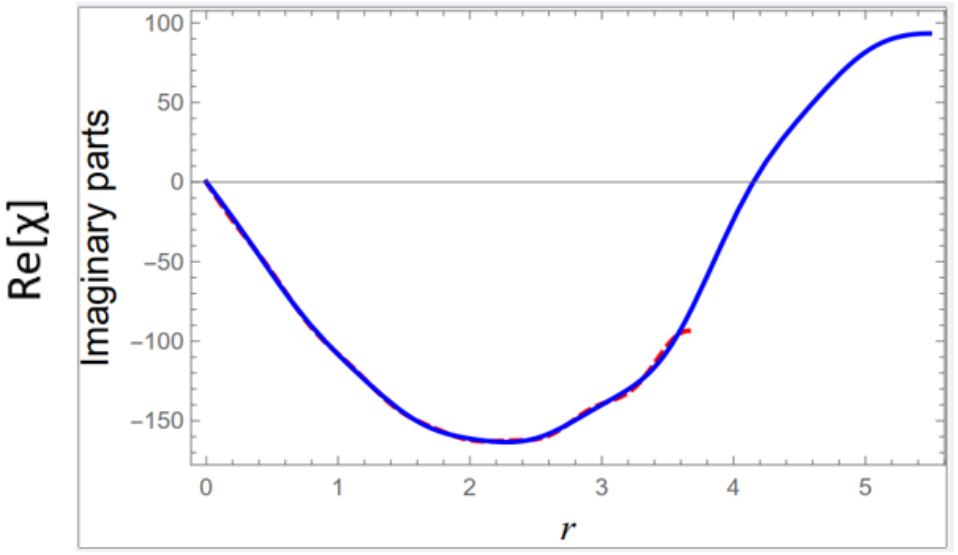

FIGURE 3.4: Real part of the pressure matching condition with 30 terms (χ_1: left shell, dotted line; χ_2: right shell, blue line).

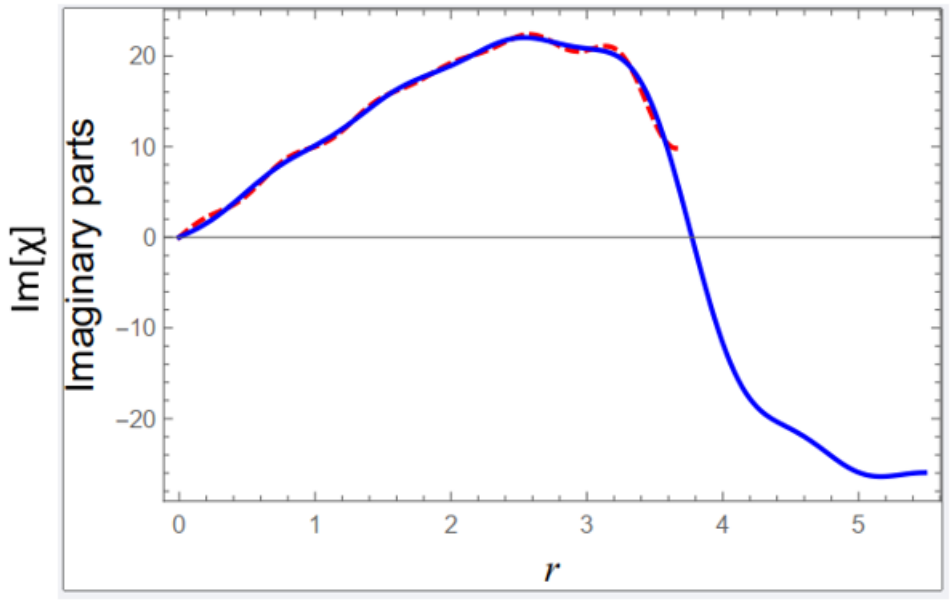

FIGURE 3.5: Imaginary part of the pressure matching condition with 30 terms (χ_1: left shell, dotted line; χ_2: right shell, blue line).

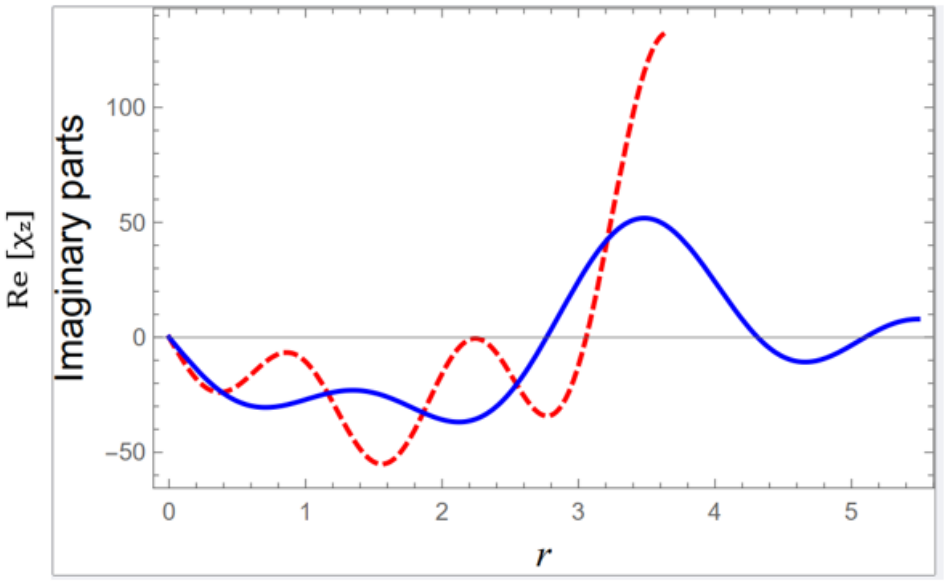

FIGURE 3.6: Real part of the matching condition for the normal component of velocity with 15 terms (χ_1: left shell, dotted line; χ_2: right shell, blue line)

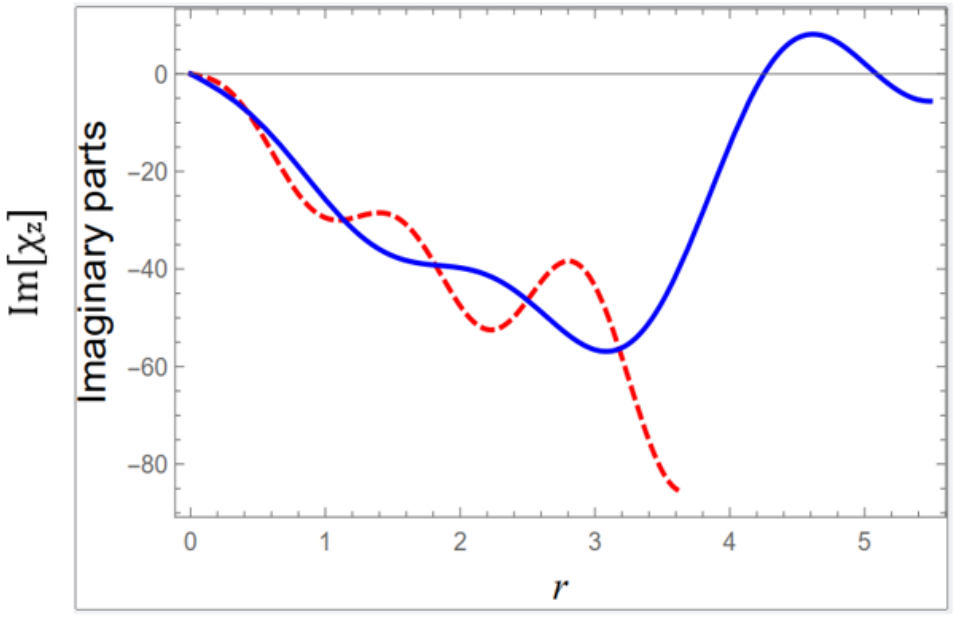

FIGURE 3.7: Imaginary part of the matching condition for the normal component of velocity with 15 terms (χ_1: left shell, dotted line; χ_2: right shell, blue line)

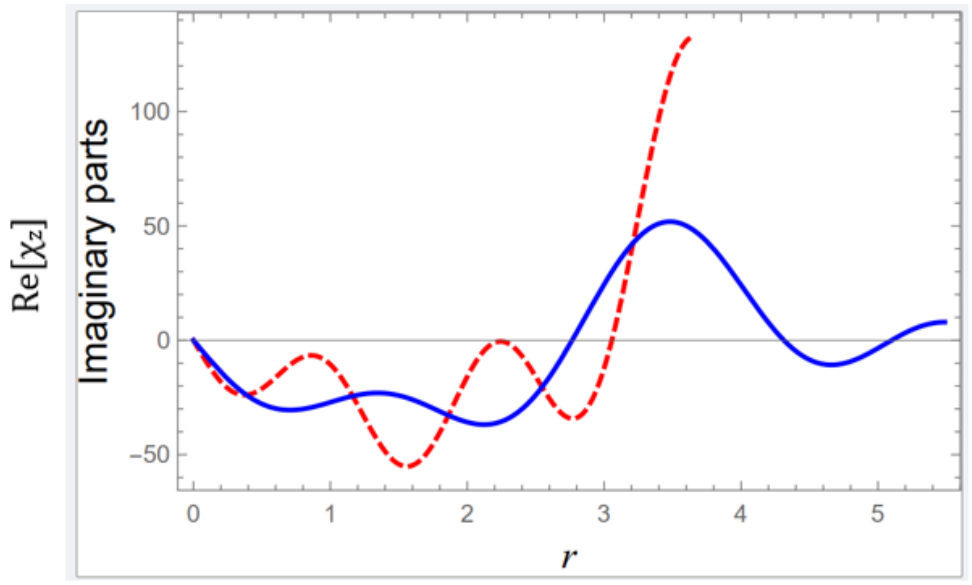

FIGURE 3.8: Real part of the normal velocity matching condition with 30 terms (χ_1: left shell, dotted line; χ_2: right shell, blue line).

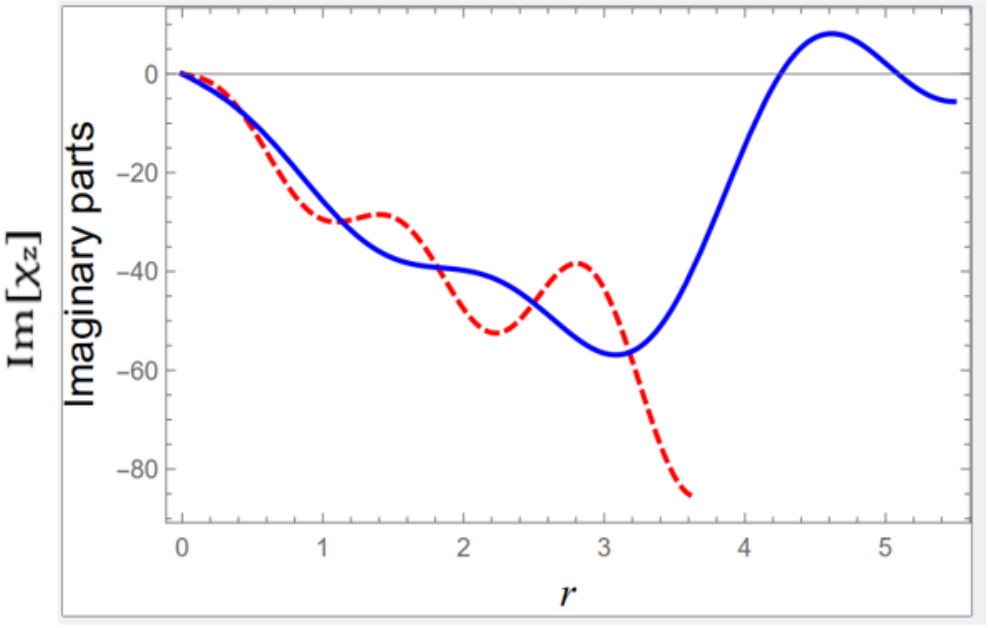

FIGURE 3.9: Imaginary part of the normal velocity matching condition with 30 terms (χ_1: left shell, dotted line; χ_2: right shell, blue line).

Chapter 4

Scattering of Non-axisymmetric Shell Radiation with Membrane Disc

Introduction

In Chapter 3, we analyzed acoustic scattering in a cylindrical membrane shell system, focusing on both transverse and longitudinal modes. Using MM techniques, the eigenvalue problem was solved, and the coefficients C_{qm} and D_{qm} were calculated using the Galerkin expansion method under clamped edge conditions. This chapter builds on that analysis by focusing exclusively on transverse modes (non-axisymmetric), which are critical for understanding the system's dynamic behavior in practical scenarios. The system consists of a finite expansion chamber surrounded by flexible membrane discs and two semi-infinite shells.. These flexible boundaries significantly influence wave propagation and energy transmission, making them essential for accurate modeling and analysis. The analysis separates the transverse modes into symmetric and anti-symmetric subproblems in order to simplify the issue. Because of this division, the governing equations are less complicated, making it possible to apply MM techniques more simply. These subproblems must be resolved in order to calculate the coefficients for the

transmitted and reflected waves, which give a numerical representation of the energy transmission and scattering across the expansion chamber. Furthermore, this chapter explores how the clamped edge conditions and the membrane's flexibility contribute to the overall acoustic scattering process. The findings from this analysis are particularly valuable for applications in noise control and vibration reduction, as they shed light on how symmetry and boundary conditions influence the acoustic performance of such systems.

4.1 Problem Formulation

The system under consideration consists of two semi-infinite flexible shells connected by a finite expansion chamber with a dimensional length of $2z_0$. The inlet shell occupies the region $0 \leq \rho \leq r_a, z \leq -z_0$, while the outlet shell lies in $0 \leq \rho \leq r_a, z \geq z_0$. The expansion chamber spans $-z_0 \leq z \leq z_0$ and $0 \leq \rho \leq r_b$, bounded by flexible membrane discs at $r_a \leq \rho \leq r_b, z = \pm z_0$. These membrane discs introduce dynamic boundary conditions, significantly influencing wave scattering and transmission within the system. In the inlet shell, the velocity potential χ_1 represents the incident wave as well as the reflected field at the initial interface. The scattered waves interact with the flexible shell and membrane discs, leading to complex wave coupling effects. Additionally, the transmitted field in the outlet shell is governed by the continuity conditions at the interfaces, ensuring conservation of acoustic energy.The velocity potential in the inlet shell can be expressed as follows:

$$\chi_1(\rho,\theta,z) = F_{1\ell}R_{1p\ell}(\rho)\cos(p\theta)e^{is_{1p\ell}(z+z_0)} + \sum_{p=1}^{\infty}\sum_{n=0}^{\infty} C_{pn}R_{1pn}(\rho)\cos(p\theta)e^{-is_{1pn}(z+z_0)}, \tag{4.1}$$

Here, ℓ stands for the fundamental mode ($\ell = 0$ or $\ell = 1$), $F_{1\ell}$ for the incident wave amplitude, C_{pn} for the amplitude of the n-th reflected mode, and τ_{1pn} for the formula $\sqrt{1 - s_{1pn}^2}$.

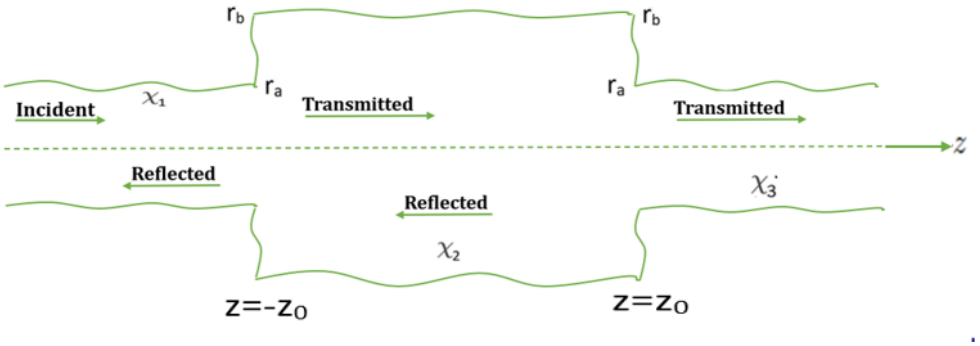

FIGURE 4.1: Physical arrangement of the system of expansion chambers between two shells.

In the expansion chamber, χ_2 characterizes both the waves reflected at the second junction and the transmitted waves coming from the first junction.

$$\chi_2(\rho,\theta,z) = \sum_{p=1}^{\infty}\sum_{n=0}^{\infty}\left(D_{pn}e^{-is_{2pn}(z)} + P_{pn}e^{is_{2pn}(z)}\right)R_{2pn}(\rho)\cos(p\theta). \tag{4.2}$$

In this case, D_{pn} and P_{pn} represent the respective strengths of the reflected and transmitted waves. Likewise, the expression for the velocity potential in the outlet shell, χ_3, is given by:

$$\chi_3(\rho,\theta,z) = \sum_{p=1}^{\infty}\sum_{n=0}^{\infty}E_{pn}R_{1pn}(\rho)\cos(p\theta)e^{-is_{1pn}(z-L)}, \tag{4.3}$$

where E_{pn} is the amplitude of the nth transmitted wave. The analysis is divided into two subproblems: symmetric and anti-symmetric expansion chambers.For the symmetric subproblem, a line of symmetry is established at $z = 0$ (as shown in Figure 4.2). Two incident waves are considered: one traveling from the left section ($z \leq -z_0$) directed toward the first junction, and the right section ($z \geq z_0$) directed toward the second junction. In the anti-symmetric subproblem, a phase shift of π is introduced to the wave from the right section, resulting in a negative amplitude. This creates an anti-symmetry line at $z = 0$ (as shown in Figure 4.3). These symmetry conditions simplify the equations, reducing the problem to a radial variation analysis. The reflection and transmission coefficients for both subproblems are subsequently utilized to determine the overall response of the expansion chamber system.

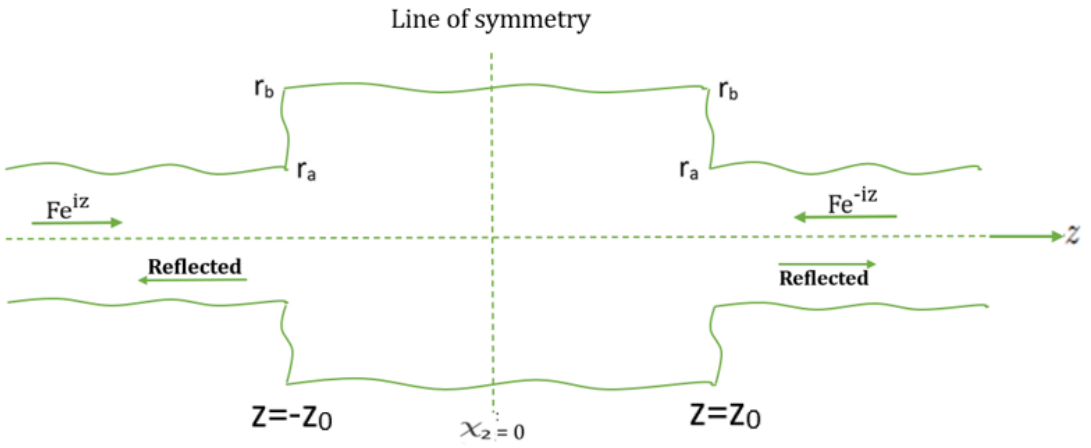

FIGURE 4.2: The symmetric subproblem's physical setup.

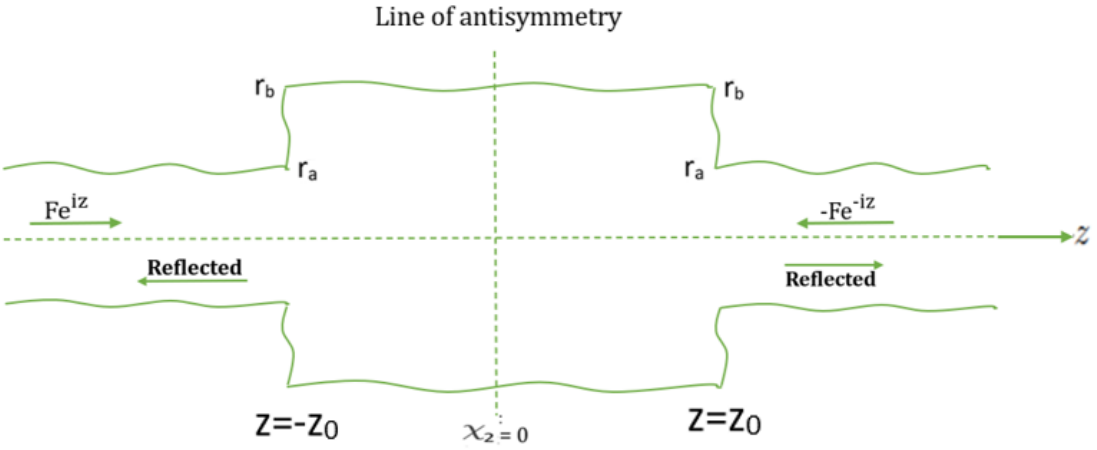

FIGURE 4.3: The antisymmetric subproblem's physical setup.

4.1.1 Symmetric Sub-problem

The symmetry of the subproblem allows for a simplification into an equivalent system that includes a sudden radius increase and a flexible end plate (see Figure 4.4). This subsection aims to calculate the energy radiated by a forcing wave at the point of the abrupt radius increase. The system consists of two semi-infinite shells: the left shell spans $0 \leq \rho \leq r_a$, $z \leq -z_0$, and the right shell spans $0 \leq \rho \leq r_b$, $-z_0 \leq z \leq 0$. The system is enclosed by a flexible membrane disc at $r_a \leq \rho \leq r_b$, $z = -z_0$, and a flexible plate at $0 \leq \rho \leq r_b$, $z = 0$. A wave propagating in the left shell, traveling in the positive z-direction toward the abrupt increase in radius, acts as the forcing.

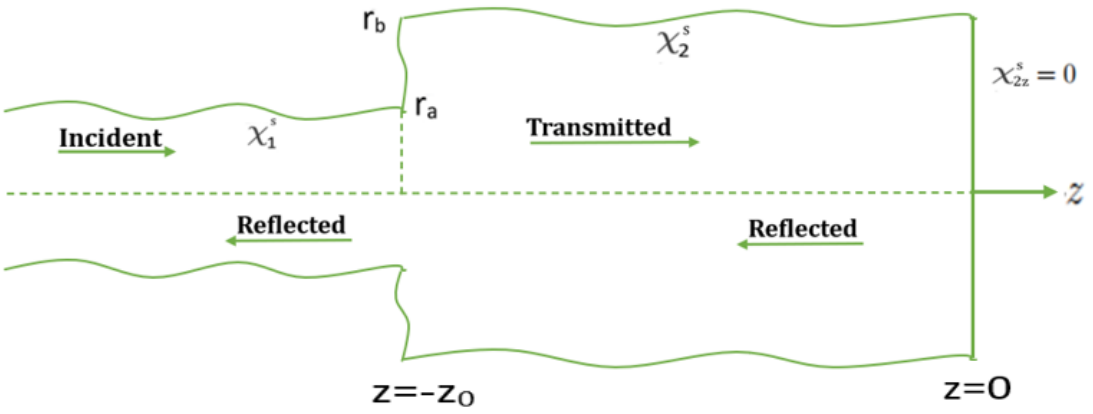

FIGURE 4.4: The simplified symmetric subproblem's physical setup.

The velocity potential in the left shell consists of both the incoming wave and the reflected field, expressed as: Due to the discontinuity at $z = -z_0$, part of the incident energy is transmitted into the right shell, while the remaining energy is scattered back into the left shell. The interaction between the shell flexibility and the membrane disc plays a crucial role in defining the reflection and transmission characteristics.

$$\chi_1^s(\rho,\theta,z) = F_{1\ell}R_{1p\ell}(\rho)\cos(p\theta)e^{is_{1p\ell}(z+z_0)} + \sum_{p=1}^{\infty}\sum_{n=0}^{\infty} C_{pn}^s R_{1pn}(\rho)\cos(p\theta)e^{-is_{1pn}(z+z_0)}, \tag{4.4}$$

where the superscript s refers to the symmetric subsystem. ℓ identifies the selected fundamental mode for forcing ($\ell = 0$ or $\ell = 1$), $F_{1\ell}$ represents the amplitude of the forcing wave. and C_{pn}^s is the amplitude of the nth reflected wave. The displacement components are as follows:

$$\begin{aligned}\varphi_1^s(\theta,z) = {} & U_{1p\ell}F_{1\ell}R_{1p\ell}(r_a)\cos(p\theta)e^{is_{1p\ell}(z+z_0)} \\ & - \sum_{p=1}^{\infty}\sum_{n=0}^{\infty} U_{1pn}C_{pn}^s R_{1pn}(r_a)\cos(p\theta)e^{-is_{1pn}(z+z_0)}.\end{aligned} \tag{4.5}$$

$$\begin{aligned}\vartheta_1^s(\theta,z) = {} & V_{1p\ell}F_{1\ell}R_{1p\ell}(r_a)\sin(p\theta)e^{is_{1p\ell}(z+z_0)} \\ & + \sum_{p=1}^{\infty}\sum_{n=0}^{\infty} V_{1pn}C_{pn}^s R_{1pn}(r_a)\sin(p\theta)e^{-is_{1pn}(z+z_0)}.\end{aligned} \tag{4.6}$$

$$\Omega_1^s(\theta,z) = -F_{1\ell}R_{1p\ell}(r_a)\cos(p\theta)e^{is_{1p\ell}(z+z_0)} - \sum_{p=1}^{\infty}\sum_{n=0}^{\infty} C_{pn}^s R_{1pn}(r_a)\cos(p\theta)e^{-is_{1pn}(z+z_0)}. \tag{4.7}$$

The velocity potential χ_2^s for the finite section consists of waves transmitted across the junction and those reflected from the plate at $z = 0$, expressed as:

$$\chi_2^s(\rho,\theta,z) = \sum_{p=1}^{\infty}\sum_{n=0}^{\infty} D_{pn}^s R_{2pn}(\rho)\cos(p\theta)e^{-is_{2pn}z} + \sum_{p=1}^{\infty}\sum_{n=0}^{\infty} P_{pn}^s R_{2pn}(\rho)\cos(p\theta)e^{is_{2pn}z}, \tag{4.8}$$

The transmitted and reflected wave amplitudes are denoted by P_{pn}^s and D_{pn}^s, respectively. Applying the boundary condition $\chi_2^s = 0$ at the rigid duct simplifies the velocity potential χ_2^s to: Since the duct is rigid, this condition implies that no normal velocity exists at its surface, restricting the transmitted wave behavior and influencing the overall wave propagation in the right shell.

$$\frac{\partial\chi_2^s}{\partial z} = i\sum_{p=1}^{\infty}\sum_{n=0}^{\infty}\left(-D_{pn}^s + P_{pn}^s\right)s_{2pn}\cos(p\theta)R_{2pn}(\rho) = 0. \tag{4.9}$$

This condition is satisfied only when $D_{pn} = P_{pn}$, allowing the velocity potential χ_2^s to be simplified to:

$$\chi_2^s = 2\sum_{p=1}^{\infty}\sum_{n=0}^{\infty} D_{pn}^s R_{2pn}(\rho)\cos(p\theta)\frac{\cos(s_{2pn}z)}{\sin(s_{2pn}z_0)}. \tag{4.10}$$

The expressions for the axial and radial displacements in the right-hand section are given by:

$$\varphi_2^s(\theta,z) = 2\sum_{p=1}^{\infty}\sum_{n=0}^{\infty} W_{2pn}D_{pn}^s R_{2pn}(r_b)\cos(p\theta)\frac{\cos(s_{2pn}z)}{\sin(s_{2pn}z_0)}, \tag{4.11}$$

$$\vartheta_2^s(\theta,z) = 2\sum_{p=1}^{\infty}\sum_{n=0}^{\infty} X_{2pn}D_{pn}^s R_{2pn}(r_b)\sin(p\theta)\frac{\cos(s_{2pn}z)}{\sin(s_{2pn}z_0)}, \tag{4.12}$$

$$\Omega_2^s(\theta,z) = -2\sum_{p=1}^{\infty}\sum_{n=0}^{\infty} D_{pn}^s R_{2pn}(r_b)\cos(p\theta)\frac{\cos(s_{2pn}z)}{\sin(s_{2pn}z_0)}. \tag{4.13}$$

At $z = -z_0$, the continuity of pressure across the interface is ensured by equating the velocity potentials:

$$\chi_1^s(\theta, -z_0) = \chi_2^s(\theta, -z_0). \tag{4.14}$$

The pressure condition defined in terms of the eigenfunction of equation (4.14) is obtained by applying the velocity potentials χ_1^s and χ_2^s to it.

$$F_{1\ell} R_{1p\ell}(\rho)\cos(p\theta) + \sum_{p=1}^{\infty}\sum_{n=0}^{\infty} C_{pn}^{s} R_{1pn}(\rho)\cos(p\theta) = 2\sum_{p=1}^{\infty}\sum_{n=0}^{\infty} D_{pn}^{s} R_{2pn}(\rho)\cos(p\theta)\frac{\cos(s_{2pn}z)}{\sin(s_{2pn}z_0)}, \quad 0 \le \rho \le r_a. \tag{4.15}$$

Multiplying equation (4.15) by $\cos(q\theta)$ and integrating over $0 \le \theta \le 2\pi$, followed by some rearrangements, gives:

$$F_{1\ell} R_{1p\ell}(\rho)\delta_{pq} + \sum_{n=0}^{\infty} C_{qn}^{s} R_{1qn}(\rho) = 2\sum_{n=0}^{\infty} D_{qn}^{s} R_{2qn}(\rho)\frac{\cos(s_{2pn}z)}{\sin(s_{2pn}z_0)}, \tag{4.16}$$

where

$$\int_0^{2\pi} \cos(p\theta)\cos(q\theta) = \pi\delta_{pq}.$$

Multiplying both sides of (4.16) by $\frac{\alpha}{r_a}\rho R_{1qm}(\rho)$ and integrating over $0 \le \rho \le r_a$ gives:

$$F_{1\ell}\delta_{pq}\frac{\alpha}{r_a}\int_0^{r_a} \rho R_{1qm}R_{1p\ell}d\rho + \sum_{p=1}^{\infty}\sum_{n=0}^{\infty} C_{qn}^{s}\frac{\alpha}{r_a}\int_0^{r_a}\rho R_{1qm}R_{1qn}d\rho = 2\frac{\alpha}{r_a}\sum_{n=0}^{\infty} D_{qn}^{s}P_{mn}\frac{\cos(s_{2pn}z)}{\sin(s_{2pn}z_0)}. \tag{4.17}$$

Using the orthogonality relation from (3.54), the left-hand integrals simplify to:

$$F_{1\ell}\delta_{pq}\left[\delta_{m\ell}A_{q\ell} - \frac{H_q(s_{1m}, s_{1\ell})R'_{1p\ell}R'_{1qm}}{\eta_p(s_{1\ell})\eta_q(s_{1m})}\right] + \sum_{n=0}^{\infty} C_{qn}^{s}\left[\delta_{mn}A_{qn} - \frac{H_q(s_{1m}, s_{1n})R'_{1qn}R'_{1qm}}{\eta_q(s_{1n})\eta_q(s_{1m})}\right] = 2\frac{\alpha}{r_a}\sum_{n=0}^{\infty} D_{qn}^{s}P_{mn}\frac{\cos(s_{2pn}z)}{\sin(s_{2pn}z_0)}. \tag{4.18}$$

From this, we obtain:

$$C^s_{qm} = -\frac{F_{1\ell}\delta_{pq}\delta_{m\ell}A_{q\ell}}{A_{qm}} + \frac{2\alpha}{r_a A_{qm}}\sum_{n=0}^{\infty} D^s_{qn}P_{mn}\frac{\cos(s_{2qn}z_0)}{\sin(s_{2qn}z_0)} + \frac{R'_{1qm}(r_a)}{\eta_q(s_{1m})A_{qm}}\left[H^6_q(s_{1m})E^s_1 + H^4_q(s_{1m})E^s_2 + H^2_q(s_{1m})E^s_3 + H^0_q(s_{1m})E^s_4\right], \quad (4.19)$$

where

$$E^s_1 = \frac{F_{1\ell}\delta_{pq}s^6_{1p\ell}R'_{1p\ell}(r_a)}{\eta_p(s_{1\ell})} + \sum_{n=0}^{\infty}\frac{C^s_{qn}s^6_{1qn}R'_{1qn}(r_a)}{\eta_q(s_{1n})},$$

$$E^s_2 = \frac{F_{1\ell}\delta_{pq}s^4_{1p\ell}R'_{1p\ell}r_(a)}{\eta_p(s_{1\ell})} + \sum_{n=0}^{\infty}\frac{C^s_{qn}s^4_{1qn}R'_{1qn}(r_a)}{\eta_p(s_{1n})},$$

$$E^s_3 = \frac{F_{1\ell}\delta_{pq}s^2_{1p\ell}R'_{1p\ell}(r_a)}{\eta_p(s_{1\ell})} + \sum_{n=0}^{\infty}\frac{C^s_{qn}s^2_{1qn}R'_{1qn}(r_a)}{\eta_q(s_{1n})},$$

$$E^s_4 = \frac{F_{1\ell}\delta_{pq}R'_{1p\ell}(r_a)}{\eta_p(s_{1\ell})} + \sum_{n=0}^{\infty}\frac{C^s_{qn}R'_{1qn}(r_a)}{\eta_q(s_{1n})}.$$

At the interface, the continuity of the normal velocity component in the fluid region is maintained while fulfilling the vertical membrane condition.

$$\left(\frac{\partial^2}{\partial\rho^2} + \frac{1}{\rho}\frac{\partial}{\partial\rho} + \frac{1}{\rho^2}\frac{\partial^2}{\partial\theta^2} + \mu^2\right)U^s(\rho,\theta) = \gamma\chi^s_2, \quad \text{for} \quad z = -z_0, \quad r_a \le \rho \le r_b, \quad (4.20)$$

where $U(\rho,\theta)$ represents the radial and angular displacements. The displacement $U^s(\rho,\theta)$ is expressed as a Fourier series in both ρ and θ:

$$U^s(\rho,\theta) = \sum_{n=1}^{\infty}\sum_{m=0}^{\infty} g^s_{mn}\chi_{mn}. \quad (4.21)$$

This satisfies the boundary conditions $U^s(r_a,\theta) = U^s(r_b,\theta) = 0$. Substituting this expansion and the eigenfunction expansion from equation (4.10) into the membrane condition yields:

$$\sum_{n=0}^{\infty}\sum_{m=0}^{\infty} g^s_{mn}\left(\mu^2 - \lambda^2_{mn}\right)\chi_{mn} = 2\gamma\sum_{p=1}^{\infty}\sum_{n=0}^{\infty} D^s_{pn}R_{2pn}(\rho)\cos(p\theta)\frac{\cos(s_{2pn}z_0)}{\sin(s_{2pn}z_0)}. \quad (4.22)$$

Both sides of equation (4.22) are multiplied by $\rho\chi_{m'n'}$ and integrated across the range $r_a \le \rho \le r_b$ and $0 \le \theta \le 2\pi$ to obtain:

$$\sum_{m=0}^{\infty}\sum_{n=0}^{\infty} g_{mn}^{s}\left(\mu^{2}-\lambda_{mn}^{2}\right)\delta_{mm'}\delta_{nn'}N_{mn}=2\gamma\sum_{p=1}^{\infty}\sum_{n=0}^{\infty} D_{pn}^{s}I_{m'nn'}\delta_{m'p}\cot(s_{2pn}z_{0}), \tag{4.23}$$

After rearranging equation (4.23), we find the expression for g_{mn}^{s}:

$$g_{m'n'}^{s}=\frac{2\gamma}{\Delta_{m'n'}N_{m'n'}}\sum_{n=0}^{\infty}\cot(s_{2m'n}z_{0})D_{m'n}^{s}I_{m'nn'}. \tag{4.24}$$

The normal velocity component is governed by the following condition:

$$\frac{\partial\chi_{2}^{s}}{\partial z}(\rho,\theta,-z_{0})=\begin{cases}\frac{\partial\chi_{1}^{s}}{\partial z}(\rho,\theta,-z_{0}), & \text{if } 0\leq\rho\leq r_{a},\\ U^{s}(\rho,\theta), & \text{if } r_{a}\leq\rho\leq r_{b}.\end{cases} \tag{4.25}$$

By substituting the values of (4.4), (4.10), and (4.21) into (4.25), the resulting equation is:

$$\begin{aligned}2\sum_{n=0}^{\infty}s_{2qn}D_{qn}^{s}R_{2qn}(\rho)=is_{1p\ell}F_{1\ell}\delta_{pq}R_{1p\ell}(\rho)-i\sum_{n=0}^{\infty}C_{qn}^{s}s_{1qn}R_{1qn}(\rho)\\ +\sum_{n=0}^{\infty}g_{qn}^{s}R_{qn}(\rho).\end{aligned} \tag{4.26}$$

Multiplying equation (4.26) by $\frac{\alpha}{r_b}\rho R_{2qm}(\rho)$ and performing the integration over the range $0\leq\rho\leq r_b$, along with some rearrangements and the use of the orthogonality relation (3.61), we obtain:

$$\begin{aligned}D_{qm}^{s}=\frac{i\alpha s_{1p\ell}F_{1\ell}P_{\ell m}\delta_{pq}}{2r_{b}s_{2qm}B_{qm}}+\frac{\alpha}{2r_{b}}\sum_{n=0}^{\infty}\frac{g_{qn}^{s}h_{qmn}}{s_{2qm}B_{qm}}-\frac{i\alpha}{2r_{b}}\sum_{n=0}^{\infty}\frac{s_{1qn}C_{qn}^{s}P_{nm}}{s_{2qm}B_{qm}}+\\ \frac{R'_{2qm}(r_{b})}{\eta_{q}(s_{2m})}\left[\frac{H_{q}^{6}(s_{2m})E_{5}^{s}+H_{q}^{4}(s_{2m})E_{6}^{s}+H_{q}^{2}(s_{2m})E_{7}^{s}+H_{q}^{0}(s_{2m})E_{8}^{s}}{s_{2qm}B_{qm}}\right],\end{aligned} \tag{4.27}$$

where

$$E_{5}^{s}=\frac{\sum_{n=0}^{\infty}D_{qn}^{s}s_{2qn}s_{2qn}^{6}R'_{2qn}(r_{b})}{\eta_{q}(s_{2n})},\ E_{6}^{s}=\frac{\sum_{n=0}^{\infty}D_{qn}^{s}s_{2qn}s_{2qn}^{4}R'_{2qn}(r_{b})}{\eta_{q}(s_{2n})},$$

$$E_{7}^{s}=\frac{\sum_{n=0}^{\infty}D_{qn}^{s}s_{2qn}s_{2qn}^{2}R'_{2qn}(r_{b})}{\eta_{q}(s_{2n})},\ E_{8}^{s}=\frac{\sum_{n=0}^{\infty}D_{qn}^{s}s_{2qn}R'_{2qn}(r_{b})}{\eta_{q}(s_{2n})}.$$

The interface conditions determine the constants: E_1^s to E_4^s for the left shell edge, and E_5^s to E_8^s for the right shell edge.

By utilizing the displacement equations from (4.5), (4.6), (4.11), and (4.12), the clamped edge conditions can be expressed as:

$$\varphi_1^s = \vartheta_1^s = \frac{\partial \chi_1^s}{\partial \rho} = \frac{\partial^2 \chi_1^s}{\partial \rho \partial z} = 0, \quad 0 \le \rho \le r_a, \quad z \le 0. \tag{4.28}$$

$$\varphi_2^s = \vartheta_2^s = \frac{\partial \chi_2^s}{\partial \rho} = \frac{\partial^2 \chi_2^s}{\partial \rho \partial z} = 0, \quad 0 \le \rho \le r_b, \quad z \ge 0. \tag{4.29}$$

Applying the clamped edge conditions from (4.28) leads to the following system of equations, which can be written in matrix form as:

$$\begin{bmatrix} S_{11} & S_{12} & S_{13} & S_{14} \\ S_{21} & S_{22} & S_{23} & S_{24} \\ S_{31} & S_{32} & S_{33} & S_{34} \\ S_{41} & S_{42} & S_{43} & S_{44} \end{bmatrix} \begin{bmatrix} E_1^s \\ E_2^s \\ E_3^s \\ E_4^s \end{bmatrix} = \begin{bmatrix} \xi_{11} \\ \xi_{21} \\ \xi_{31} \\ \xi_{41} \end{bmatrix}. \tag{4.30}$$

where

$$\xi_{11} = F_{1\ell}\delta_{pq}\left[W_{1p\ell}R_{1p\ell}(r_a) + W_{1q\ell}R_{1q\ell}(r_a)\right] - \frac{2\alpha}{r_a}\sum_{m=0}^{\infty}\sum_{n=0}^{\infty}\frac{D_{qn}^s W_{1qm}R_{1qm}(r_a)P_{mn}\cot(s_{2qn}z_0)}{A_{qm}}.$$

$$\xi_{21} = F_{1\ell}\delta_{pq}\left[X_{1q\ell}R_{1q\ell}(r_a) - X_{1p\ell}R_{1p\ell}(r_a)\right] - \frac{2\alpha}{r_a}\sum_{m=0}^{\infty}\sum_{n=0}^{\infty}\frac{D_{qn}^s X_{1qm}R_{1qm}(r_a)P_{mn}\cot(s_{2qn}z_0)}{A_{qm}}.$$

$$\xi_{31} = F_{1\ell}\delta_{pq}\left[R'_{1q\ell}(r_a) - R'_{1p\ell}(r_a)\right] - \frac{2\alpha}{r_a}\sum_{m=0}^{\infty}\sum_{n=0}^{\infty}\frac{D_{qn}^s R'_{1qm}(r_a)P_{mn}\cot(s_{2qn}z_0)}{A_{qm}},$$

$$\xi_{41} = F_{1\ell}\delta_{pq}\left[R'_{1q\ell}(r_a)s_{1q\ell} + R'_{1p\ell}(r_a)s_{1p\ell}\right] - \frac{2\alpha}{r_a}\sum_{m=0}^{\infty}\sum_{n=0}^{\infty}\frac{D_{qn}^s R'_{1qm}(r_a)s_{1qm}P_{mn}\cot(s_{2qn}z_0)}{A_{qm}}.$$

The remaining clamped edge conditions from (4.29) yield another system of equations in matrix form as:

$$\begin{bmatrix} \Psi^s_{11} & \Psi^s_{12} & \Psi^s_{13} & \Psi^s_{14} \\ \Psi^s_{21} & \Psi^s_{22} & \Psi^s_{23} & \Psi^a_{24} \\ \Psi^s_{31} & \Psi^s_{32} & \Psi^s_{33} & \Psi^a_{34} \\ \Psi^s_{41} & \Psi^s_{42} & \Psi^s_{43} & \Psi^a_{44} \end{bmatrix} \begin{bmatrix} E^s_5 \\ E^s_6 \\ E^s_7 \\ E^s_8 \end{bmatrix} = \begin{bmatrix} \Gamma_{11} \\ \Gamma_{21} \\ \Gamma_{31} \\ \Gamma_{41} \end{bmatrix}. \tag{4.31}$$

where

$$\Psi^s_{11} = \sum_{m=0}^{\infty} \frac{W_{2qm} R_{2qm}(r_b) \cot(s_{2qm} z_0) H^6_q(s_{2m}) R'_{2qm}(r_b)}{\eta_q(s_{2m}) B_{qm} s_{2qm}},$$

$$\Psi^s_{12} = \sum_{m=0}^{\infty} \frac{W_{2qm} R_{2qm}(r_b) \cot(s_{2qm} z_0) H^4_q(s_{2m}) R'_{2qm}(r_b)}{\eta_q(s_{2m}) B_{qm} s_{2qm}},$$

$$\Psi^s_{13} = \sum_{m=0}^{\infty} \frac{W_{2qm} R_{2qm}(r_b) \cot(s_{2qm} z_0) H^2_q(s_{2m}) R'_{2qm}(r_b)}{\eta_q(s_{2m}) B_{qm} s_{2qm}},$$

$$\Psi^s_{14} = \sum_{m=0}^{\infty} \frac{W_{2qm} R_{2qm}(r_b) \cot(s_{2qm} z_0) H^0_q(s_{2m}) R'_{2qm}(r_b)}{\eta_q(s_{2m}) B_{qm} s_{2qm}},$$

$$\Psi^s_{21} = \sum_{m=0}^{\infty} \frac{X_{2qm} R_{2qm}(r_b) \cot(s_{2qm} z_0) H^6_q(s_{2m}) R'_{2qm}(r_b)}{\eta_q(s_{2m}) B_{qm} s_{2qm}},$$

$$\Psi^s_{22} = \sum_{m=0}^{\infty} \frac{X_{2qm} R_{2qm}(r_b) \cot(s_{2qm} z_0) H^4_q(s_{2m}) R'_{2qm}(r_b)}{\eta_q(s_{2m}) B_{qm} s_{2qm}},$$

$$\Psi^s_{23} = \sum_{m=0}^{\infty} \frac{X_{2qm} R_{2qm}(r_b) \cot(s_{2qm} z_0) H^2_q(s_{2m}) R'_{2qm}(r_b)}{\eta_q(s_{2m}) B_{qm} s_{2qm}},$$

$$\Psi^s_{24} = \sum_{m=0}^{\infty} \frac{X_{2qm} R_{2qm}(r_b) \cot(s_{2qm} z_0) H^0_q(s_{2m}) R'_{2qm}(r_b)}{\eta_q(s_{2m}) B_{qm} s_{2qm}},$$

$$\Psi^s_{31} = \sum_{m=0}^{\infty} \frac{R'_{2qm}(r_b) \cot(s_{2qm} z_0) H^6_q(s_{2m}) R'_{2qm}(r_b)}{\eta_q(s_{2m}) B_{qm} s_{2qm}},$$

$$\Psi^s_{32} = \sum_{m=0}^{\infty} \frac{R'_{2qm}(r_b) \cot(s_{2qm} z_0) H^4_q(s_{2m}) R'_{2qm}(r_b)}{\eta_q(s_{2m}) B_{qm} s_{2qm}},$$

$$\Psi^s_{33} = \sum_{m=0}^{\infty} \frac{R'_{2qm}(r_b) \cot(s_{2qm} z_0) H^2_q(s_{2m}) R'_{2qm}(r_b)}{\eta_q(s_{2m}) B_{qm} s_{2qm}},$$

$$\Psi^s_{34} = \sum_{m=0}^{\infty} \frac{R'_{2qm}(r_b) \cot(s_{2qm} z_0) H^0_q(s_{2m}) R'_{2qm}(r_b)}{\eta_q(s_{2m}) B_{qm} s_{2qm}}.$$

$$\Psi^s_{41}=\sum_{m=0}^{\infty}\frac{R'_{2qm}(r_b)H^6_q(s_{2m})R'_{2qm}(r_b)}{\eta_q(s_{2m})B_{qm}},\quad \Psi^s_{42}=\sum_{m=0}^{\infty}\frac{R'_{2qm}(r_b)H^4_q(s_{2m})R'_{2qm}(r_b)}{\eta_q(s_{2m})B_{qm}},$$

$$\Psi^s_{43}=\sum_{m=0}^{\infty}\frac{R'_{2qm}(r_b)H^2_q(s_{2m})R'_{2qm}(r_b)}{\eta_q(s_{2m})B_{qm}},\quad \Psi^s_{44}=\sum_{m=0}^{\infty}\frac{R'_{2qm}(r_b)H^0_q(s_{2m})R'_{2qm}(r_b)}{\eta_q(s_{2m})B_{qm}}.$$

$$\begin{aligned}\Gamma_{11}=&-\frac{i\alpha}{2r_b}F_{1\ell}\delta_{pq}s_{1p\ell}\sum_{m=0}^{\infty}\frac{W_{2qm}R_{2qm}(r_b)P_{\ell m}\cot(s_{2qm}z_0)}{B_{qm}s_{2qm}}\\&+\frac{i\alpha}{2r_b}\sum_{m=0}^{\infty}\sum_{n=0}^{\infty}\frac{C^s_{qn}W_{2qm}R_{2qm}(r_b)s_{1qn}P_{nm}\cot(s_{2qm}z_0)}{B_{qm}s_{2qm}}\\&-\frac{\alpha}{2r_b}\sum_{m=0}^{\infty}\sum_{n=0}^{\infty}\frac{W_{2qm}R_{2qm}(r_b)g^s_{qn}h_{qmn}\cot(s_{2qm}z_0)}{B_{qm}s_{2qm}}.\end{aligned}$$

$$\begin{aligned}\Gamma_{21}=&-\frac{i\alpha}{2r_b}F_{1\ell}\delta_{pq}s_{1p\ell}\sum_{m=0}^{\infty}\frac{V_{2qm}R_{2qm}(r_b)P_{\ell m}\cot(s_{2qm}z_0)}{B_{qm}s_{2qm}}\\&-\frac{\alpha}{2r_b}\sum_{m=0}^{\infty}\sum_{n=0}^{\infty}\frac{V_{2qm}R_{2qm}(r_b)g^s_{qn}h_{qmn}\cot(s_{2qm}z_0)}{B_{qm}s_{2qm}}\\&+\frac{i\alpha}{2r_b}\sum_{m=0}^{\infty}\sum_{n=0}^{\infty}\frac{C^s_{qn}V_{2qm}R_{2qm}(r_b)s_{1qn}P_{nm}\cot(s_{2qm}z_0)}{B_{qm}s_{2qm}}.\end{aligned}$$

$$\begin{aligned}\Gamma_{31}=&-\frac{i\alpha}{2r_b}F_{1\ell}\delta_{pq}s_{1p\ell}\sum_{m=0}^{\infty}\frac{R'_{2qm}(r_b)P_{\ell m}\cot(s_{2qm}z_0)}{B_{qm}s_{2qm}}\\&-\frac{\alpha}{2r_b}\sum_{m=0}^{\infty}\sum_{n=0}^{\infty}\frac{R'_{2qm}(r_b)g^s_{qn}h_{qmn}\cot(s_{2qm}z_0)}{B_{qm}s_{2qm}}\\&+\frac{i\alpha}{2r_b}\sum_{m=0}^{\infty}\sum_{n=0}^{\infty}\frac{C^s_{qn}R'_{2qm}(r_b)s_{1qn}P_{nm}\cot(s_{2qm}z_0)}{B_{qm}s_{2qm}}.\end{aligned}$$

$$\begin{aligned}\Gamma_{41}=&-\frac{i\alpha}{2r_b}F_{1\ell}\delta_{pq}s_{1p\ell}\sum_{m=0}^{\infty}\frac{R'_{2qm}(r_b)P_{\ell m}}{B_{qm}}-\frac{\alpha}{2r_b}\sum_{m=0}^{\infty}\sum_{n=0}^{\infty}\frac{R'_{2qm}(r_b)g^s_{qn}h_{qmn}}{B_{qm}}\\&+\frac{i\alpha}{2r_b}\sum_{m=0}^{\infty}\sum_{n=0}^{\infty}\frac{C^s_{qn}R'_{2qm}(r_b)s_{1qn}P_{nm}}{B_{qm}},\end{aligned}$$

To determine the mth amplitude of the reflected field (C_{qm}) and the transmitted field (D_{qm}), equations (4.19) and (4.27) are truncated and solved utilizing the

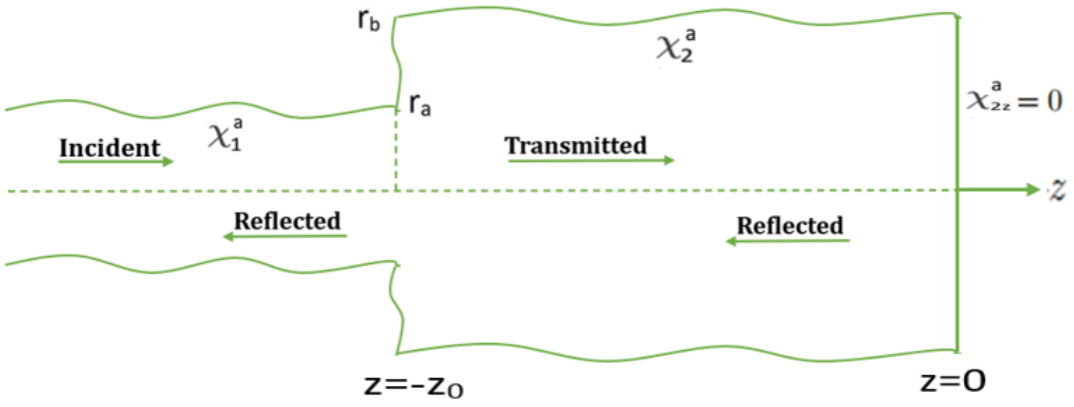

FIGURE 4.5: The simplified antisymmetric subproblem's physical setup.

constants E_1^s to E_8^s.

4.1.2 Antisymmetric Subproblem

This subproblem's antisymmetric nature allows it to be modeled as a system with a sharp radius discontinuity, enclosed by a flexible membrane disc and a sound-reflecting end plate (refer to Figure 4.5). This subsection aims to analyze the emitted energy at the radius discontinuity due to a forcing wave.The system consists of two unbounded shells, with the left shell extending from $0 \leq \rho \leq r_a$ and $z \leq -z_0$, while the right shell extends from $0 \leq \rho \leq r_b$ and $-z_0 \leq z \leq 0$. For $0 \leq \rho \leq r_b$. A sound-absorbing end plate is located at $0 \leq \rho \leq r_b$, and a membrane disc stretches across $r_a \leq \rho \leq r_b$ at $z = -z_0$. A wave propagating in the positive z-direction within the left shell initiates the forcing, moving towards the radius discontinuity. The left shell's velocity potential is expressed as:

$$\chi_1^a(\rho,\theta,z) = F_{1\ell}R_{1p\ell}(\rho)\cos(p\theta)e^{is_{1p\ell}(z+z_0)} + \sum_{p=1}^{\infty}\sum_{n=0}^{\infty} C_{pn}^a R_{1pn}(\rho)\cos(p\theta)e^{-is_{1pn}(z+z_0)}, \tag{4.32}$$

where the superscript a denotes the antisymmetric subsystem, ℓ specifies the fundamental mode for forcing ($\ell = 0$ or $\ell = 1$), the amplitude of the forcing wave is represented by $F_{1\ell}$, and the Reflection amplitude of the nth wave in the antisymmetric subsystem is indicated by C_{pn}^a. For the finite section, the velocity potential resembles that of the symmetric case but replaces $\cos(s_{2pn}z)$ with $i\sin(s_{2pn}z)$:

$$\chi_2^a = 2i \sum_{p=1}^{\infty} \sum_{n=0}^{\infty} D_{pn}^a R_{2pn}(\rho) \cos(p\theta) \frac{\sin(s_{2pn} z)}{\cos(s_{2pn} z_0)}, \tag{4.33}$$

ensuring the acoustic compliance condition, $\chi_2^a = 0$, at $z = 0$.

The displacements for the right-hand section in terms of χ_2^a are given by:

$$\varphi_2^a = 2i \sum_{p=1}^{\infty} \sum_{n=0}^{\infty} W_{2pn} D_{pn}^a R_{2pn}(r_b) \cos(p\theta) \frac{\sin(s_{2pn} z)}{\cos(s_{2pn} z_0)}, \tag{4.34}$$

$$\vartheta_2^a = 2i \sum_{p=1}^{\infty} \sum_{n=0}^{\infty} X_{2n} D_n^a R_{2n}(r_b) \sin(p\theta) \frac{\sin(s_{2pn} z)}{\cos(s_{2pn} z_0)}. \tag{4.35}$$

The solution steps mirror those of the symmetric problem. Applying the pressure condition yields the reflected wave amplitude equation:

$$\begin{aligned} C_{qm}^a = &- \frac{F_{1\ell} \delta_{pq} \delta_{m\ell} A_{q\ell}}{A_{qm}} + \frac{R'_{1qm}(r_a)}{\eta_q(s_{1m}) A_{qm}} \Big[H_q^6(s_{1m}) E_1^a + H_q^4(s_{1m}) E_2^a \\ &+ H_q^2(s_{1m}) E_3^a + H_q^0(s_{1m}) E_4^a \Big] - \frac{2i\alpha}{a A_{qm}} \sum_{n=0}^{\infty} D_{qn}^a P_{mn} \tan(s_{2qn} z_0). \end{aligned} \tag{4.36}$$

where,

$$E_1^a = \frac{F_{1\ell} \delta_{pq} s_{1p\ell}^6 R'_{1p\ell}(r_a)}{\eta_q(s_{1\ell})} + \sum_{n=0}^{\infty} \frac{C_{qn}^a s_{1qn}^6 R'_{1qn}(r_a)}{\eta_q(s_{1n})},$$

$$E_2^a = \frac{F_{1\ell} \delta_{pq} s_{1p\ell}^4 R'_{1p\ell}(r_a)}{\eta_q(s_{1\ell})} + \sum_{n=0}^{\infty} \frac{C_{qn}^a s_{1qn}^4 R'_{1qn}(r_a)}{\eta_p(s_{1n})},$$

$$E_3^a = \frac{F_{1\ell} \delta_{pq} s_{1p\ell}^2 R'_{1p\ell}(r_a)}{\eta_q(s_{1\ell})} + \sum_{n=0}^{\infty} \frac{C_{qn}^a s_{1qn}^2 R'_{1qn}(r_a)}{\eta_q(s_{1n})},$$

$$E_4^a = \frac{F_{1\ell} \delta_{pq} R'_{1p\ell}(r_a)}{\eta_q(s_{1\ell})} + \sum_{n=0}^{\infty} \frac{C_{qn}^a R'_{1qn}(r_a)}{\eta_q(s_{1n})}.$$

Similarly, applying the velocity condition gives:

$$D^a_{qm} = \frac{\alpha s_{1p\ell} F_{1\ell} \delta_{pq} P_{\ell m}}{2 r_b s_{2qm} B_{qm}} - \frac{i\alpha}{2r_b} \sum_{n=0}^{\infty} \frac{g^a_{qn} h_{mn}}{s_{2qm} B_{qm}} - \frac{\alpha}{2r_b} \sum_{n=0}^{\infty} \frac{s_{1qn} C^a_{qn} P_{nm}}{s_{2qm} B_{qm}} + \frac{R'_{2qm}(r_b)}{\eta_q(s_{2m})} \left[\frac{H^6_q(s_{2m}) E^a_5 + H^q_p(s_{2m}) E^a_6 + H^2_q(s_{2m}) E^a_7 + H^0_q(s_{2m}) E^a_8}{s_{2qm} B_{qm}} \right]. \quad (4.37)$$

where

$$E^a_5 = \frac{\sum_{n=0}^{\infty} D^a_{qn} s_{2qn} s^6_{2qn} R'_{2qn}(r_b)}{\eta_q(s_{2n})}, \quad E^a_6 = \frac{\sum_{n=0}^{\infty} D^a_{qn} s_{2qn} s^4_{2qn} R'_{2qn}(r_b)}{\eta_q(s_{2n})},$$

$$E^a_7 = \frac{\sum_{n=0}^{\infty} D^a_{qn} s_{2qn} s^2_{2qn} R'_{2qn}(r_b)}{\eta_q(s_{2n})}, \quad E^a_8 = \frac{\sum_{n=0}^{\infty} D^a_{qn} s_{2qn} R'_{2qn}(r_b)}{\eta_q(s_{2n})}.$$

The function $U^a_1(\rho, \theta)$ is expressed as:

$$U^a_1(\rho, \theta) = \sum_{m=0}^{\infty} \sum_{n=0}^{\infty} g^a_{mn} \chi_{mn},$$

where

$$g^a_{mn} = \frac{2i\gamma}{\Delta_{m'n'} N_{m'n'}} \sum_{n=0}^{\infty} D^a_{m'n} I_{m'nn'} \tan(s_{2m'n} z_0).$$

The constants E^a_1 to E^a_4 arise from the left shell's edge conditions, while E^a_5 to E^a_8 are derived from the right shell's edge conditions.

Clamped Edges

$$\varphi^a_1 = \vartheta^a_1 = \chi^a_{1\rho} = \chi^a_{1\rho z} = 0, \quad 0 \le \rho \le a.$$

$$\varphi^a_2 = \vartheta^a_2 = \chi^a_{2\rho} = \chi^a_{2\rho z} = 0, \quad 0 \le r \le b.$$

After applying the edge condition in region I, the resulting system of equations is in matrix form as:

$$\begin{bmatrix} S_{11} & S_{12} & S_{13} & S_{14} \\ S_{21} & S_{22} & S_{23} & S_{24} \\ S_{31} & S_{32} & S_{33} & S_{34} \\ S_{41} & S_{42} & S_{43} & S_{44} \end{bmatrix} \begin{bmatrix} E_1^a \\ E_2^a \\ E_3^a \\ E_4^a \end{bmatrix} = \begin{bmatrix} \Lambda_{11} \\ \Lambda_{21} \\ \Lambda_{31} \\ \Lambda_{41} \end{bmatrix}, \tag{4.38}$$

where the Λ_{ij} terms are given by:

$$\Lambda_{11} = F_{1\ell}\delta_{pq}\Big[W_{1p\ell}R_{1p\ell}(r_a) + W_{1q\ell}R_{1q\ell}(r_a)\Big] + \frac{2i\alpha}{r_a}\sum_{m=0}^{\infty}\sum_{n=0}^{\infty}\frac{D_{qn}^a U_{1qm}R_{1qm}(r_a)P_{mn}\tan(s_{2qn}z_0)}{A_{qm}},$$

$$\Lambda_{21} = F_{1\ell}\delta_{pq}\Big[V_{1q\ell}R_{1q\ell}(r_a) - X_{1p\ell}R_{1p\ell}(r_a)\Big] + \frac{2i\alpha}{r_a}\sum_{m=0}^{\infty}\sum_{n=0}^{\infty}\frac{D_{qn}^a X_{1qm}R_{1qm}(r_a)P_{mn}\tan(s_{2qn}z_0)}{A_{qm}},$$

$$\Lambda_{31} = F_{1\ell}\delta_{pq}\Big[R'_{1q\ell}(r_a) - R'_{1p\ell}(r_a)\Big] + \frac{2i\alpha}{r_a}\sum_{m=0}^{\infty}\sum_{n=0}^{\infty}\frac{D_{qn}^a R'_{1qm}(r_a)P_{mn}\tan(s_{2qn}z_0)}{A_{qm}},$$

$$\Lambda_{41} = F_{1\ell}\delta_{pq}\Big[R'_{1q\ell}(r_a)s_{1q\ell} + R'_{1p\ell}(r_a)s_{1p\ell}\Big] + \frac{2i\alpha}{r_a}\sum_{m=0}^{\infty}\sum_{n=0}^{\infty}\frac{D_{qn}^a R'_{1qm}(r_a)s_{1qm}P_{mn}\tan(s_{2qn}z_0)}{A_{qm}}.$$

For region II, the edge conditions yield a system of equations in matrix form as:

$$\begin{bmatrix} \Psi_{11}^a & \Psi_{12}^a & \Psi_{13}^a & \Psi_{14}^a \\ \Psi_{21}^a & \Psi_{22}^a & \Psi_{23}^a & \Psi_{24}^a \\ \Psi_{31}^a & \Psi_{32}^a & \Psi_{33}^a & \Psi_{34}^a \\ \Psi_{41}^a & \Psi_{42}^a & \Psi_{43}^a & \Psi_{44}^a \end{bmatrix} \begin{bmatrix} E_5^a \\ E_6^a \\ E_7^a \\ E_8^a \end{bmatrix} = \begin{bmatrix} \Pi_{11} \\ \Pi_{21} \\ \Pi_{31} \\ \Pi_{41} \end{bmatrix}, \tag{4.39}$$

where

$$\Psi^a_{11} = \sum_{m=0}^{\infty} \frac{W_{2qm} R_{2qm}(r_b) \tan(s_{2qm} z_0) H^6_q(s_{2m}) R'_{2qm}(r_b)}{\eta_q(s_{2m}) B_{qm} s_{2qm}},$$

$$\Psi^a_{12} = \sum_{m=0}^{\infty} \frac{W_{2qm} R_{2qm}(r_b) \tan(s_{2qm} z_0) H^4_q(s_{2m}) R'_{2qm}(r_b)}{\eta_q(s_{2m}) B_{qm} s_{2qm}},$$

$$\Psi^a_{13} = \sum_{m=0}^{\infty} \frac{W_{2qm} R_{2qm}(r_b) \tan(s_{2qm} z_0) H^2_q(s_{2m}) R'_{2qm}}{\eta_q(s_{2m}) B_{qm} s_{2qm}},$$

$$\Psi^a_{14} = \sum_{m=0}^{\infty} \frac{W_{2qm} R_{2qm}(r_b) \tan(s_{2qm} z_0) H^0_q(s_{2m}) R'_{2qm}(r_b)}{\eta_q(s_{2m}) B_{qm} s_{2qm}},$$

$$\Psi^a_{21} = \sum_{m=0}^{\infty} \frac{X_{2qm} R_{2qm}(r_b) \tan(s_{2qm} z_0) H^6_q(s_{2m}) R'_{2qm}(r_b)}{\eta_q(s_{2m}) B_{qm} s_{2qm}},$$

$$\Psi^a_{22} = \sum_{m=0}^{\infty} \frac{X_{2qm} R_{2qm}(r_b) \tan(s_{2qm} z_0) H^4_q(s_{2m}) R'_{2qm}(r_b)}{\eta_q(s_{2m}) B_{qm} s_{2qm}},$$

$$\Psi^a_{23} = \sum_{m=0}^{\infty} \frac{X_{2qm} R_{2qm}(r_b) \tan(s_{2qm} z_0) H^2_q(s_{2m}) R'_{2qm}(r_b)}{\eta_q(s_{2m}) B_{qm} s_{2qm}},$$

$$\Psi^a_{24} = \sum_{m=0}^{\infty} \frac{X_{2qm} R_{2qm}(r_b) \tan(s_{2qm} z_0) H^0_q(s_{2m}) R'_{2qm}}{\eta_q(s_{2m}) B_{qm} s_{2qm}},$$

$$\Psi^a_{31} = \sum_{m=0}^{\infty} \frac{R'_{2qm}(r_b) \tan(s_{2qm} z_0) H^6_q(s_{2m}) R'_{2qm}(r_b)}{\eta_q(s_{2m}) B_{qm} s_{2qm}},$$

$$\Psi^a_{32} = \sum_{m=0}^{\infty} \frac{R'_{2qm}(r_b) \tan(s_{2qm} z_0) H^4_q(s_{2m}) R'_{2qm}(r_b)}{\eta_q(s_{2m}) B_{qm} s_{2qm}},$$

$$\Psi^a_{33} = \sum_{m=0}^{\infty} \frac{R'_{2qm}(r_b) \tan(s_{2qm} z_0) H^2_q(s_{2m}) R'_{2qm}}{\eta_q(s_{2m}) B_{qm} s_{2qm}},$$

$$\Psi^a_{34} = \sum_{m=0}^{\infty} \frac{R'_{2qm}(r_b) \tan(s_{2qm} z_0) H^0_q(s_{2m}) R'_{2qm}(r_b)}{\eta_q(s_{2m}) B_{qm} s_{2qm}},$$

$$\Psi^a_{41} = \sum_{m=0}^{\infty} \frac{R'_{2qm}(r_b) H^6_q(s_{2m}) R'_{2qm}(r_b)}{\eta_q(s_{2m}) B_{qm}},$$

$$\Psi^a_{42} = \sum_{m=0}^{\infty} \frac{R'_{2qm}(r_b) H^4_q(s_{2m}) R'_{2qm}(r_b)}{\eta_q(s_{2m}) B_{qm}},$$

$$\Psi^a_{43} = \sum_{m=0}^{\infty} \frac{R'_{2qm}(r_b)H^2_q(s_{2m})R'_{2qm}(r_b)}{\eta_q(s_{2m})B_{qm}},$$

$$\Psi^a_{44} = \sum_{m=0}^{\infty} \frac{R'_{2qm}(r_b)H^0_q(s_{2m})R'_{2qm}(r_b)}{\eta_q(s_{2m})B_{qm}}.$$

$$\Pi_{11} = -\frac{\alpha}{2r_b}F_{1\ell}\delta_{pq}s_{1p\ell}\sum_{m=0}^{\infty}\frac{W_{2qm}R_{2qm}(r_b)P_{\ell m}\tan(s_{2qm}z_0)}{B_{qm}s_{2qm}} + \frac{\alpha}{2r_b}\sum_{m=0}^{\infty}\sum_{n=0}^{\infty}\frac{C^a_{qn}W_{2qm}R_{2qm}(r_b)s_{1qn}P_{nm}\tan(s_{2qm}z_0)}{B_{qm}s_{2qm}} + \frac{i\alpha}{2r_b}\sum_{m=0}^{\infty}\sum_{n=0}^{\infty}\frac{W_{2qm}R_{2qm}(r_b)g^a_{qn}h_{qmn}\tan(s_{2qm}z_0)}{B_{qm}s_{2qm}},$$

$$\Pi_{21} = -\frac{\alpha}{2r_b}F_{1\ell}\delta_{pq}s_{1p\ell}\sum_{m=0}^{\infty}\frac{X_{2qm}R_{2qm}(r_b)P_{\ell m}\tan(s_{2qm}z_0)}{B_{qm}s_{2qm}} + \frac{i\alpha}{2r_b}\sum_{m=0}^{\infty}\sum_{n=0}^{\infty}\frac{X_{2qm}R_{2qm}(r_b)g^a_{qn}h_{qmn}\tan(s_{2qm}z_0)}{B_{qm}s_{2qm}} + \frac{\alpha}{2r_b}\sum_{m=0}^{\infty}\sum_{n=0}^{\infty}\frac{C^a_{qn}X_{2qm}R_{2qm}(r_b)s_{1qn}P_{nm}\tan(s_{2qm}z_0)}{B_{qm}s_{2qm}},$$

$$\Pi_{31} = -\frac{\alpha}{2r_b}F_{1\ell}\delta_{pq}s_{1p\ell}\sum_{m=0}^{\infty}\frac{R'_{2qm}(r_b)P_{\ell m}\tan(s_{2qm}z_0)}{B_{qm}s_{2qm}} + \frac{i\alpha}{2r_b}\sum_{m=0}^{\infty}\sum_{n=0}^{\infty}\frac{R'_{2qm}(r_b)g^a_{qn}h_{qmn}\tan(s_{2qm}z_0)}{B_{qm}s_{2qm}} + \frac{\alpha}{2r_b}\sum_{m=0}^{\infty}\sum_{n=0}^{\infty}\frac{C^a_{qn}R'_{2qm}(r_b)s_{1qn}P_{nm}\tan(s_{2qm}z_0)}{B_{qm}s_{2qm}},$$

$$\Pi_{41} = -\frac{\alpha}{2r_b}F_{1\ell}\delta_{pq}s_{1p\ell}\sum_{m=0}^{\infty}\frac{R'_{2qm}(r_b)P_{\ell m}}{B_{qm}} + \frac{i\alpha}{2r_b}\sum_{m=0}^{\infty}\sum_{n=0}^{\infty}\frac{R'_{2qm}(r_b)g^a_{qn}h_{qmn}}{B_{qm}} + \frac{\alpha}{2r_b}\sum_{m=0}^{\infty}\sum_{n=0}^{\infty}\frac{C^a_{qn}R'_{2qm}(r_b)s_{1qn}P_{nm}}{B_{qm}}. \quad (4.40)$$

The amplitude (C^a_{qm}) of the (m)th reflected field and the amplitude (D^a_{qm}) of the mth transmitted field can be obtained by truncating and solving the system once

the constants E_1 to E_8 from equations (4.38) and (4.39) have been established. By solving the symmetric and anti-symmetric problems after truncation, the following amplitudes can be computed:

$$C_{pn} = \frac{C^s_{pn} + C^a_{pn}}{2}, E_{pn} = \frac{C^s_{pn} - C^a_{pn}}{2},$$

$$D_{pn} = \frac{D^s_{pn} + D^a_{pn}}{2}, P_{pn} = \frac{D^s_{pn} - D^a_{pn}}{2}.$$

After truncating and determining the amplitudes, the problem can be analyzed numerically.

4.2 Numerical Solution

Numerical solutions are obtained by truncating the system to N terms, where N is a fixed number. This is done to simplify the complex mathematical equations and make them easier to solve. Computations are performed using Mathematica software, which is a powerful tool for numerical calculations. The following parameters are used in the computations: $\bar{a} = 0.2$ (dimensional radius of duct I), $\bar{b} = 0.28$ (dimensional radius of duct II), $\varrho = 1.2$ kg/m^3 (air density), $c = 343.5$ m/s (sound speed in air), $T = 350$ N (tension), and $f = 1000$ Hz (frequency). The results of the computations are plotted in Figs. 4.2-4.21, which show the pressure matching conditions and normal velocity for symmetric and antisymmetric subproblems. The plots demonstrate that the pressure matching conditions show good agreement between corresponding modes, indicating accurate pressure matching, especially when 30 modes are used. In contrast, when 15 modes are used, the pressure matching is not as accurate. However, the velocity matching conditions exhibit some discrepancies, suggesting room for improvement in velocity matching. Notably, the normal component of velocity shows poor matching for both 15 and 30 modes. Overall, the numerical solution is verified, and the results provide valuable insights into the acoustic behavior of the system.

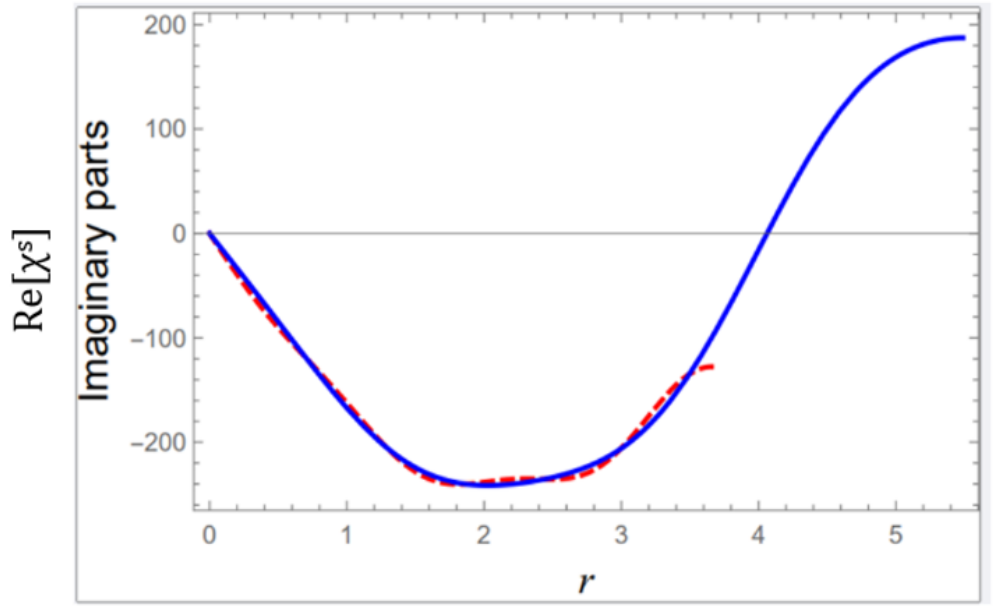

FIGURE 4.6: Real part of pressure matching for symmetric subproblem with 15 terms (χ_1^s: left shell, dotted; χ_2^s: right shell, blue).

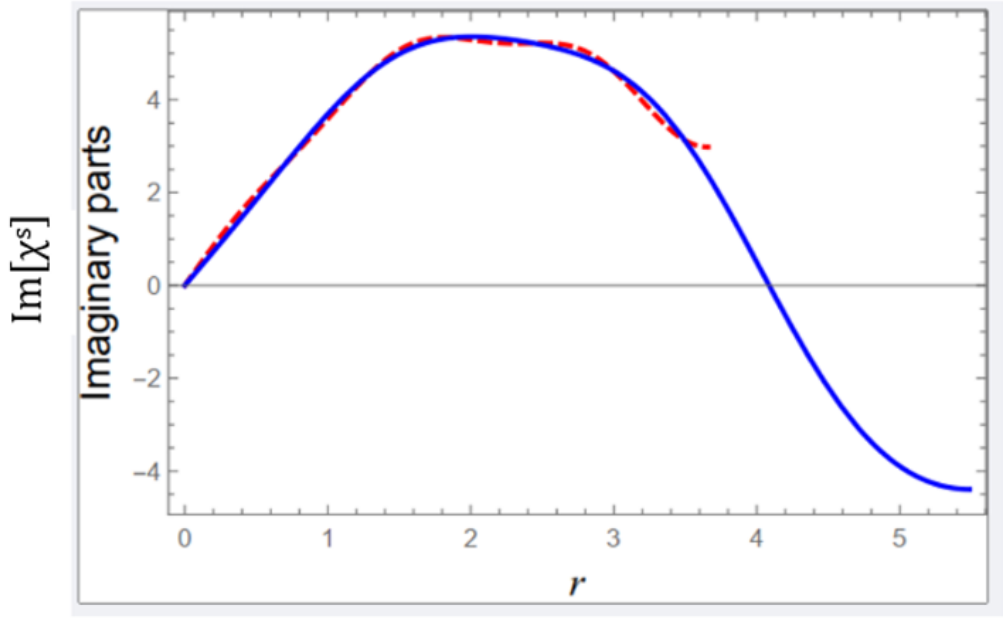

FIGURE 4.7: Imaginary part of the pressure matching condition for the symmetric subproblem with 15 terms (χ_1^s : left shell, dotted line; χ_2^s : right shell, blue line).

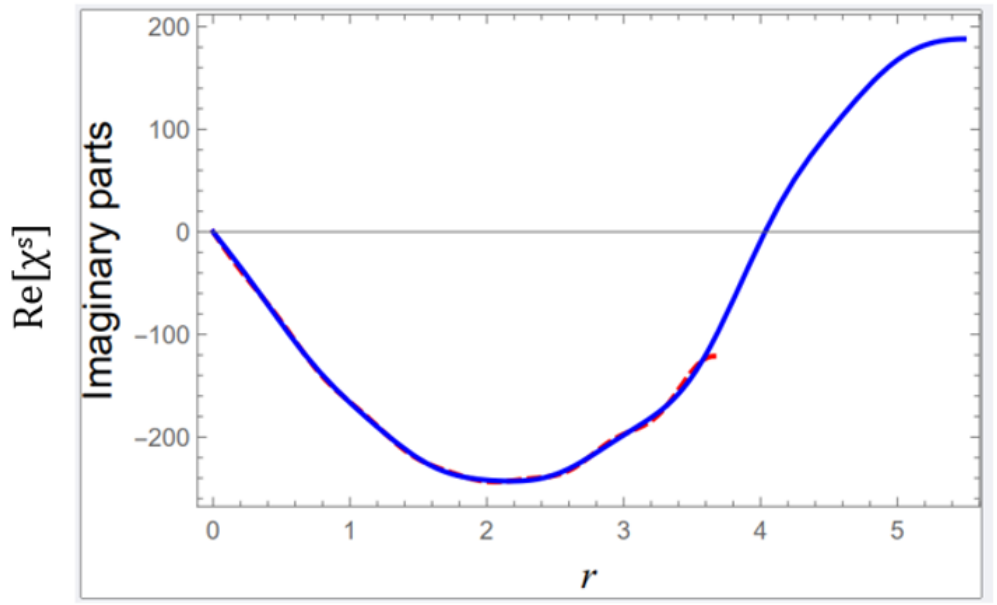

FIGURE 4.8: Real part of pressure matching for symmetric subproblem with 30 terms (χ_1^s: left shell, dotted; χ_2^s: right shell, blue).

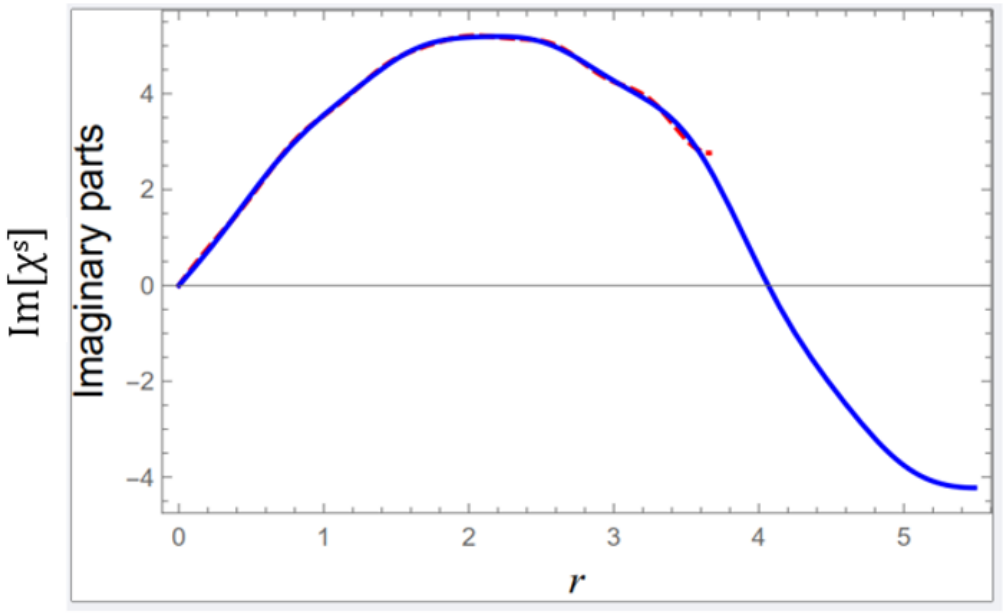

FIGURE 4.9: Imaginary part of the pressure matching condition for the symmetric subproblem with 30 terms (χ_1^s : left shell, dotted line; χ_2^s : right shell, blue line).

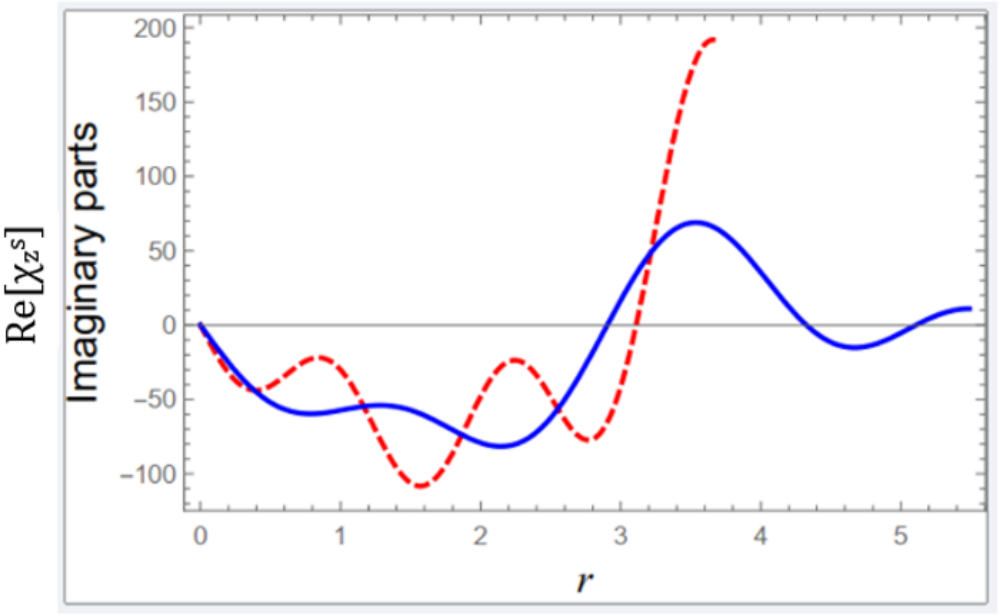

FIGURE 4.10: Real part of the matching condition for normal velocity in symmetric subproblem with 15 terms (χ_1^s: left shell, dotted line; χ_2^s: right shell, blue line). .

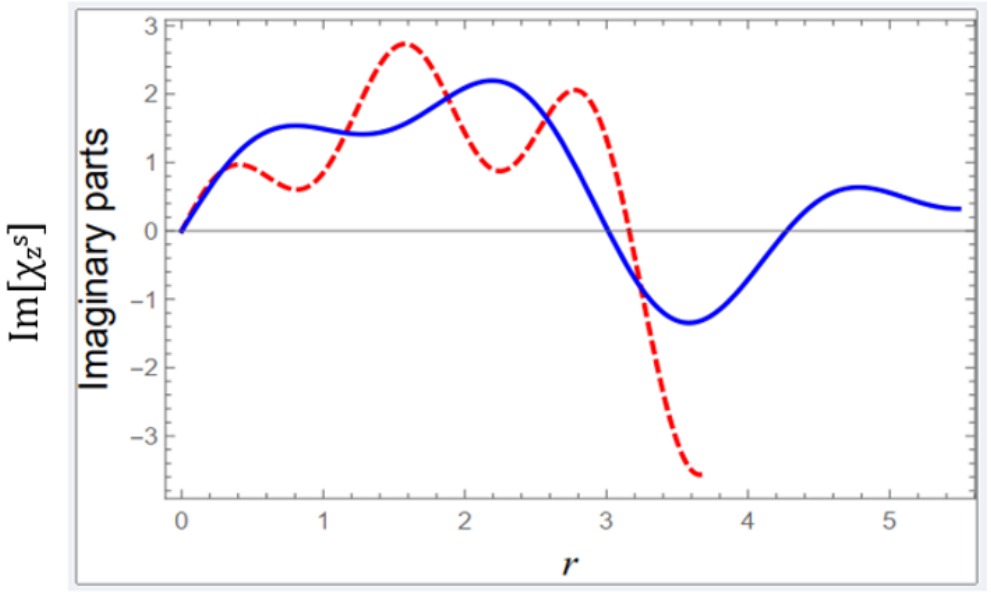

FIGURE 4.11: Imaginary part of the matching condition for normal velocity in symmetric subproblem with 15 terms (χ_1^s: left shell, dotted line; χ_2^s: right shell, blue line). .

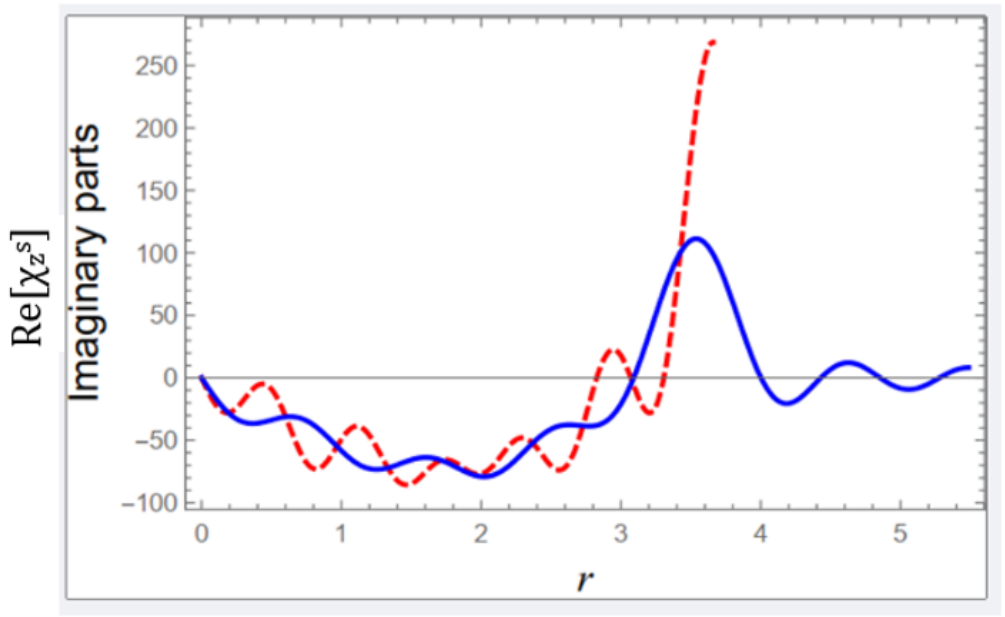

FIGURE 4.12: Real part of the matching condition for normal velocity in symmetric subproblem with 30 terms (χ_1^s: left shell, dotted line; χ_2^s: right shell, blue line). .

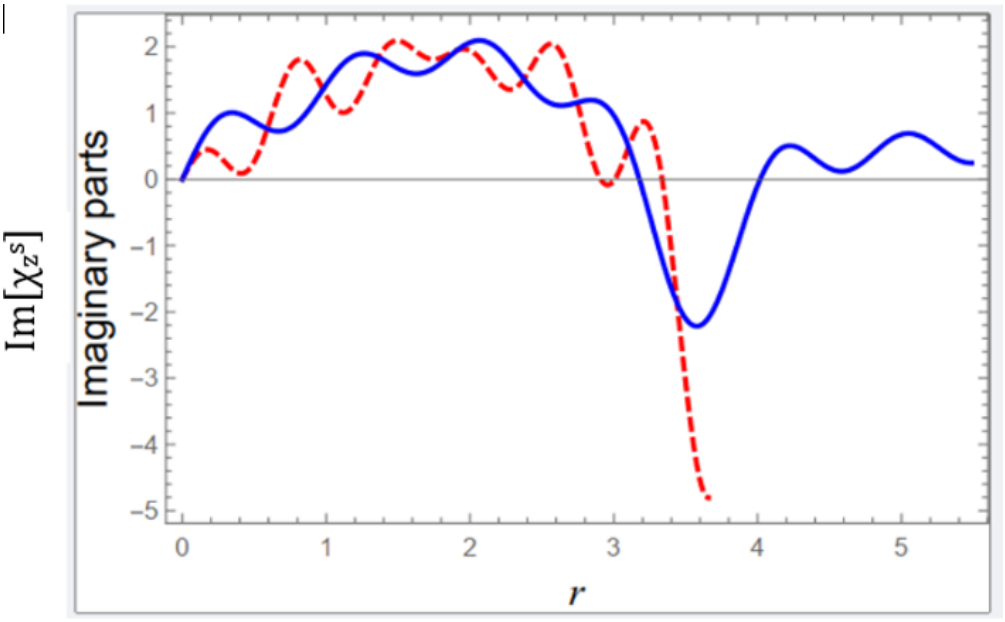

FIGURE 4.13: Imaginary part of the matching condition for normal velocity in symmetric subproblem with 30 terms (χ_1^s: left shell, dotted line; χ_2^s: right shell, blue line). .

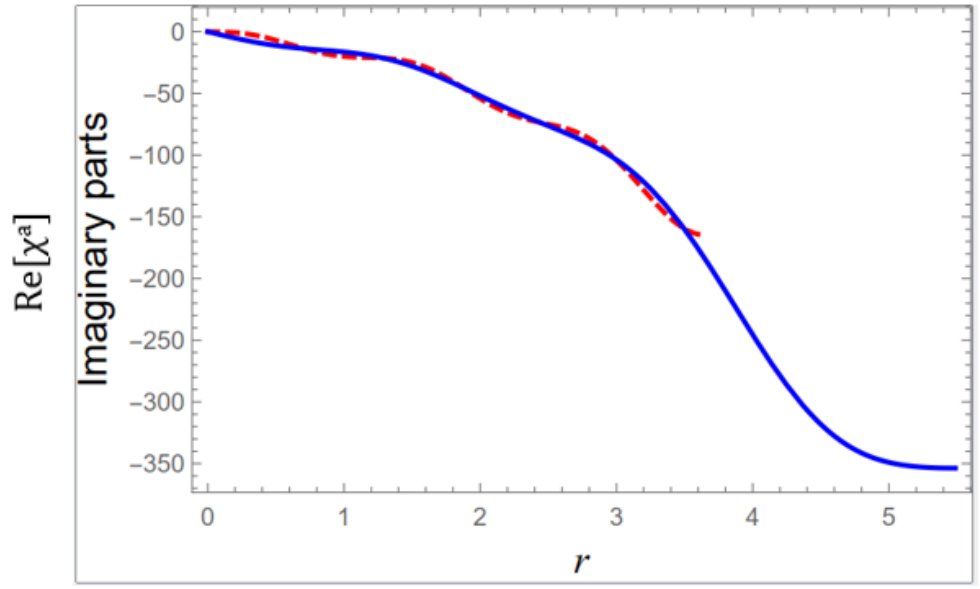

FIGURE 4.14: Real part of pressure matching for antisymmetric subproblem with 15 terms (χ_1^a: left shell, dotted; χ_2^a: right shell, blue).

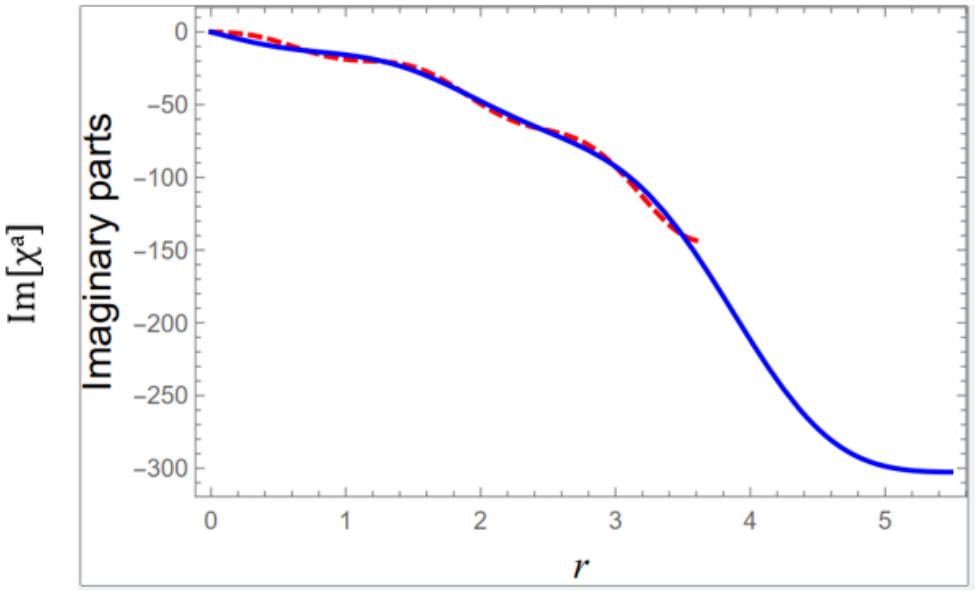

FIGURE 4.15: Imaginary part of the pressure matching condition for the antisymmetric subproblem with 15 terms (χ_1^a : left shell, dotted line; χ_2^a : right shell, blue line).

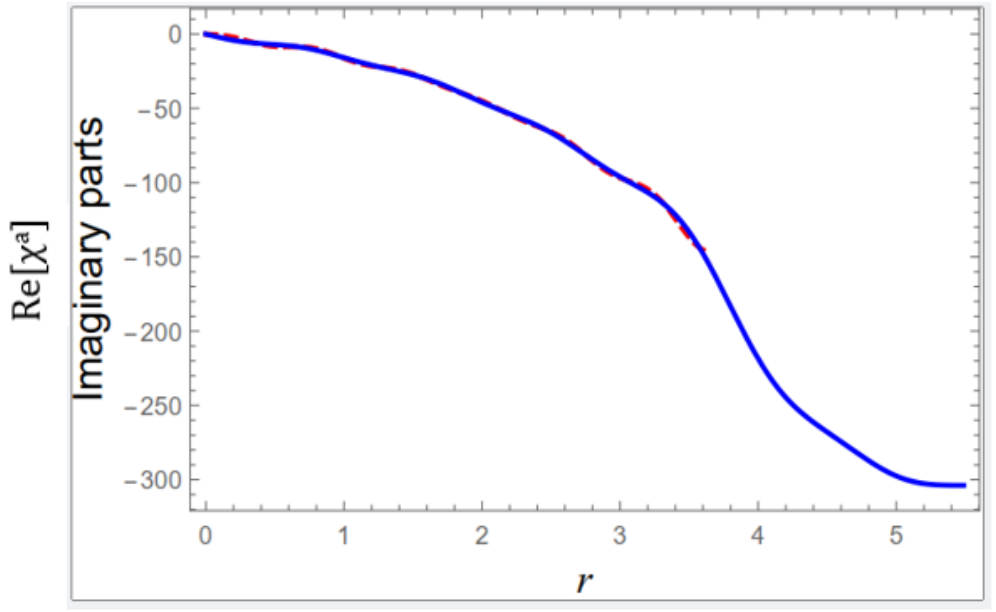

FIGURE 4.16: Real part of pressure matching for antisymmetric subproblem with 30 terms (χ_1^a: left shell, dotted; χ_2^a: right shell, blue).

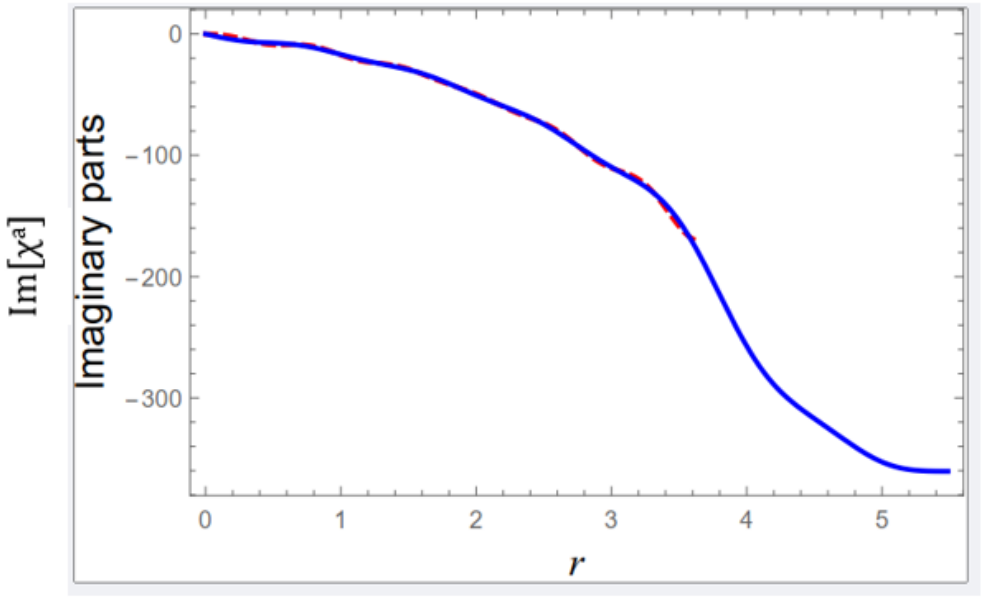

FIGURE 4.17: Imaginary part of the pressure matching condition for the antisymmetric subproblem with 30 terms (χ_1^a : left shell, dotted line; χ_2^a : right shell, blue line).

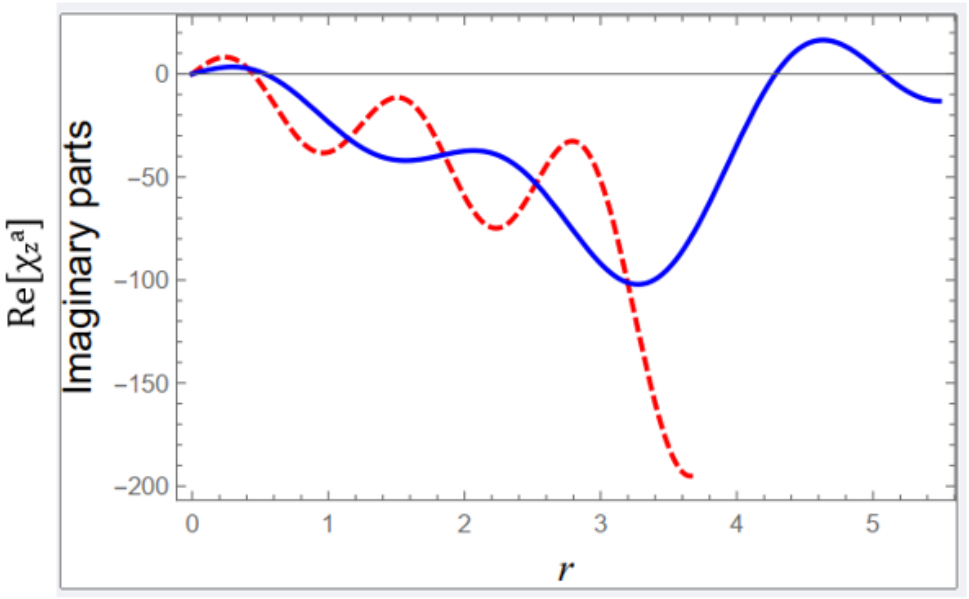

FIGURE 4.18: Real part of the matching condition for the normal component of velocity in the antisymmetric subproblem with 15 terms (χ_1^a : left shell, dotted line; χ_2^a : right shell, blue line).

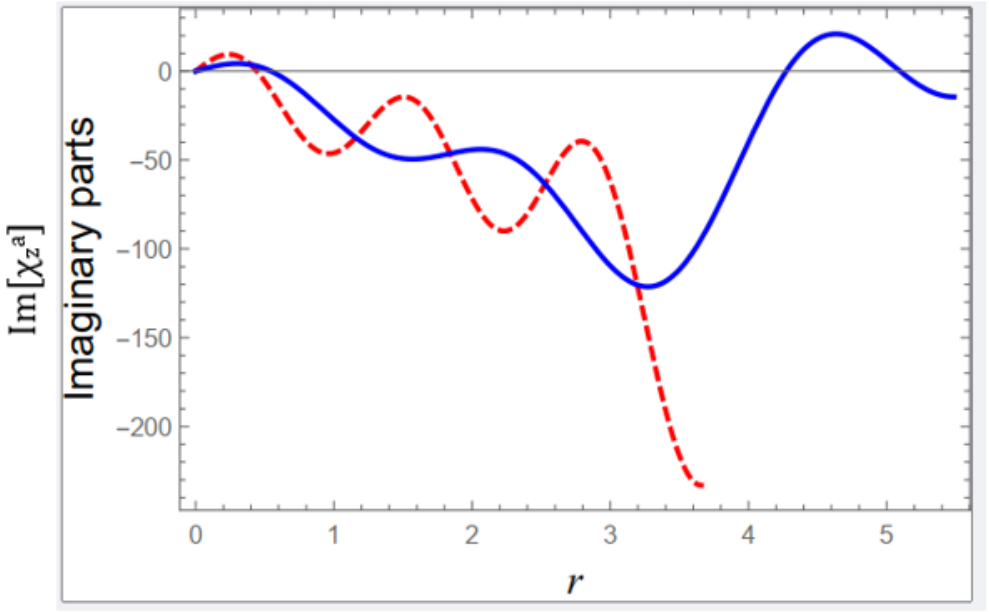

FIGURE 4.19: Imaginary part of the matching condition for the normal component of velocity in the antisymmetric subproblem with 15 terms (χ_1^a : left shell, dotted line; χ_2^a : right shell, blue line).

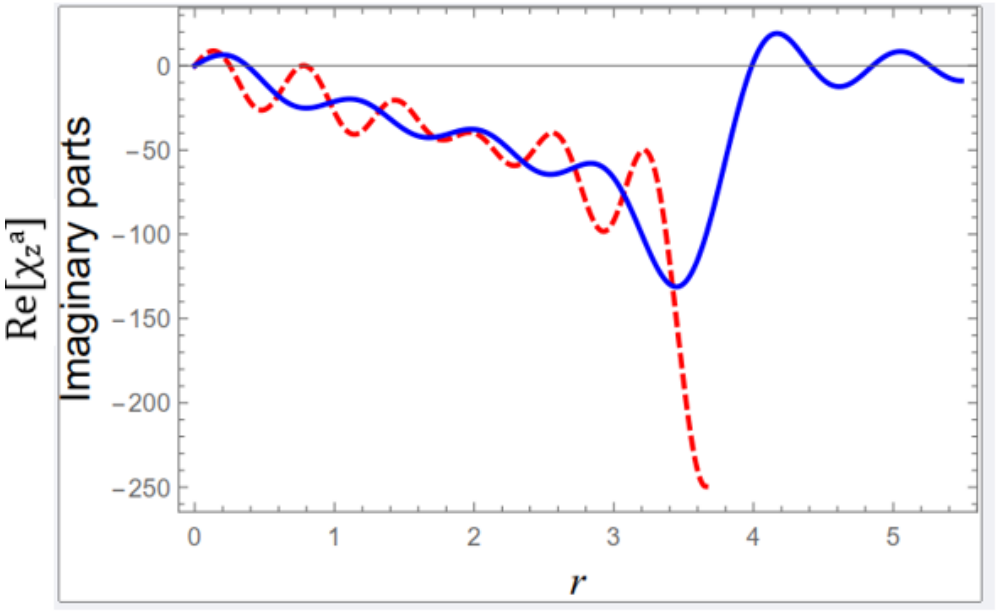

FIGURE 4.20: Real part of the matching condition for the normal component of velocity in the antisymmetric subproblem with 30 terms (χ_1^a : left shell, dotted line; χ_2^a : right shell, blue line).

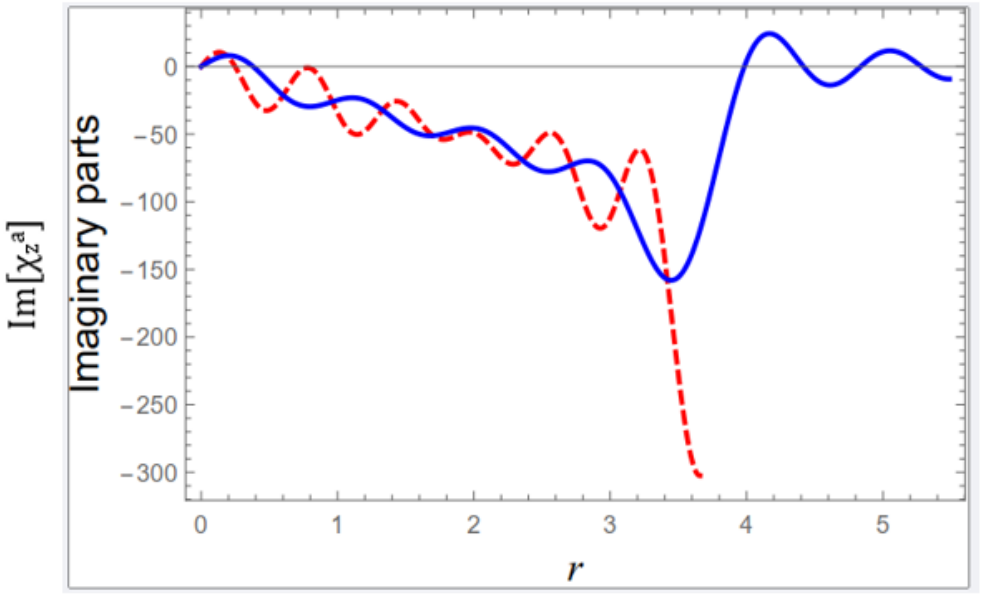

FIGURE 4.21: Imaginary part of the matching condition for the normal component of velocity in the antisymmetric subproblem with 30 terms (χ_1^a : left shell, dotted line; χ_2^a : right shell, blue line).

Chapter 5

Conclusion

This thesis has presented a comprehensive study on acoustic scattering in cylindrical membrane shells, focusing on the interaction between flexible shells and membrane discs. Through detailed mathematical modeling, the wave equation, Donnell-Mushtari theory, and membrane dynamics were formulated to analyze the behavior of sound waves in the given structure.

In **Chapter3**, we examined the case of non-axisymmetric radiation in an infinite waveguide with a bridging membrane disc. The system was modeled using two semi-infinite flexible shells, and the effects of longitudinal axisymmetric motion, transverse axisymmetric motion, and transverse non-axisymmetric motion were explored. The mode-matching method (MM) and Galerkin approach were applied to determine the scattered wave amplitudes, proving the orthogonality of mode shapes and capturing the complex interactions between the membrane disc and the surrounding fluid.

In **Chapter4**, the study was extended to acoustic scattering through expansion chambers with membrane disc interfaces. Unlike Chapter 3, only non-axisymmetric transverse modes were considered. The expansion chamber, bounded by two flexible membrane discs, introduced additional complexity due to the presence of three velocity potential fluids. The clamped edge conditions derived in Chapter 3 were also applied here, ensuring consistency in boundary constraints.

The results obtained highlight the critical role of membrane flexibility, wave propagation, and boundary conditions in determining the acoustic response of the system. The findings provide insights into sound transmission and scattering in cylindrical structures, which are relevant to engineering applications such as aerospace, underwater acoustics, and structural health monitoring.

Bibliography

[1] R. Nawaz, M. Afzal, and M. Ayub. Acoustic propagation in two-dimensional waveguide for membrane bounded ducts. *Communications in Nonlinear Science and Numerical Simulation*, 20(2):421–433, 2015.

[2] M. Afzal, R. Nawaz, and A. Ullah. Attenuation of dissipative device involving coupled wave scattering and change in material properties. *Applied Mathematics and Computation*, 290:154–163, 2016.

[3] S. Shafique, M. Afzal, and R. Nawaz. On mode-matching analysis of fluid-structure coupled wave scattering between two flexible waveguides. *Canadian Journal of Physics*, 95(6):581–589, 2017.

[4] J. B. Lawrie and M. Afzal. Acoustic scattering in a waveguide with a height discontinuity bridged by a membrane: a tailored galerkin approach. *Journal of Engineering Mathematics*, 105:99–115, 2017.

[5] R. Nawaz, A. U. Jan, and M. Afzal. Fluid-structure coupled wave scattering in a flexible duct at the junction of planar discontinuities. *Advances in Mechanical Engineering*, 9(7):1687814017713187, 2017.

[6] M. Afzal and H. Bilal. Acoustic wave scattering from a wave-bearing cavity in a rectangular waveguide. *The Journal of the Acoustical Society of America*, 144(3_Supplement):1681–1681, 2018.

[7] T. Nawaz, M. Afzal, and R. Nawaz. The scattering analysis of trifurcated waveguide involving structural discontinuities. *Advances in Mechanical Engineering*, 2019.

[8] J. U. Satti, M. Afzal, and R. Nawaz. Scattering analysis of a partitioned wave-bearing cavity containing different material properties. *Physica Scripta*, 94(11):115223, 2019.

[9] M. Afzal, J. U. Satti, and R. Nawaz. Scattering characteristics of non-planar trifurcated waveguides. *Meccanica*, 55(5):977–988, 2020.

[10] M. Afzal and M. Safdar. Mode-matching technique for analyzing scattering in elastic shell chambers: Applications in trifurcated waveguide systems. *Communications in Nonlinear Science and Numerical Simulation*, 130:107723, 2024.

[11] A. D. Alruwaili, M. Afzal, H. N. Alahmadi, and A. Wahab. Wave scattering in cylindrical waveguides: Analyzing flexible shells and liner conditions. *Alexandria Engineering Journal*, 91:610–619, 2024.

[12] M. Afzal, M. Safdar, and H. N. Alahmadi. Analyzing the impact of flexible shells and sound absorbent lining on acoustic wave behavior in ducts. *Mathematical Methods in the Applied Sciences*, 47(12):10462–10477, 2024.

[13] M. Afzal, T. Aziz, and H. M. Bahaidarah. Dynamical behavior of fluid–structure interaction in ducts with rigid and flexible interfaces: modeling and analysis. *Partial Differential Equations in Applied Mathematics*, 11:100789, 2024.

[14] M. Afzal, M. O. Alkinidri, M. Safdar, and H. Bilal. On the scattering of cylindrical elastic shell having trifurcation and structural variations at interfaces. *Chaos, Solitons Fractals*, 175:114033, 2023.

[15] J. W. Miles. The analysis of plane discontinuities in cylindrical tubes. part i. *The Journal of the Acoustical Society of America*, 17(3):259–271, 1946.

[16] E. L. Shenderov. Helmholtz equation solutions corresponding to multiple roots of the dispersion equation for a waveguide with impedance walls. *Acoustical Physics*, 46(3), 2000.

[17] R. L. Cummings. The reflection of sound at a sudden expansion in a rigid cylindrical duct. *Journal of the Acoustical Society of America*, 26(1):1–7, 1954.

[18] D. Homentcovschi and J. W. Miles. Wave scattering at points of size change in rigid cylindrical ducts. *Journal of Sound and Vibration*, 118(2):315–327, 1987.

[19] R. C. Lawrie and I. L. Abrahams. Sound propagation between cylindrical ducts with different sizes and gaps. *Journal of Sound and Vibration*, 13(3):289–294, 1969.

[20] R. C. Lawrie. Behavior of flexible shells bonded to hollow cylindrical shells. *Journal of Sound and Vibration*, 28(2):247–253, 1972.

[21] M. Afzal and S. Shafique. Attenuation analysis of flexural modes with absorbent lined flanges and different edge conditions. *The Journal of the Acoustical Society of America*, 148(1):85–99, 2020.

[22] S. Shafique, M. Afzal, and R. Nawaz. On the attenuation of fluid–structure coupled modes in a non-planar waveguide. *Mathematics and Mechanics of Solids*, 25(10):1831–1850, 2020.

[23] H. Bilal and M. Afzal. On the extension of the mode-matching procedure for modeling a wave-bearing cavity. 2022.

[24] M. Afzal, S. Shafique, and A. Wahab. Analysis of traveling waveform of flexible waveguides containing absorbent material along flanged junctions. *Communications in Nonlinear Science and Numerical Simulation*, 97:105737, 2021.

[25] Mathematics and Mechanics of Solids. 27(2):348–367, 2023.

[26] H. Bilal and M. Afzal. Reflection and transmission of acoustic waves through the bridging membrane junctions. *Waves in Random and Complex Media*, pages 1–24, 2022.

[27] M. Afzal and H. Bilal. Silencing performance analysis of a membrane cavity with different edge conditions. *Journal of Vibration and Control*, 29(19–20):4466–4478, 2023.

[28] M. Afzal, N. Akhtar, M. O. Alkinidri, and M. Shutaywi. A mode-matching tailored-galerkin approach for higher order interface conditions and geometric variations. *Mathematics*, 11(3):755, 2023.

[29] M. Safdar, N. Ahmed, M. Afzal, and A. Wahab. Acoustic scattering in lined panel cavities with membrane interfaces. *The Journal of the Acoustical Society of America*, 154(2):1138–1151, 2023.

[30] M. Afzal, H. Bilal, N. Ahmed, and A. Wahab. Acoustic scattering from a wave–bearing cavity with flexible inlet and outlet. *Mathematical Methods in the Applied Sciences*, 46(18):19404–19428, 2023.

[31] M. Afzal, J. U. Satti, A. Wahab, and R. Nawaz. Scattering analysis of a partitioned membrane-bounded cavity with material contrast. *The Journal of the Acoustical Society of America*, 151(1):31–44, 2022.

[32] M. Afzal and J. U. Satti. The traveling wave formulation of a splitting chamber containing reactive components. *Archive of Applied Mechanics*, 91:1959–1980, 2021.

[33] T. Nawaz, M. Afzal, and A. Wahab. Scattering analysis of a flexible trifurcated lined waveguide structure with step-discontinuities. *Physica Scripta*, 96(11):115004, 2021.

[34] A. W. Leissa. *Vibrations of cylindrical shells*, volume 30. Journal of Sound and Vibration, 1973.

[35] M. L. Munjal and K. Prasad. Transfer matrix analysis of sound propagation in rigid cylindrical ducts with hot mean flow. *Journal of Sound and Vibration*, 61(3):347–353, 1979.

[36] M. L. Munjal. *Acoustic Wave Propagation in Ducts and Cylindrical Shells*. Elsevier, 2014.

[37] W. R. Peat. Measurement of sound behavior before and after cylindrical silencers. *Journal of the Acoustical Society of America*, 49(4):845–851, 1971.

[38] W. R. Peat. Transfer matrix method for analyzing sound transmission in cylindrical ducts with a temperature gradient. *Journal of the Acoustical Society of America*, 53(2):381–387, 1973.

[39] W. R. Peat. Higher-order sound modes at the junction of rigid cylindrical ducts. *Journal of Sound and Vibration*, 45(2):289–298, 1975.

[40] R. M. Pullen. *Acoustic scattering in circular cylindrical shells: A modal approach based on a generalized orthogonality relation.* Doctoral dissertation, Brunel University London, 2017.

[41] R. Nawaz, A. Yaseen, and M. O. Alkinidri. Fluid–structure coupled response of dynamical surfaces tailored in a flexible shell. *Mathematics and Mechanics of Solids*, 28(11):2404–2419, 2023.

[42] R. Nawaz, A. Yaseen, H. Alahmadi, and B. Tiryakioglu. A mode-matching analysis of flexible shells and waveguides with partitioning and muffler conditions. *International Journal of Mechanics and Materials in Design*, 20(5):1009–1028, 2024.

[43] A. Yaseen and R. Nawaz. Acoustic radiation through a flexible shell in a bifurcated circular waveguide. *Mathematical Methods in the Applied Sciences*, 46(5):6262–6278, 2023.

[44] H. Afsar, R. Nawaz, and A. Yaseen. Scattering through a flexural trifurcated waveguide by varying the material properties. *Physica Scripta*, 96(9):095208, 2021.

[45] H. Bilal, M. Uzair Khan, and M. Afzal. Silencing performance of the wave-bearing cavity with porous media. *Journal of Vibration and Control*, 30(19-20):4368–4382, 2024.

[46] A. D. Alruwaili, M. Afzal, M. Tanveer, and H. N. Alahmadi. Analyzing monopole sources modeling with structural variations and material contrast: An analytical perspective. *Chaos, Solitons Fractals*, 179:114434, 2024.

[47] S. Shafique, M. A. Ahmad, and M. Afzal. Optimizing the noise control in a two-layer conduit. *Physica Scripta*, 99(6):065227, 2024.

[48] T. Nawaz and M. Afzal. Trifurcated lined ducts: A comprehensive study on noise reduction strategies. *PloS One*, 19(7):e0306115, 2024.

[49] H. Bilal and M. Afzal. Application of the matrix element method: A mode-matching approach for wave-bearing cavities in complex media. *Chaos, Solitons Fractals*, 189:115589, 2024.

[50] M. Afzal, N. Ahmed, M. Safdar, and M. Umar. On the modeling of sound sources in waveguides with structural variations and sound-absorbent materials. *Communications in Nonlinear Science and Numerical Simulation*, page 108714, 2025.

[51] S. A. Nazarov and S. D. Kamenetsky. Acoustic wave scattering by a circular membrane in a cylindrical shell. *Acoustics Journal*, 56(3):253–265, 1989.

[52] S. W. Lee. *Elastic Waves in Cylindrical Shells: Theory and Applications*. Springer, 2011.

[53] P. C. T. R. Raju. Wave scattering by thin membranes in cylindrical shells: Analytical and numerical methods. *Journal of Sound and Vibration*, 328(3):456–469, 2012.

[54] B. R. Mitchell et al. Analysis of acoustic wave propagation in flexible shells and membranes. *Journal of Acoustics*, 61:283–293, 2014.

[55] J. B. Lawrie and I. D. Abrahams. An orthogonality relation for a class of problems with high-order boundary conditions; applications in sound-structure interaction. *The Quarterly Journal of Mechanics and Applied Mathematics*, 52(2):161–181, 1999.

[56] M. Afzal, H. Bilal, N. Ahmed, and A. Wahab. Analyzing the impact of flexible shells and sound absorbent lining on acoustic wave behavior in ducts. *Journal of Sound and Vibration*, 523:116711, 2024.

[57] A. Yaseen and R. Nawaz. Acoustic radiation through a flexible shell in a bifurcated circular waveguide. *Mathematical Methods in the Applied Sciences*, 46(5):6262–6278, 2023.

[58] M. C. Junger and D. Feit. *Sound, Structures, and Their Interaction*. MIT Press, 1972.